

**S M A L L F I E L D D O S I M E T R Y O F  
H I G H - E N E R G Y  
E L E C T R O N B E A M S**

**Barbara Chanda M'ule**

# **SMALL FIELD DOSIMETRY OF HIGH -ENERGY ELECTRON BEAMS**

**Barbara Chanda M'ule**

A research report submitted to the Faculty of Science, University of the Witwatersrand, Johannesburg, in partial fulfilment of the requirements for the degree of Master of Science

Johannesburg, 2008

## DECLARATION

I declare that this research report is my own, unaided work. It is submitted for the Degree of Master of Science in the University of the Witwatersrand, Johannesburg. It has not been submitted before for any degree or examination in any other University.

---

(Signature of candidate)

\_\_\_\_\_ day of \_\_\_\_\_ 2008

## ABSTRACT

**Purpose:** A comparative dosimetric study was conducted with four detectors manufactured by PTW-Freiburg (Germany) (Markus – type 23343, Advanced Markus – type 34045, PinPoint – type 31006 and a diode type – 60012) for small field high-energy electron beams. The dosimetry of Intraoperative Radiation Therapy (IORT) is challenging because of the type of tertiary collimation used. The cones increase low energy electron contamination and detectors with low energy dependence and high spatial resolution should be used.

**Materials and Methods:** Dosimetric measurements were made using all four detectors. Two applicator systems were studied: The small-field system has 9 cylindrical straight end cones of inner diameters 2 to 8 cm increasing in steps of 1 cm, and two bevel end cones of 2 and 3 cm with a bevel angle of 45°. The periscopic electron cone system is provided with three set of cylindrical cones of inner diameter 3.2, 3.8 and 4.5 cm with straight and bevel ends with bevel angle 30°.

**Results:** All dosimetric data was compared to the Markus chamber. The percent error for the absolute dose measurements for the Advanced Markus and the PinPoint were found to be 3.2% and 5.1% respectively. For the small-field cone system the percent difference in output factors (OF) for the Markus chamber and all other detectors was found to be less than 2.6% for the straight cones and less than 4.8% for the bevelled cones. The percent difference for the Markus and all other detectors was found to be less than 1.9% for straight cones and 4.2% for the bevelled cones for the periscopic system.

**Conclusions:** The Markus, Advanced Markus and the diode detector, may be used for the relative dosimetry of small electron fields. The Markus and diode detector should be cross-calibrated for absolute dose measurements. The PinPoint chamber should not be used for the absolute dosimetry of small electron fields, unless the quality correction factor  $k_{QE}$  is determined for the beam quality used. A comparative study should be made with the PinPoint oriented in the two possible positions to determine which position is more suitable for electron dosimetry. Spencer-Attix stopping power ratios for water to air ( $S_{w,air}$ ) must be calculated using Monte Carlo simulations for the two applicator systems used.

# DEDICATION

For my “Ambuya”

Egneiah Kawama Victoria Nguni Chulu

(1928.01.01 – 2006.01.21)

and my mother

Elizabeth Bupe Kalambo-M’ule

without your love of education this would never have been possible

## ACKNOWLEDGEMENTS

The department of Radiation Oncology, Division Medical Physics, at the Johannesburg Hospital, is acknowledged for permitting this work on a part-time basis. My supervisor Professor D. G. van der Merwe is acknowledged for suggesting the area of small field electron dosimetry and for the guidance.

The Canon Collins Trust is acknowledged for the scholarship awarded to me for 2007.

Mr. A Rule is acknowledge for his help in setting up and assisting with some of the measurements (sacrificing many a Saturday), and for taking the pictures used in the report. Mr. N A Mwale, Mr. S A Ngcezu, Mr. T Nyati, Mr. P Segone and Miss L Pule for sparing a moment and assisting when they could, also for their interest and encouragement.

My friends Wisani and Landry, for the use of their laptops for some of the data analysis when mine gave up thank you!

My mother, Mrs. E Kalambo-M'ule, my siblings Chita, Kawela, my cousins Kawama and Tapiwa, for the great sacrifice in view of all else so that I could finish, even when I could have given up "Zikomo".

# CONTENTS

<b>DECLARATION.....</b>	<b>II</b>
<b>ABSTRACT.....</b>	<b>III</b>
<b>DEDICATION.....</b>	<b>IV</b>
<b>ACKNOWLEDGEMENTS.....</b>	<b>V</b>
<b>CONTENTS.....</b>	<b>VI</b>
<b>LIST OF FIGURES.....</b>	<b>VIII</b>
<b>LIST OF TABLE.....</b>	<b>XI</b>
<b>CHAPTER 1 INTRODUCTION.....</b>	<b>1</b>
1.1 GENERAL INTRODUCTION.....	1
1.2 HISTORICAL BACKGROUND.....	2
1.3 STATEMENT OF THE PROBLEM.....	3
1.3.1 Objectives.....	4
<b>CHAPTER 2 LITERATURE REVIEW.....</b>	<b>6</b>
2.1 APPLICATOR SYSTEM.....	6
2.1.1 Field size.....	7
2.2 DOSIMETRY SYSTEM.....	8
2.2.1 Air ionisation chambers.....	8
2.2.2 Solid-State Detectors.....	10
2.3 DOSIMETRIC MEASUREMENTS.....	11
2.3.1 Output measurements.....	12
2.3.2 Percent Depth Dose.....	14
2.3.3 Lateral therapeutic coverage (Isodoses).....	15
2.3.4 Output Factors (OF).....	15
2.3.5 Gap factors (GF).....	16
2.4 SUMMARY OF METHODOLOGY TO BE USED.....	17
<b>CHAPTER 3 EXPERIMENTAL PROCEDURES AND RESULTS.....</b>	<b>18</b>
3.1 EQUIPMENT.....	18
3.1.1 Applicator system.....	19

3.1.2	<i>Dosimetry System</i> .....	23
3.2	ABSOLUTE DOSIMETRY .....	23
3.2.1	<i>Output measurements</i> .....	23
3.2.2	<i>Output Factors (OF)</i> .....	25
3.3	RELATIVE DOSIMETRY .....	29
3.3.1	<i>Percent depth dose (PDD)</i> .....	29
3.3.2	<i>Two dimensional relative beam data (isodose curves)</i> .....	61
3.3.3	<i>SSD corrections on air gap</i> .....	76
<b>CHAPTER 4 DISCUSSION</b> .....		<b>78</b>
4.1	ABSOLUTE DOSIMETRY.....	78
4.1.1	<i>Output measurements</i> .....	78
4.1.2	<i>Output factor measurements</i> .....	79
4.2	RELATIVE DOSIMETRY.....	81
<b>CHAPTER 5 CONCLUSIONS AND RECOMMENDATIONS</b> .....		<b>83</b>
<b>REFERENCES</b> .....		<b>85</b>

## LIST OF FIGURES

Figure 2-1: Diagram illustrating the definition of the clinical central axes and geometric central axes for dosimetry measurements, where $g$ is the air gap distance, SCED is the Source-to-cone-end distance and SSD is the Source-to-surface distance (figure adapted from Palta et al 1995; Nyerick et al 1991) .....	12
Figure 2-2: Mass collision stopping-power ratios for water/carbon and water/silicon as a function of electron energy (from Björk et al 2000a).....	14
Figure 3-3: Small-field cone system (a) the main adaptor (b) acrylic cone (c) stainless steel cone (d) the assembled applicator system with the stainless steel cone mounted directly on to the main adaptor and (e) the assembled applicator system with the acrylic cone mounted on to a docking adaptor and on the main adaptor.....	20
Figure 3-4: (a) The main adaptor for the periscopic electron cone system (b) the top part of the cone showing the three spacer rings and the brass plate on top of the cone (c) a straight cone and (d) a bevelled cone (bevel angle $30^\circ$ ).....	22
Figure 3-5: Comparison of the PDD as measured with the Markus, Advanced Markus, PinPoint chambers and diode detector for 10 cm x 10 cm reference field for energies 5 and 6 MeV.....	30
Figure 3-6: Comparison of the PDD as measured with the Markus, Advanced Markus, PinPoint chambers and diode detector for 10 cm x 10 cm reference field for energies 7 and 9 MeV.....	31
Figure 3-7: PDD measured along the clinical central-axis for different cones for the small field applicator system cones for energies 5 and 6 MeV (bevel angle $45^\circ$ ).....	33
Figure 3-8: PDD measured along the clinical central-axis for different cones for the small field applicator system cones for energies 7 and 9 MeV (bevel angle $45^\circ$ ) (Markus chamber).....	34
Figure 3-9: PDD measured along the clinical central-axis for the different cones for the Periscopic electron cone system cones for energies 5 and 6 MeV (bevel angle $30^\circ$ ) .....	35
Figure 3-10: PDD measured along the clinical central-axis for the different cones for the Periscopic electron cone system cones for energies 7 and 9 MeV (bevel angle $30^\circ$ ) (7 MeV and 9 MeV) (Markus chamber).....	36

Figure 3-11: Comparison of the PDD as measured with the Markus, Advanced Markus, PinPoint and the diode detector for the 8 cm cone for energies 5 and 6 MeV (small field cone system) .....38

Figure 3-12: Comparison of the PDD as measured with the Markus, Advanced Markus, PinPoint and the diode detector for the 8 cm cone for energies 7 and 9 MeV (small field cone system).....39

Figure 3-13: Comparison of the PDD as measured with the Markus, Advanced Markus, PinPoint and the diode detector for the 3 cm straight cone for energies 5 and 6 MeV (small field cone system).....40

Figure 3-14: Comparison of the PDD as measured with the Markus, Advanced Markus, PinPoint and the diode detector for the 3 cm straight cone for energies 7 and 9 MeV (small field cone system).....41

Figure 3-15: Comparison of the PDD as measured with the Markus, Advanced Markus, PinPoint and the diode detector for the 3 cm bevelled cone for energies 5 and 6 MeV (small field cone system) (bevel angle 45°).....42

Figure 3-16: Comparison of the PDD as measured with the Markus, Advanced Markus, PinPoint and the diode detector for the 3 cm bevelled cone for energies 7 and 9 MeV (small field cone system) (bevel angle 45°).....43

Figure 3-17: Comparison of the PDD as measured with the Markus, Advanced Markus, PinPoint and the diode detector for the 4.5 cm straight cone for energies 5 and 6 MeV (periscopic electron cone system).....44

Figure 3-18: Comparison of the PDD as measured with the Markus, Advanced Markus, PinPoint and the diode detector for the 4.5 cm straight cone for energies 7 and 9 MeV (periscopic electron cone system).....45

Figure 3-19: Comparison of the PDD as measured with the Markus, Advanced Markus, PinPoint and the diode detector for the 4.5 cm bevelled cone for energies 5 and 6 MeV (periscopic electron cone system).....46

Figure 3-20: Comparison of the PDD as measured with the Markus, Advanced Markus, PinPoint and the diode detector for the 4.5 cm bevelled cone for energies 7 and 9 MeV (periscopic electron cone system) (bevel angle 30°).....47

Figure 3-21: Isodose charts for the 8 cm straight cone (small cone system) for electron energies (a) 5, (b) 6, (c) 7, and ( d) 9 MeV measured with the Markus

chamber.....	62
Figure 3-22: Isodose charts for the 5 cm straight cone (small cone system) for electron energies (a) 5, (b) 6, (c) 7, and ( d) 9 MeV measured with the Markus chamber.....	63
Figure 3-23: Isodose charts for the 3 cm straight cone (small cone system) for electron energies (a) 5, (b) 6, (c) 7, and ( d) 9 MeV measured with the Markus chamber.....	64
Figure 3-24: Isodose charts for the 3 cm bevelled cone (bevel angle 45°) (small cone system) for electron energies (a) 5, (b) 6, (c) 7, and ( d) 9 MeV measured with the Markus chamber, measured along the major elliptical axis of the cone) .....	65
Figure 3-25: Isodose charts for the 3 cm bevelled applicator (bevel angle 45°) (small applicator system) for electron energies (a) 5, (b) 6, (c) 7, and ( d) 9 MeV measured with the Markus chamber, measured along the minor elliptical axis of the applicator.....	66
Figure 3-26: Isodose charts for the 4.5 cm straight cone (periscopic electron system) for electron energies (a) 5, (b) 6, (c) 7, and ( d) 9 MeV measured with the Markus chamber.....	67
Figure 3-27: Isodose charts for the 4.5 cm bevelled cone (bevel angle 45°) (periscopic electron system) for electron energies (a) 5, (b) 6, (c) 7, and ( d) 9 MeV measured with the Markus chamber, measured along the major elliptical axis of the cone.....	68
Figure 3-28: Isodose charts for the 4.5 cm bevelled applicator (bevel angle 45°) (periscopic electron cone system) for electron energies (a) 5, (b) 6, (c) 7, and ( d) 9 MeV measured with the Markus chamber, measured along the minor elliptical axis of the applicator.....	69
Figure 3-29: Comparison of isodose curves as measured with the Markus (M), Advanced Markus (AM), PinPoint (P) and Diode (D) detector for energies for the 8 cm straight cone (small cone system) (a) 5 MeV (b) 6 MeV (c) 7 MeV and ( d) 9 MeV .....	71
Figure 3-30: Comparison of isodose curves as measured with the Markus (M), Advanced Markus (AM), PinPoint (P) and Diode (D) detector for energies for the 3 cm straight cone (small cone system) (a) 5 MeV (b) 6 MeV (c) 7 MeV and ( d) 9 MeV .....	72

Figure 3-31: Comparison of isodose curves as measured with the Markus (M), Advanced Markus (AM), PinPoint (P) and Diode (D) detector for energies for the 3 cm bevelled cone (bevel angle 45°) (small cone system) (a) 5 MeV (b) 6 MeV (c) 7 MeV and ( d) 9 MeV.....73

Figure 3-32: Comparison of isodose curves as measured with the Markus (M), Advanced Markus (AM), PinPoint (P) and Diode (D) detector for energies for the 4.5 cm straight cone (periscopic electron cone system) (a) 5 MeV (b) 6 MeV (c) 7 MeV and ( d) 9 MeV.....74

Figure 3-33: Comparison of isodose curves as measured with the Markus (M), Advanced Markus (AM), PinPoint (P) and Diode (D) detector for energies for the 4.5 cm bevelled cone (bevel angle 30°) (periscopic electron cone system) (a) 5 MeV (b) 6 MeV (c) 7 MeV and ( d) 9 MeV.....75

## LIST OF TABLE

Table 3-1: Characteristics of the electron energies from the Siemens PRIMUS linear accelerator used for this study.....	18
Table 3-2: Ionisation chambers and detector specifications.....	23
Table 3-3: Measured output for the reference applicator 10 cm x 10 cm.....	25
Table 3-4: Output Factors for the small-field cone system measured with different types of detectors.....	27
Table 3-5: Output Factors for the periscopic electron cone system measured with different types of detectors.....	28
Table 3-6: Summary of the electron depth dose characteristics as measured with the Markus chamber (small-field cone system).....	48
Table 3-7: Summary of the electron depth dose characteristics as measured with the Advanced Markus chamber (small-field cone system).....	50
Table 3-8: Summary of the electron depth dose characteristics as measured with the PinPoint chamber (small-field cone system).....	51
Table 3-9: Summary of the electron depth dose characteristics as measured with the Diode detector (small-field cone system).....	52
Table 3-10: Summary of the electron depth dose characteristics as measured with the Markus chamber (periscopic electron cone system).....	54
Table 3-11: Summary of the electron depth dose characteristics as measured with the Advanced Markus chamber (periscopic electron cone system).....	56
Table 3-12: Summary of the electron depth dose characteristics as measured with the PinPoint chamber (periscopic electron cone system).....	58
Table 3-13: Summary of the electron depth dose characteristics as measured with the Diode detector (periscopic electron cone system).....	60
Table 3-14: Inverse square factors for the 2 and 3 cm bevelled cones for the small field cone system.....	76
Table 3-15: Gap factors for the 2 and 3 bevelled cones (bevel angle 45°) for the small field cone system.....	77

# CHAPTER 1 INTRODUCTION

## 1.1 General Introduction

Major advances in clinical radiation oncology have often been due to the difference that can be achieved in the dose distribution between the target volume and the normal surrounding tissue (Biggs 1985, Willett *et al* 2007). The probability of achieving local tumour control of a localized tumour mass generally increases as larger radiation doses are delivered to the tumour. The dose that can safely be delivered to a tumour is however restricted by the radiation tolerance of the surrounding normal tissue. Intraoperative Radiation Therapy (IORT) is one method of increasing the dose to the local target volume. IORT is a multidisciplinary procedure that combines two conventional modalities of cancer treatment: Surgery and Radiation Therapy (Palta and Suntharalingham 1989). IORT delivers a single large radiation dose in a sterile environment to a surgically exposed tumour, to tumour remaining after partial resection or to unresected tissue that may contain microscopic disease (Hogstrom *et al* 2006, Podgorsak and Podgorsak 1999).

As is the case with conventional radiation therapy, it is necessary to spare normal radiosensitive tissue that may inadvertently be irradiated during IORT. IORT aims to expose the tumour-bearing structure and applying a large radiation dose directly to the target volume, while avoiding the irradiation of normal sensitive structures (Biggs 1985). Normal sensitive structures can be spared by selecting a radiation modality with a rapid dose fall-off beyond the treatment volume or by shielding or displacing the sensitive structures from primary radiation. There are three different radiation modalities (Podgorsak and Podgorsak 1999) that are used in IORT:

1. HDR brachytherapy sources
2. Orthovoltage x-rays

### 3. Megavoltage electron beams

## 1.2 Historical Background

Less than 20 years after the discovery of x-rays Carl Beck, MD, performed the first documented cases of IORT in an attempt to treat patients with gastric cancer, (Beddar *et al* 2001, Conkey *et al* 1987, Palta *et al* 1995) The rationale for the treatments was that normal radiosensitive tissue could be excluded from the target volume and an improved therapeutic ratio of local control to major tissue complication could be achieved for deep seated tumours (Palta *et al* 1995). However these treatments were unsuccessful due to the low energy of the beams that were used.

The introduction of megavoltage x-rays in radiation therapy in the 1950's resulted in a decrease of interest in IORT as a treatment modality. Megavoltage x-ray beams could be used to deliver high doses of radiation to deep seated tumours without the limitation of skin-tolerance (as experienced with kilo-voltage x-ray beams). Even with the availability of penetrating x-rays, the target volume is surrounded by normal tissues, which may limit the maximum dose that can be delivered to the target volume (Podgorsak and Podgorsak 1999). The use of megavoltage electron beams for IORT was pioneered by Abe and Takahashi in 1964 (Abe 1984, Ellis *et al* 2000). The reasoning was that electron-IORT offered a definite advantage over conventional megavoltage radiation therapy and surgery alone. In conventional megavoltage therapy the dose delivered to a target volume maybe limited by critical structures surrounding the target volume. With surgery there is a chance that microscopic disease may be contained in adjacent tissue may not be removed by surgery. To overcome the limitation of external beam radiation therapy and surgery alone IORT was developed (Abe 1984, Palta *et al* 1995).

Most IORT programs today utilise megavoltage electron beams produced by a linear accelerator (linac) (Palta *et al* 1995, Podgorsak and Podgorsak 1999). Electron beams

have several properties that are unique and make them advantageous for use in IORT. Firstly, dose is deposited within a definite range resulting in the characteristic electron beam depth-dose curve, with relatively uniform dose delivered on the central axis superficially followed by a region of rapid dose fall-off resulting in low doses to distal tissue. Secondly, depending on the thickness of the target volume and energy, the dose can be delivered homogeneously throughout the target volume. Thirdly, unlike low-energy x-rays, there is less difference between tissue and bone absorption in megavoltage electron beams (Palta *et al* 1995, Podgorsak and Podgorsak 1999).

According to Palta *et al* (1995) the ideal setup for IORT is to have a dedicated radiation machine in an operating theatre, the disadvantage with this setup is that the workload and resources sometimes do not justify its implementation. An alternative is to have an operating theatre adjoining a radiation treatment room. The advantage of having a functional operating theatre in the radiotherapy department adjacent to the radiation treatment vault, allows the accelerator to be used for regular treatments as well as the IORT procedures.

### **1.3 Statement of the problem**

The electron beam distribution in a medium is characterised by a rapidly changing fluence and by the ease with which electrons are scattered by interaction with the medium (Klevenhagen 1985). These electron beam features present a unique problem in electron beam dosimetry and have considerable bearing on the dosimetry methodology used. Due to the large dose gradients of electron beams, the detectors used must be able to adequately resolve these. There is therefore a need to use detectors which have a high spatial resolution.

IORT utilises a dedicated collimation system and the passage of electrons through these collimators results in a large amount of scattered electrons in the clinical beam, as

compared to the reference field. The increase of scatter changes the characteristics of the radiation beam at the measuring point, which influences the mass collision stopping power ratio between water and the detector material.

According to Verellen (2006), the dosimetry of small fields is complicated by two factors, firstly the lack of charged particle equilibrium and secondly, the relationship between the detector size and the field. The choice of detector system depends on the field size and as such, the volume of an ionisation chamber should be taken into consideration when choosing a detector for small fields. According to Sharma *et al* (2005) it is crucial that the detector used for measurements in small fields be smaller than the dimensions of the field.

Although many measurement techniques have been used in degraded electron beams, such as in IORT, comparison of results obtained with different detectors in the same irradiation geometry have not been thoroughly studied (Björk *et al* 2004). The aim of this study was to compare beam data obtained with different detector systems. Four types of PTW detectors manufactured by PTW-Freiburg, Germany were investigated:

1. a cylindrical chamber (PinPoint – type 31006)
2. and two parallel-plate chambers with different collecting volumes (Markus – type 23343 and Advanced Markus – type 34045) and
3. a diode detector (type – 60012)

### **1.3.1 Objectives**

The aim of the study was obtain dosimetric data for small electron IORT fields, focusing on 5, 6, 7 and 9 MeV energies, using the different detector systems and to compare the data obtained for two different applicator systems.

The objectives of the study were to:

- Determine the absolute (dose rate) dose at a reference depth of measurement for a series of small electron IORT beams.
- Measure the output factors for small electron beams for the range of energies.
- Determine the 1D and 2D relative beam data for the small electron fields.
- Compare the beam data obtained with different detector systems.

The commissioning dosimetry of IORT system is unique and requires a complete set of measurements (Palta *et al* 1995). Beam characteristics at all energies for all IORT cones sizes must be measured and presented in a form that is easily usable in the Operating Theatre environment (Palta *et al* 1995). Before IORT can be used as a modality at the Johannesburg Hospital the IORT applicators have to be commissioned. Acquiring beam data (including the output) is one of the tasks required in the commissioning process. Suitable data obtained from this study will be used in the commissioning of IORT at the Johannesburg Hospital.

## CHAPTER 2 LITERATURE REVIEW

### 2.1 Applicator System

A standard linear accelerator (linac) can be adapted for IORT delivery without making adjustments to the linac head, gantry, dose rate or the mechanism by which the electron beams are produced (Palta *et al* 1995, Podgorsak and Podgorsak 1999). Applicator systems for IORT include docking adapters, IORT adapters and different sets of cones (Fraass *et al* 1985). IORT applicator designs are determined by the volume to be treated and by other technical details of IORT procedures (Fraass *et al* 1985). The cones used in IORT may include elliptical, rectangular and circular cross-sectional designs and may also include specially made shapes such as the squircle (half circle-half square) used by Fraass *et al* (1985). The cones may be made of polymethylmethacrylate (PMMA/acrylic) or metal (brass or aluminium), and they must allow for the viewing of the treatment area (Podgorsak and Podgorsak 1999). Applicator systems in IORT serve three major functions.

1. Collimation of the electron beam
2. delineation of the treatment volume
3. retraction of normal tissue (Björk *et al* 2000b, Podgorsak and Podgorsak 1999)

There are two different methods by which cones are attached to the applicator system that have been developed for IORT: soft-docking and hard-docking systems. In the case of a soft-docking system the cone is not physically attached to the accelerator head of the linac, whereas for a hard-docking system the cone is physically attached to the accelerator head (Hogstrom *et al* 2006, ICRU 2004, Palta *et al* 1995). Different IORT systems are available commercially or are designed by the institution utilising IORT. Previous studies by Björk *et al* (2000a, 2000b, 2004) and Nyerick *et al* (1991) in IORT utilised soft-docking IORT systems. Studies by Biggs *et al* (1981) and Fraass *et al* (1985) used custom designed hard-docking systems.

### 2.1.1 Field size

It is well known that the characteristics of the depth-dose distribution as well as the output of electron beams are dramatically affected by decreasing the field [AAPM 1991, Bova 1995, ICRU 2004, Khan 2003, Strydom *et al* 2005, Sharma *et al* 1984, Sharma *et al* 2005, Venselaar *et al* 1998]. When the field size is large such that its dimensions are larger than the practical range ( $R_p$ ) of electrons in the medium, there is equilibrium between electrons scattered into and out of the area. As such the dependence of depth-dose on the field size is almost negligible. However if the field size decreases such that the dimensions are less than the  $R_p$  there is a lack of electronic equilibrium because the number of electrons scattered into area does not compensate for those scattered out of area. Clinically there is little change in depth dose for field sizes greater than 10 cm x 10 cm [Bova 1995, Strydom *et al* 2005]. For IORT fields the added collimation also results in increased scatter at the edges of the field and this also results in a lack of electronic equilibrium.

According to Fraass *et al* (1985), Sharma *et al* (1984) and the ICRU (2004) several features of the percent depth dose (PDD) common to all beam energies can be observed with added collimation or treatment fields such as is common in small-fields and IORT fields:

1. the depth of maximum dose ( $d_{max}$ ) moves toward the surface
2. the depth of the therapeutic ( $R_t$ ) range becomes smaller
3. the fall off region of the curve becomes less steep
4. the relative surface dose increases

Biggs (1985) concluded that there were significant changes in  $d_{max}$  and the steepness of the descending part of the depth dose for bevelled applicators as the angle of bevel increased and the energy decreased.

## 2.2 Dosimetry System

Although extensive data on IORT can be found in literature, these are dependent on the radiation modality and the applicator system (soft- or hard-docking) chosen for IORT (Podgorsak and Podgorsak 1999). Relative electron beam dosimetry in electron beam therapy can be carried out using:

1. air ionisation chambers
2. solid state detectors
3. film
4. thermoluminescent detectors (TLDs)

Because of the steep dose gradients associated with electron beams, it is preferable to use detectors with a high spatial resolution. In addition, because of the increased scatter in IORT beams detectors with low energy and angular dependence are preferable (Björk *et al* 2004).

### 2.2.1 Air ionisation chambers

Ionisation methods are the most developed and widely used methods in dosimetry measurements (Klevenhagen 1985). There are two types of air ionisation chambers that are routinely used in electron dosimetry: cylindrical chambers and parallel-plate chambers.

*Cylindrical chambers:* The standard cylindrical chamber (volume 0.6 cm<sup>3</sup>) has wide application in photon dosimetry and is thus readily available in a clinical environment. The positional accuracy of the standard cylindrical chamber is compromised due to the shape change in electron fluence (van der Merwe 1994).

*Parallel-Plate chambers:* The parallel-plate chamber was specifically designed for electron use. To some extent the parallel-plate chamber overcomes the problem of

positional accuracy encountered when using standard cylindrical chambers (Klevenhagen 1985). Any dosimeter that is placed in an electron beam should cause minimal disturbance of the electron fluence. Parallel-plate chambers meet this criterion better than other types of ionisation chambers. Parallel-plate chambers are designed with a small air chamber volume, particularly in the beam's direction and the chamber body is made of tissue equivalent material, thus minimising the electron fluence perturbation effect (Klevenhagen 1985). The AAPM (AAPM 1991) recommends the use of Parallel-plate chambers, which have a collection volume with height and diameter not exceeding 2 mm and 2 cm respectively for lower energies.

In previous IORT studies different dosimetry systems were used, cylindrical ionisation chambers with volumes ranging between 0.1 and 0.3 cm<sup>3</sup>, (Biggs 1985, Dahl and McCullough 1989, Fraass *et al* 1985, Hogstrom *et al* 1990, Nyerick *et al* 1991, Palta and Suntharalingham 1989), and parallel-plate chambers, (Biggs 1985, Björk *et al* 2000a, 2002, 2004, Fraass *et al* 1985), were used.

The PinPoint chamber (ion chamber) is specifically designed for relative beam profile measurements where superior spatial resolution is needed in IMRT and Stereotactic radiotherapy beams. When calibrated against a Farmer chamber, the PinPoint chamber can be used for depth dose and absolute dose measurements. To date there is no published information on the use of the PinPoint in electron dosimetry. It has a small measuring volume and a high spatial resolution. The Advanced Markus has the same physical dimensions as the Markus however it has a smaller measuring volume, potentially giving it a better spatial resolution. The improved guard ring is said to reduce the effect of scattered radiation from the housing which makes it possible to perform absolute dosimetry without perturbation effects ([www.elimpex.com](http://www.elimpex.com)).

### **2.2.2 Solid-State Detectors**

Silicon diodes: Silicon diodes are widely used in relative dosimetry measurements in high-energy electron beam therapy. Silicon diodes have well defined volumes and hence a high spatial resolution (Björk *et al* 2000a, AAPM 1991). Silicon diodes can be used for relative dosimetry measurements without the need for depth dose corrections provided their accuracy has been verified by comparing them with ionisation chamber measurements of depth-dose. Due to radiation damage, the dose rate dependence of diodes can change with time and thus must be verified periodically (AAPM 1991)

Björk *et al* (2000a, 2000b, 2002, 2004), Fraass *et al* (1985), Nyerick *et al* (1991), Olsen (1995) used diode detectors in their IORT dosimetry.

In other dosimetric studies of IORT beams diamond detector (Björk *et al* 2000a, 2000b, 2002, 2004) and film were used (Fraass *et al* 1985, Nyerick *et al* 1991, Wilenzick *et al* (unpublished)).

Dosimetric studies were conducted using the Markus, Advanced Markus, PinPoint and a diode detector. These detectors were chosen for use because these are already available for dosimetric purpose at the Johannesburg hospital. The study thus aimed to ascertain the significance of their use in small-field dosimetry without having to purchase new detectors. Other studies have used film however film was not used in this study because of the disadvantages of using film. Film cannot be used for absolute dosimetry. It needs to be calibrated against an ionisation chamber. There may be lack of consistency especially if there is variation in a batch of film. The processing of film is difficult to control. It is also not cost effective as a large number of films would be needed for the dosimetric measurements that were required for this study.

### **2.3 Dosimetric Measurements**

Dosimetry quantities that permit the calculation of the Monitor Unit (MU) setting for the delivery of a prescribed target dose at a selected depth on the central axis of the electron

beam are output factors, inverse square factors, gap factors and PDD (Palta *et al* 1995). Relative beam data are normally obtained on the geometric central-axis of the applicator, but Nyerick *et al* (1991) and Palta *et al* (1995) found that for bevelled applicators it was more relevant to determine relative beam data on the clinical central-axis. Thus the target volume is assumed to be perpendicular to the surface of the bevelled applicator and dose distribution, characterised by isodose curves parallel to the target volume are therefore more desirable (Olsen 1995). The ‘clinical central-axis’ is defined as the line projecting perpendicularly from the surface and intersecting the geometric central-axis (central-axis) of the applicator at the surface (Nyerick *et al* 1991, Palta *et al* 1995). Figure 2-1 illustrates the definition of the ‘geometric central-axis’ and the ‘clinical central-axis’. For straight applicators the angle  $\theta$  is equal to zero thus the geometric central-axis and the clinical central-axis are identical. For bevelled applicators ( $\theta$  is equal to the bevel angle) all depth dose data measurements should be measured along the clinical central-axis and normalised, to represent  $d_{\max}$  (Palta *et al* 1995). Thus for this study all 1D and 2D beam data were measured on the clinical central-axis of the IORT applicators. The minimum data necessary for clinical use of IORT include: isodose distributions, percent depth-doses, output factors, air gap correction factors, corrections factors for field blocking and leakage through applicator walls.

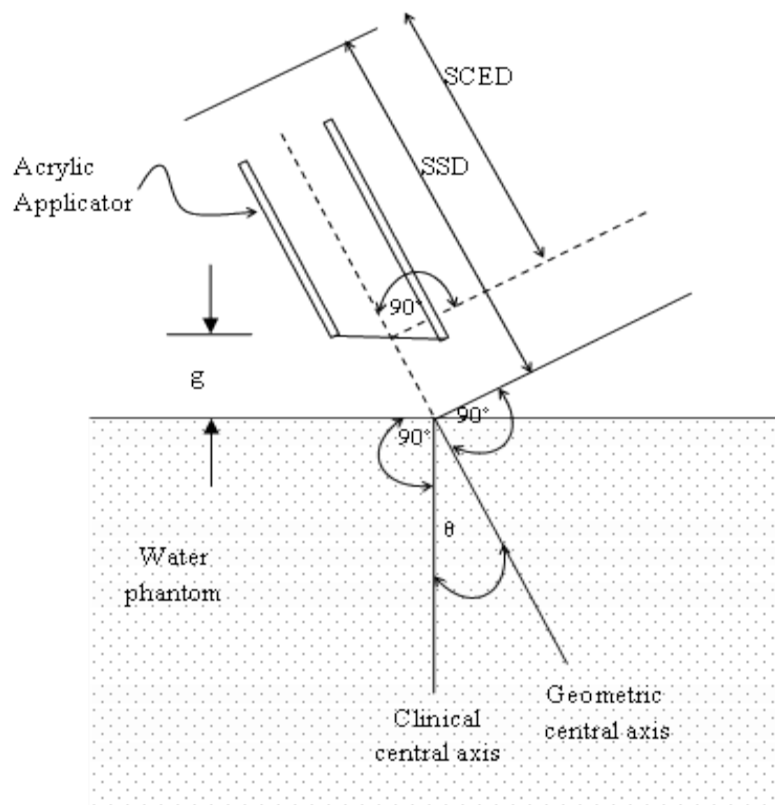


**Figure 2-1: Diagram illustrating the definition of the clinical central axes and geometric central axes for dosimetry measurements, where  $g$  is the air gap distance, SCED is the Source-to-cone-end distance and SSD is the Source-to-surface distance (figure adapted from Palta *et al* 1995; Nyerick *et al* 1991)**

### 2.3.1 Output measurements

A linac is calibrated to deliver 1 cGy/MU at  $d_{\max}$  for a standard electron applicator at a source-surface-distance (SSD) of 100 cm on the central axis. International protocols (AAPM 1983, 1991, 1999, IAEA 1987, 1997, 2000) are used to calculate output for electron beams, however the conversion and perturbation factors listed in these protocols are applicable to broad beam geometries (field sizes 10 cm x 10 cm or greater). The extra collimation of IORT beams results in a broader energy spectrum and a wider angular distribution and therefore IORT fields do not fulfil the requirements for broad beam geometry and relative methods have to be used to determine the output (Björk *et al* 2000b). When ionisation chambers are used to determine the output at  $d_{\max}$ , errors are

introduced because of the variations in the correction factors (stopping-power ratios and perturbation factors) between the two measurement geometries (reference and IORT fields).

Figure 2-2 shows the mass collision stopping-power ratios for water to carbon and water to silicon as a function of energy. For energies greater than 5 MeV the mass collision stopping-power ratios for silicon to water are almost independent of energy (Björk *et al* 2000b). Therefore measurements involving a diode can be considered directly proportional to the absorbed dose to water ( $D_w$ ). The output of IORT field can therefore be determined directly by (Björk *et al* 2000b):

$$D_{w,d_{max}}^{IORT} = \frac{M_{u,diode}^{IORT}}{M_{u,diode}^{Reference}} D_{w,d_{max}}^{reference}$$

2-1

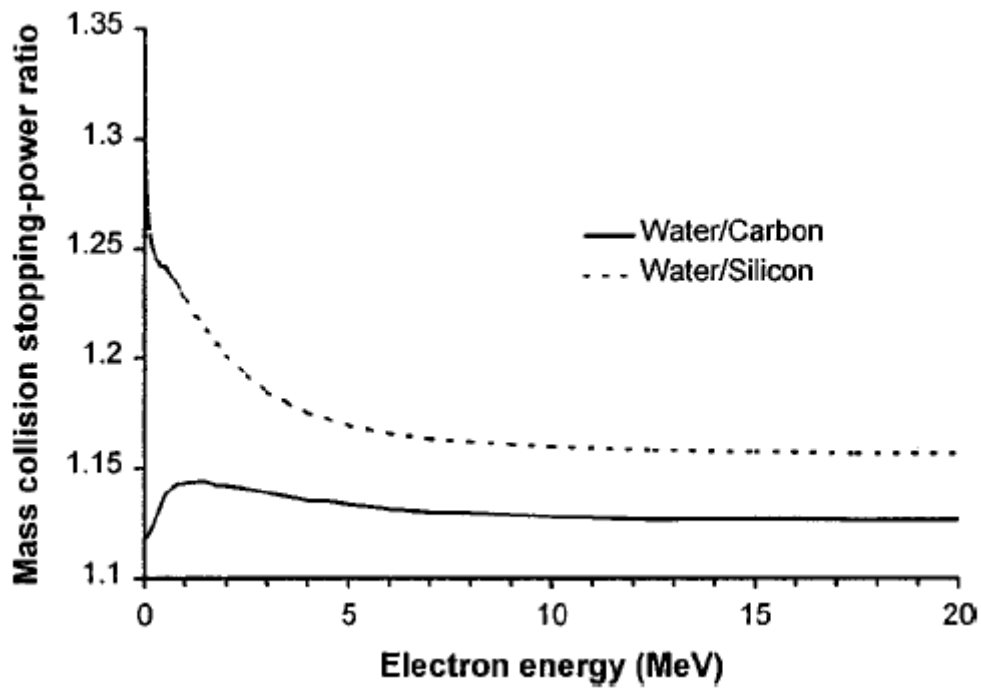


Figure 2-2: Mass collision stopping-power ratios for water/carbon and water/silicon as a function of electron energy (from Björk *et al* 2000a)

### 2.3.2 Percent Depth Dose

According to Palta *et al* (1995) depth dose measurements can be measured in a water phantom using either an ionisation chamber or a diode detector. However, the detector characteristics for electron measurements should be taken into consideration. Because the applicators used for IORT are in contact with the treatment volume, measurements of the surface dose are critical to the IORT procedure and should be measured with great care (Palta *et al* 1995).

The therapeutic depth is defined as the distance from the surface to the depth on the clinical central axis where the prescribed dose is to be delivered e.g. the depth of the 85% isodose. The therapeutic depth dose will remain constant for a given applicator size however the clinical depth dose will decrease as the bevel angle increases (Palta *et al.*, 1995).

Studies by Biggs *et al* (1981), and Fraass *et al* (1981) and Wilenzick *et al* (unpublished work) found that the setting of the x-ray jaws affected the PDD. Biggs *et al* (1981) found that the depth of the 90% isodose curve shifted between 2 and 3 mm. Fraass *et al* (1985) also found that beam flatness was affected by the setting of the x-ray jaws.

### **2.3.3 Lateral therapeutic coverage (Isodoses)**

Isodose contours representing all available energies for each applicator should be measured, depending on the shape of the applicator. Multiple planes may have to be measured (Palta *et al* 1995).

Scattering of the electrons in a medium causes dose contours to widen with depth, which is important to note when trying to limit the dose to tissue outside the treatment field. The width of isodose contours is important (Palta *et al* 1995). Having actual isodose distributions available for review at the time of IORT is clearly recommended.

For straight end applicators where the geometrical and clinical central-axis are the same, the treatment volume would be a flattened cylindrical volume typical of an electron isodose surface with constriction of the higher and expansion of the lower isodose curves (Palta *et al* 1995). For bevelled applicators, where the geometric and clinical central-axis are not equal, the ideal treatment volume will be tilted. The isodose contours for a bevelled applicator must be measured along the elongated axis (major elliptical axis) and short axis (minor elliptical axis) of the applicator.

### **2.3.4 Output Factors (OF)**

The OF is defined as the ratio of the dose reading at the depth of maximum dose ( $d_{\max}$ ) for the IORT applicator to the absorbed dose for the reference electron applicator (10 cm x 10 cm) at  $d_{\max}$  for the same number of monitor units. Readings are taken along the central-axis at the nominal calibration SSD of 100 cm.

For small field applicators  $d_{\max}$  depth moves towards the surface and it is important to locate the actual  $d_{\max}$  point for each applicator. This is especially critical when measuring

output factors factor for bevelled applicators at lower energies.

Björk *et al* (2004) measured output factors using three detectors: a diamond detector, a diode detector and an ionisation chamber. For the diamond and diode detector the output factor was calculated directly as the ratio of detector readings for the field being measured to the reference field because the stopping power ratios of water/carbon and water/silicon were considered to be independent of energy. Dosimetry protocols were used to determine the output factors as measured with the ionisation chambers at  $d_{\max}$  (AAPM 1991 and IAEA 2000):

$$OF = \frac{M_{\text{field}}(s_{w,\text{air}})_{\text{field}}}{M_{\text{ref}}(s_{w,\text{air}})_{\text{ref}}} \quad 2-2$$

### 2.3.5 Gap factors (GF)

According to Palta *et al* (1995), some irradiation geometries do not allow for the applicator to be in flush contact with the treatment site and thus the air gap (measured) and inverse square correction (calculated) factors must be used to calculate the dose. Figure 2-1 shows the arrangement of an IORT bevelled applicator with an air gap ( $g$ ). The source-to-cone-end distance (SCED) is related to the source-to-surface distance (SSD) by:

$$SSD = SCED + g \quad 2-3$$

From Figure 2-1 the following relationship for the inverse square factor (ISF) holds for gaps less than 2 cm:

$$ISF = [(SCED + d_{\max}) / (SSD + d_{\max})]^2 \quad 2-4$$

The output of an IORT applicator can also be affected by side-scatter equilibrium and this

is accounted for by the gap factor (GF). The gap factor is a measure of the deviation of the output from that predicated by the inverse square alone and is defined as:

$$GF = \frac{\left[ \frac{O(g)}{O(g=0)} \right]}{ISF} \quad 2-5$$

Where  $(O(g)/O(g=0))$  is the ratio of absorbed dose with gap (g) relative to the absorbed dose without the air gap measured at  $d_{max}$ .

## 2.4 Summary of Methodology to be used

Dosimetric data were obtained from measurements using the ionisation chambers and a diode detector. Measurements were taken using a computerised scanning system used to control the positioning of the detector and take dose measurements for relative dosimetric measurements. Dose measurements were made using the unidos electrometer (type T10008). Measurements were taken along the clinical central-axis of the cone (figure 2-1). All dosimetric measurements were carried out in MP3 water phantom. For bevelled applicators the gantry was rotated to the angle of bevel. For bevelled applicators isodose curves were also generated on the major and minor elliptical axis of the cone. Thus the surface of the cone was parallel to the water surface and the clinical central-axis perpendicular to the water surface. Dosimetric measurements included output, OF and PDD, isodose curves and ISF and GF.

## CHAPTER 3      EXPERIMENTAL PROCEDURES AND RESULTS

### 3.1      Equipment

The linear accelerator (Siemens PRIMUS) at the Johannesburg hospital designated for IORT has six nominal electron energies: 5, 6, 7, 9, 12 and 14 MeV. Table 3-1 specifies the energies (for the reference field 10 cm x 10 cm) that were used in this study:

**Table 3-1: Characteristics of the electron energies from the Siemens PRIMUS linear accelerator used for this study**

Nominal energy [MeV]	R <sub>50</sub> (cm)	d <sub>max</sub> [cm]
5	1.956	1.1
6	2.325	1.3
7	2.629	1.5
9	3.377	2.0

The d<sub>max</sub> was obtained from the PDD for the 10 cm x 10 cm reference field. Current dosimetry protocols (AAPM 1999, IAEA 2000) specify electron beam quality in terms of R<sub>50</sub>, defined as the depth in water at which the percent depth dose is 50% of its value at the absorbed dose maximum (half-value depth in water). All relative beam measurements were performed in a MP3 (PTW-Freiburg) automated beam acquisition system with a MP3 control unit (type 43164) with an internal electrometer. Absolute dose and output factor measurements were also performed in the MP3 water tank. All absolute dose measurements were made with the dosimeters connected to an electrometer manufactured by PTW – Freiburg Germany (Unidos - type T10008).

### 3.1.1 Applicator system

Two cone systems were studied: a small-field cone system manufactured by Siemens and a periscopic electron cone system manufactured by Radiation Products Inc., for intraoperative and intracavitary radiation.

***Small-field cone system:*** The small-field cone system consisted of:

- a. the main adaptor which attaches to the head of the linac
- b. a set of docking adaptors
- c. cones made of either acrylic or stainless steel

Figure 3-1 shows the components of the applicator system for the small-field cone system. The system has 9 cylindrical cones with flat ends. The cones have inner diameters ranging from 2 to 8 cm increasing in steps of 1 cm. Also included are two cylindrical cones with inner diameters of 2 and 3 cm with bevelled ends. The angle of bevel is 45°. The cones of diameters 2 to 5 cm are made of acrylic, with a stainless steel docking adaptor, which is used to attach the cone to the main adaptor. The cones of inner diameter 6 to 8 cm are made of stainless steel and fit directly into the main adaptor (has no docking adaptor). The main adaptor is coded such that the x-ray jaw setting is 17 cm x 17 cm when using the small-field applicator system.

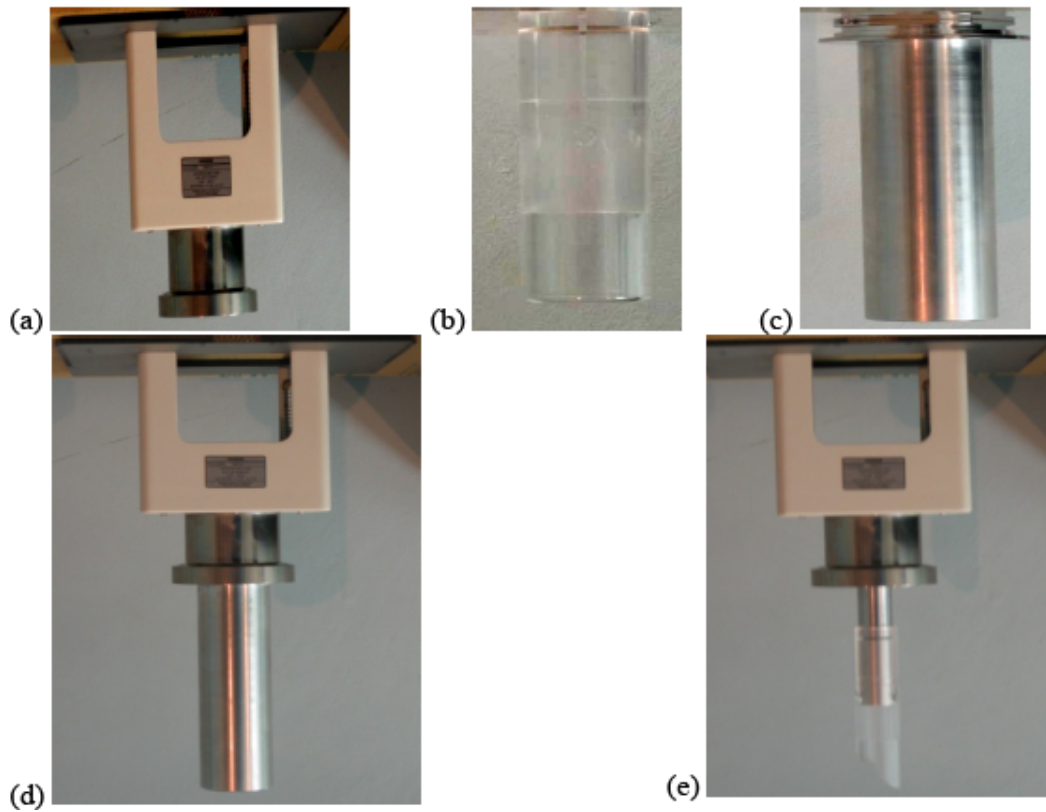


**Figure 3-3: Small-field cone system (a) the main adaptor (b) acrylic cone (c) stainless steel cone (d) the assembled applicator system with the stainless steel cone mounted directly on to the main adaptor and (e) the assembled applicator system with the acrylic cone mounted on to a docking adaptor and on the main adaptor**

***Periscopic electron cone system:*** The Periscopic electron cone system consisted of:

- a. the main adaptor which attaches to the head of the linac
- b. cylindrical cones made of acrylic

Figure 3-2 shows the components of the periscopic electron cone system. The main adaptor has a custom made Siemens adaptor plate (The adaptor plate is custom made for linac model). At the top of the barrel is a thin sheet of Mylar to prevent foreign matter from entering the treatment site. It has a periscopic viewing tube, with a highly polished stainless steel mirror. A lever at the side of the barrel controls the mirror position to allow viewing of the treatment area via the periscopic viewing tube. Above and below the viewing tube are two penlight holders which can be used for additional lighting. At the bottom of the barrel is a hinged door which allows for the lateral docking of cone. The periscopic electron cone system is provided with three sets of cylindrical electron cones of inner diameter 3.2, 3.8 and 4.5 cm, each with a flat and bevelled end. The bevel angle is 30°. At the top of the electron cones are three spacer rings which slide into the barrel of the periscopic viewer. When the third spacer is flush with the bottom of the barrel, then the cone will be at an SSD of 100 cm. A brass plate on top of the spacer rings collimates the beam and prevents electrons from entering the spacer rings. The main adaptor for the periscopic system does not have a preset code for the x-ray jaw setting. The x-ray jaw was therefore arbitrarily set to 19 cm x 19 cm when using the periscopic system for all measurements.

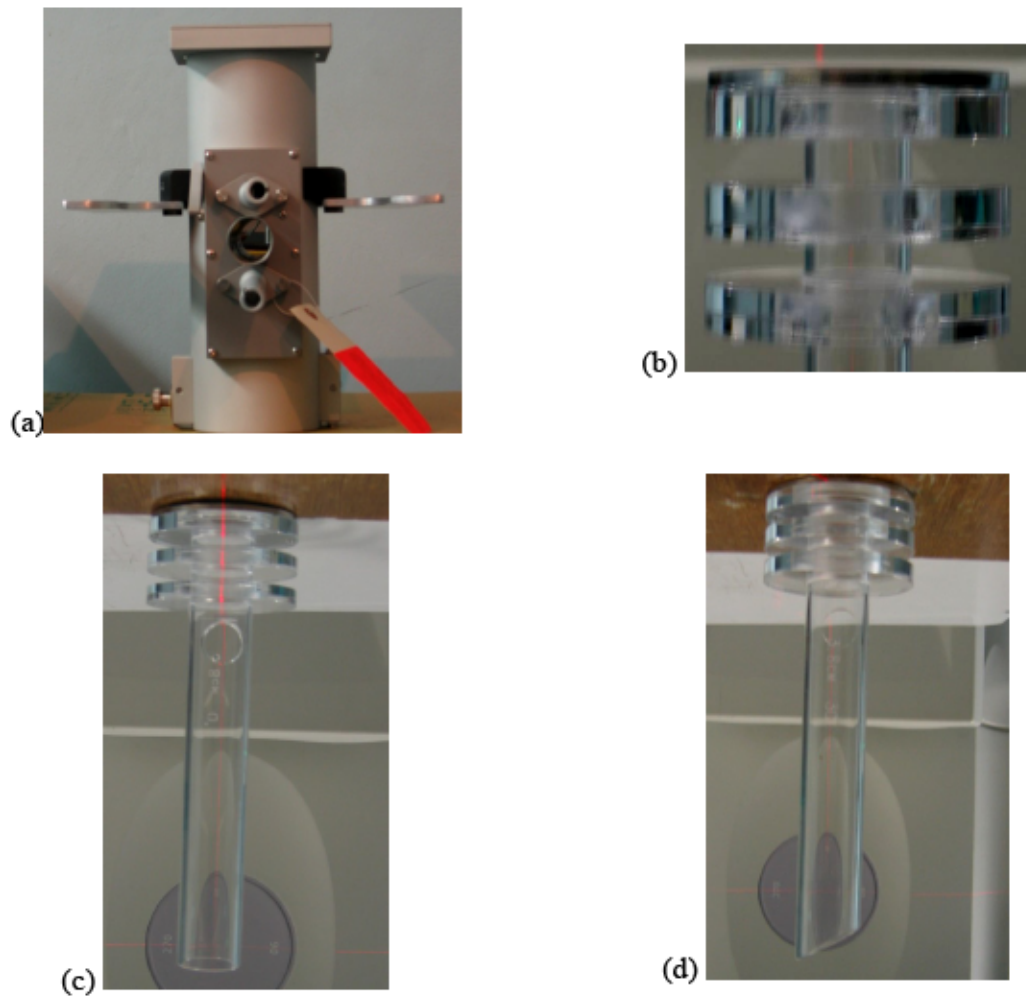


**Figure 3-4: (a) The main adaptor for the periscopic electron cone system (b) the top part of the cone showing the three spacer rings and the brass plate on top of the cone (c) a straight cone and (d) a bevelled cone (bevel angle 30°)**

### 3.1.2 Dosimetry System

Table 3-2 show the detector specifications for the four types of detectors used. The Advanced Markus chamber and the PinPoint chamber had an absorbed dose to water calibration factor obtained in a  $^{60}\text{Co}$  beam  $N_{D,w}$ . The  $N_{D,w}$  calibration factor for both chambers was traceable to international laboratories.

**Table 3-2: Ionisation chambers and detector specifications**

Chamber	Model	Manufacturer	Chamber wall material	Measuring Volume	$N_{D,w}$ [Gy/C]
Markus	23343	PTW-Freiburg	Polyethylene	0.055 cm <sup>3</sup>	
Advanced Markus	34045	PTW-Freiburg	Polyethylene	0.02 cm <sup>3</sup>	1.360 x 10 <sup>9</sup>
PinPoint	31006	PTW-Freiburg	PMMA, Graphite	0.015 cm <sup>3</sup>	2.500 x 10 <sup>9</sup>
Diode	60012	PTW-Freiburg	Silicon	1 mm <sup>2</sup> circular and 2 μm	

Because there is no documented use of the PinPoint chamber for electron beam dosimetry the effective point of measurement was determined experimentally by comparing PDD data obtained with the PinPoint chamber to the PDD data obtained with the Markus chamber. The chamber was oriented such that the stem of the chamber was parallel to the beam. This also allowed measurements to be taken at shallower depths.

## 3.2 Absolute Dosimetry

All dosimetric measurements were made on the clinical central-axis as defined in figure 2-1, and at an SSD of 100 cm.

### 3.2.1 Output measurements

Output measurements were carried out according to the IAEA TRS-398 protocol (IAEA

2000) for the range of electrons energies studied. Because of the increased scatter in the IORT beams, the beams did not meet the requirements for broad beam (beams produced by field sizes greater than 10 cm x 10 cm) and therefore relative methods were used to determine the output at  $d_{\max}$  for an IORT field. The output of the reference field 10 cm x 10 cm was confirmed first (1 cGy/MU at  $d_{\max}$ ). The output was calculated as:

$$D_{w,Q_0}(d_{\text{ref}}) = M_Q(d_{\text{ref}})N_{D,w}k_{Q_E} \quad 3-6$$

$M_Q(d_{\text{ref}})$  is the ionization chamber measurement corrected for temperature and pressure variation, polarity and ion recombination effects.

$N_{D,w}$  is the absorbed dose to water calibration factor for the ionization chamber used obtained in the reference beam  $^{60}\text{Co}$ .

$k_{Q_E}^1$  is a chamber specific quality conversion factor which corrects for the differences between beam quality  $Q_0$  and the actual beam quality  $Q_E$  (in this electron beam).

$k_{Q_E}$  for the Advanced Markus is not given in table 7.III of the IAEA TRS-398 (IAEA 2000). The  $k_{Q_E}$  values given are chamber specific, and vary according to the beam quality. However, because some of the dimensions of the Advanced Markus are identical to those of Markus chamber, the  $k_{Q_E}$  used was that prescribed for the Markus chamber.  $k_{Q_E}$  values for the PinPoint chamber were extrapolated from the existing data in table 7.III of the IAEA TRS-398 (IAEA 2000).

Then the absorbed dose at  $d_{\max}$  for the reference field 10 cm x 10 cm was calculated according to:

$$D_{w,Q}(d_{\max}) = D_{w,Q}(d_{\text{ref}}) \times \frac{100}{\text{PDD}(d_{\text{ref}})} \quad 3-7$$

<sup>1</sup>  $_{Q_0}$  and  $_{Q_E}$  are written as  $_{\text{E}}$  and  $_{\text{W}}$  if the ionisation chamber was calibrated in a  $^{60}\text{Co}$

**Table 3-3: Measured output for the reference applicator 10 cm x 10 cm**

	electron energy (MeV)	5	6	7	9
Advanced Markus	$D_{w,Q}(d_{max})$ [cGy/MU]	$0.999 \pm 0.001$	$0.997 \pm 0.001$	$1.032 \pm 0.000$	$1.019 \pm 0.002$
PinPoint	$D_{w,Q}(d_{max})$ [cGy/MU]	$1.014 \pm 0.002$	$1.009 \pm 0.002$	$1.051 \pm 0.002$	$1.031 \pm 0.002$

Table 3-3 shows the output for the 10 cm x 10 cm reference field. The uncertainty in output measurements was found to be 2.8% for the PinPoint and 3.1% the Advanced Markus. Thus the output at  $d_{max}$  for an IORT field was determined with the following equation where the OF was as calculated as shown in the next section (3.2.2).

$$D_{w,Q}^{IORT}(d_{max}) = OF \times D_{w,Q}(d_{max}) \quad 3-8$$

### 3.2.2 Output Factors (OF)

All OF were measured at  $d_{max}$  as determined from the PDD of each energy-cone combination. Measurements for the reference field (10 cm x 10 cm) were taken at  $d_{ref}$  according to the IAEA TRS-398 protocol (IAEA 2000) and a PDD correction was applied so that the output measurement was corrected to  $d_{max}$ . OF determined from ionisation chambers measurements were calculated using:

$$OF = \frac{M_{IORT}(s_{w,air})_{IORT} \frac{100}{d_{ref}}}{M_{IORT}(s_{w,air})_{IORTPDD}} \quad 3-9$$

For the diode detector  $S_{w,air}$  was assumed to be approximately constant over the range of energies studied, thus the OF was calculated directly as the ratio of  $M_{IORT}$  and  $M_{ref}$  readings taken at  $d_{max}$

$$OF = \frac{M_{IORT}}{M_{10cm \times 10cm}} \quad 3-10$$

Tables 3-12 and 3-13 shows the OF for the small-field cone system determined from measurement using all the detectors. The OF increased with an increase in cone size with a peak for the 6 cm cone and then a decrease for the 7 and 8 cm cones. This trend was observed for all energies and for all detectors. The OF for bevel end cones (2 and 3 cm) was higher due to the obliquity of the beam, given the increase in the amount of electrons scattered to  $d_{max}$ .

Table 3-13 shows the OF for the periscopic electron cone system determined from measurements using all detectors. There is an increase in OF with increase in the field diameter and increase in energy. This was observed for both the straight and bevelled cones.

**Table 3-4: Output Factors for the small-field cone system measured with different types of detectors**

Energy [MeV]	→	Markus				Advanced Markus			
		5	6	7	9	5	6	7	9
Applicator									
10 cm x 10 cm		<b>1.000 ± 0.000</b>							
2 cm circle		0.558 ± 0.001	0.613 ± 0.002	0.675 ± 0.001	0.816 ± 0.002	0.551 ± 0.000	0.619 ± 0.001	0.687 ± 0.001	0.799 ± 0.001
3 cm circle		0.830 ± 0.001	0.862 ± 0.001	0.896 ± 0.002	0.972 ± 0.000	0.817 ± 0.001	0.859 ± 0.001	0.909 ± 0.000	0.959 ± 0.002
4 cm circle		0.983 ± 0.003	1.015 ± 0.003	1.013 ± 0.001	1.048 ± 0.001	0.977 ± 0.001	1.001 ± 0.001	1.022 ± 0.001	1.036 ± 0.002
5 cm circle		1.082 ± 0.002	1.103 ± 0.002	1.099 ± 0.001	1.119 ± 0.002	1.076 ± 0.001	1.094 ± 0.001	1.111 ± 0.001	1.116 ± 0.002
6 cm circle		1.149 ± 0.001	1.157 ± 0.001	1.148 ± 0.001	1.185 ± 0.002	1.137 ± 0.002	1.154 ± 0.001	1.178 ± 0.001	1.173 ± 0.001
7 cm circle		1.071 ± 0.003	1.069 ± 0.002	1.068 ± 0.000	1.096 ± 0.002	1.083 ± 0.002	1.086 ± 0.002	1.085 ± 0.002	1.116 ± 0.002
8 cm circle		1.013 ± 0.001	1.022 ± 0.001	1.020 ± 0.002	1.047 ± 0.002	1.030 ± 0.000	1.034 ± 0.002	1.030 ± 0.002	1.067 ± 0.003
2 cm circle <sup>a</sup>		0.586 ± 0.001	0.652 ± 0.001	0.729 ± 0.001	0.841 ± 0.003	0.564 ± 0.001	0.633 ± 0.000	0.715 ± 0.001	0.855 ± 0.001
3 cm circle <sup>a</sup>		0.872 ± 0.002	0.922 ± 0.001	0.963 ± 0.001	1.007 ± 0.002	0.882 ± 0.003	0.911 ± 0.001	0.942 ± 0.002	1.007 ± 0.002
Energy [MeV]	→	PinPoint				Diode			
		5	6	7	9	5	6	7	9
Applicator									
10 cm x 10 cm		<b>1.000 ± 0.000</b>							
2 cm circle		0.558 ± 0.003	0.628 ± 0.001	0.687 ± 0.001	0.805 ± 0.001	0.569 ± 0.001	0.625 ± 0.001	0.690 ± 0.000	0.796 ± 0.001
3 cm circle		0.831 ± 0.001	0.873 ± 0.001	0.903 ± 0.003	0.959 ± 0.002	0.840 ± 0.001	0.881 ± 0.001	0.919 ± 0.001	0.963 ± 0.002
4 cm circle		0.985 ± 0.002	1.008 ± 0.002	1.020 ± 0.002	1.037 ± 0.003	0.985 ± 0.001	1.012 ± 0.000	1.030 ± 0.001	1.045 ± 0.002
5 cm circle		1.075 ± 0.003	1.102 ± 0.002	1.105 ± 0.003	1.111 ± 0.002	1.067 ± 0.001	1.089 ± 0.001	1.104 ± 0.001	1.117 ± 0.002
6 cm circle		1.143 ± 0.011	1.156 ± 0.003	1.157 ± 0.002	1.170 ± 0.003	1.134 ± 0.003	1.146 ± 0.002	1.159 ± 0.002	1.176 ± 0.001
7 cm circle		1.063 ± 0.003	1.076 ± 0.002	1.075 ± 0.003	1.087 ± 0.002	1.054 ± 0.001	1.068 ± 0.002	1.074 ± 0.001	1.088 ± 0.004
8 cm circle		1.020 ± 0.003	1.030 ± 0.002	1.030 ± 0.003	1.033 ± 0.003	1.008 ± 0.001	1.021 ± 0.001	1.032 ± 0.001	1.042 ± 0.001
2 cm circle <sup>a</sup>		0.570 ± 0.003	0.643 ± 0.001	0.718 ± 0.001	0.838 ± 0.002	0.585 ± 0.001	0.654 ± 0.001	0.724 ± 0.001	0.832 ± 0.002
3 cm circle <sup>a</sup>		0.832 ± 0.002	0.891 ± 0.003	0.930 ± 0.002	1.050 ± 0.003	0.851 ± 0.000	0.903 ± 0.000	0.946 ± 0.001	0.993 ± 0.003
<sup>a</sup> bevel angle 45°									

**Table 3-5: Output Factors for the periscopic electron cone system measured with different types of detectors**

Energy [MeV]	→	Markus				Advanced Markus			
		5	6	7	9	5	6	7	9
Applicator									
10 cm x 10 cm		<b>1.000 ± 0.000</b>							
3.2 cm circle		0.839 ± 0.002	0.891 ± 0.001	0.949 ± 0.001	1.026 ± 0.001	0.847 ± 0.001	0.898 ± 0.001	0.959 ± 0.001	1.036 ± 0.002
3.8 cm circle		0.966 ± 0.001	1.022 ± 0.001	1.060 ± 0.001	1.115 ± 0.004	0.974 ± 0.001	1.028 ± 0.001	1.074 ± 0.002	1.122 ± 0.001
4.5 cm circle		1.047 ± 0.002	1.093 ± 0.002	1.125 ± 0.001	1.164 ± 0.001	1.052 ± 0.001	1.105 ± 0.002	1.135 ± 0.002	1.166 ± 0.003
3.2 cm circle <sup>b</sup>		0.836 ± 0.001	0.894 ± 0.001	0.952 ± 0.001	1.045 ± 0.003	0.843 ± 0.001	0.897 ± 0.001	0.964 ± 0.002	1.054 ± 0.002
3.8 cm circle <sup>b</sup>		0.967 ± 0.001	1.019 ± 0.002	1.058 ± 0.002	1.124 ± 0.000	0.977 ± 0.001	1.016 ± 0.001	1.078 ± 0.002	1.132 ± 0.002
4.5 cm circle <sup>b</sup>		1.043 ± 0.002	1.095 ± 0.000	1.133 ± 0.000	1.183 ± 0.002	1.043 ± 0.001	1.091 ± 0.002	1.136 ± 0.002	1.175 ± 0.002
Energy [MeV]	→	PinPoint				Diode			
		5	6	7	9	5	6	7	9
Applicator									
10 cm x 10 cm		<b>1.000 ± 0.000</b>							
3.2 cm circle		0.823 ± 0.001	0.905 ± 0.002	0.949 ± 0.001	1.023 ± 0.004	0.841 ± 0.001	0.903 ± 0.000	0.960 ± 0.001	1.034 ± 0.002
3.8 cm circle		0.974 ± 0.002	1.025 ± 0.002	1.062 ± 0.002	1.115 ± 0.002	0.967 ± 0.002	1.021 ± 0.001	1.071 ± 0.000	1.119 ± 0.001
4.5 cm circle		1.038 ± 0.000	1.087 ± 0.002	1.118 ± 0.003	1.155 ± 0.002	1.035 ± 0.002	1.083 ± 0.001	1.121 ± 0.002	1.162 ± 0.002
3.2 cm circle <sup>b</sup>		0.821 ± 0.001	0.883 ± 0.003	0.940 ± 0.001	1.034 ± 0.002	0.824 ± 0.000	0.885 ± 0.002	0.945 ± 0.000	1.027 ± 0.001
3.8 cm circle <sup>b</sup>		0.950 ± 0.002	1.005 ± 0.003	1.046 ± 0.002	1.109 ± 0.002	0.942 ± 0.002	0.994 ± 0.001	1.044 ± 0.001	1.104 ± 0.001
4.5 cm circle <sup>b</sup>		1.013 ± 0.002	1.069 ± 0.003	1.103 ± 0.002	1.154 ± 0.004	1.001 ± 0.001	1.052 ± 0.000	1.106 ± 0.000	1.158 ± 0.001
<sup>b</sup> bevel angle 30°									

### 3.3 Relative dosimetry

Relative beam data obtained for the two applicator systems included the PDD, isodose charts and OF. All measurements were taken on the clinical central-axis and at a SSD of 100 cm. For bevelled cones, the gantry was rotated to the bevel angle such that the cone end was parallel to the water surface and the clinical central-axis was perpendicular to the water surface. Comparative dosimetry measurements using the Markus, Advanced Markus and PinPoint and diode detector, described in table 3-2, were taken to demonstrate the advantages and disadvantages of the dosimetric systems.

#### 3.3.1 Percent depth dose (PDD)

The measured depth ionisation curves were converted to depth dose using the Spencer-Attix stopping-power ratios for water to air ( $S_{w,air}$ ). The  $S_{w,air}$  values used in this study were obtained from table 7.V of the IAEA TRS-398 protocol (IAEA 2000) and are a function beam quality  $R_{50}$  and the relative depth ( $d/R_{50}$ ).  $S_{w,air}$  corrections applied to the Markus, Advanced Markus, PinPoint chambers were interpolated from the same data set (Table 7.V TRS-398 (IAEA 2000)). All depth dose values were normalised such that 100% represented the value of maximum dose. Figures 3-3 and 3-4 shows normalised PDD curves for 5, 6, 7 and 9 MeV electron beams for the 10 cm x 10 cm reference applicator, as measured with the Markus, Advanced Markus and PinPoint chambers and diode detector. The PDD curves for the Advanced Markus and PinPoint chambers and the diode detector were offset such that the  $d_{max}$  values corresponded to that measured by the Markus chamber. The PDD were offset by 2 mm for the Advanced Markus chamber and the diode detector and by -1 mm for the diode detector. Figures 3-3 and 3-4 shows PDD curves where the offset has been applied. This offset was also applied to all other measurements that were performed.

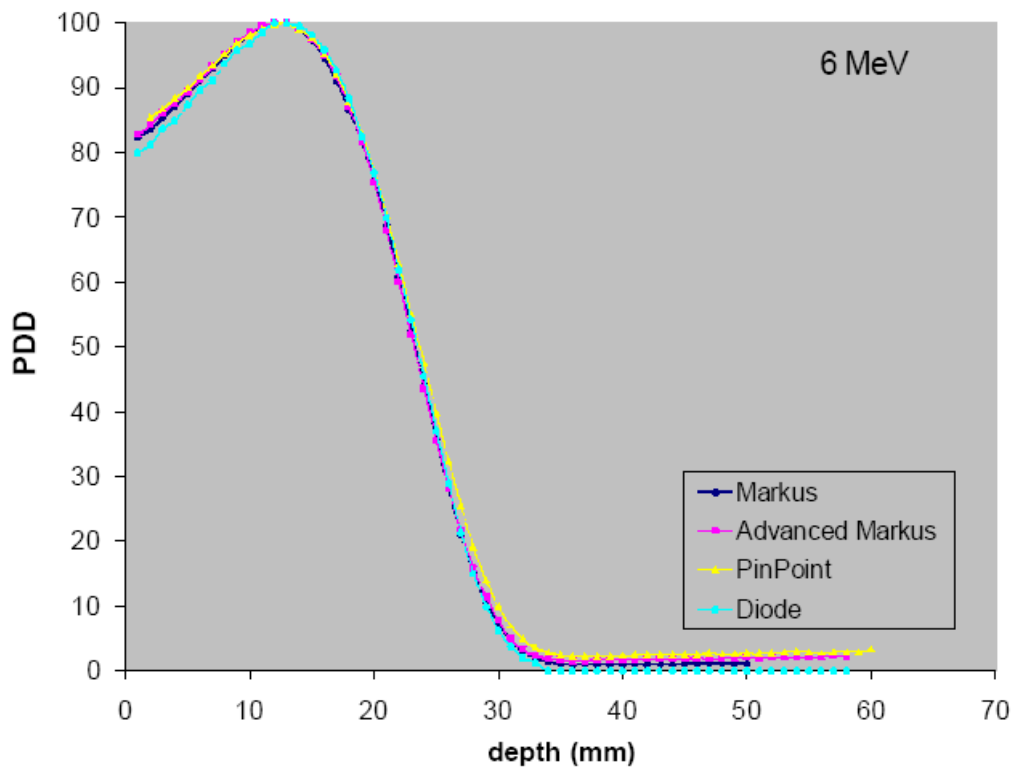
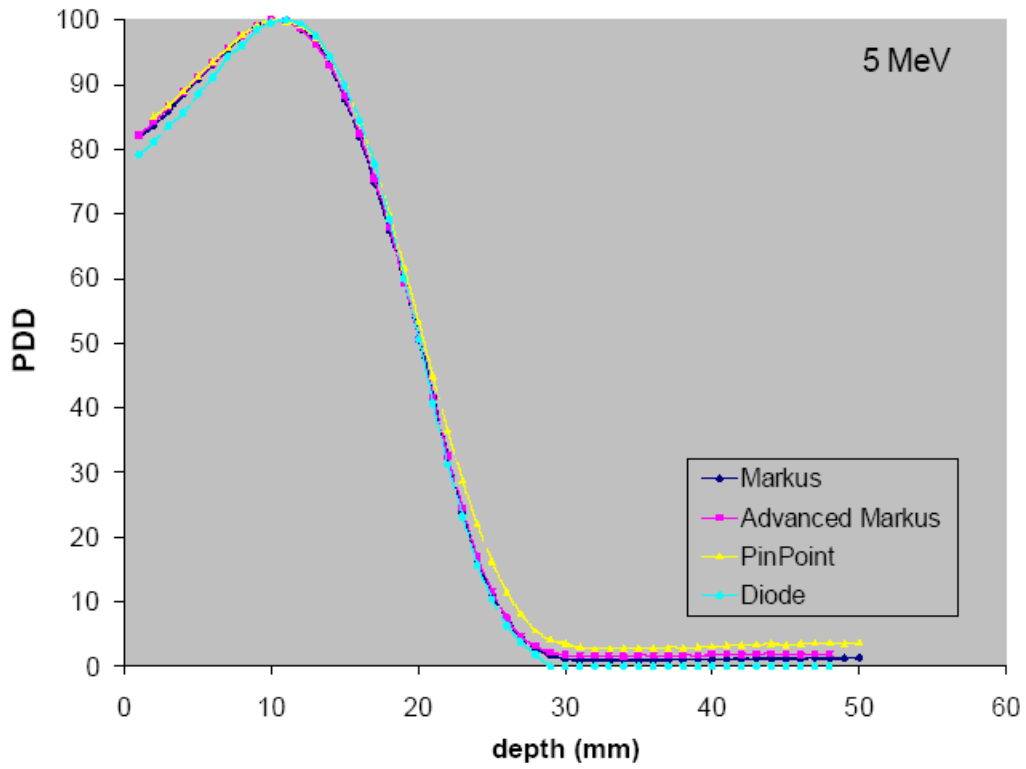


**Figure 3-5: Comparison of the PDD as measured with the Markus, Advanced Markus, PinPoint chambers and diode detector for 10 cm x 10 cm reference field for energies 5 and 6 MeV**

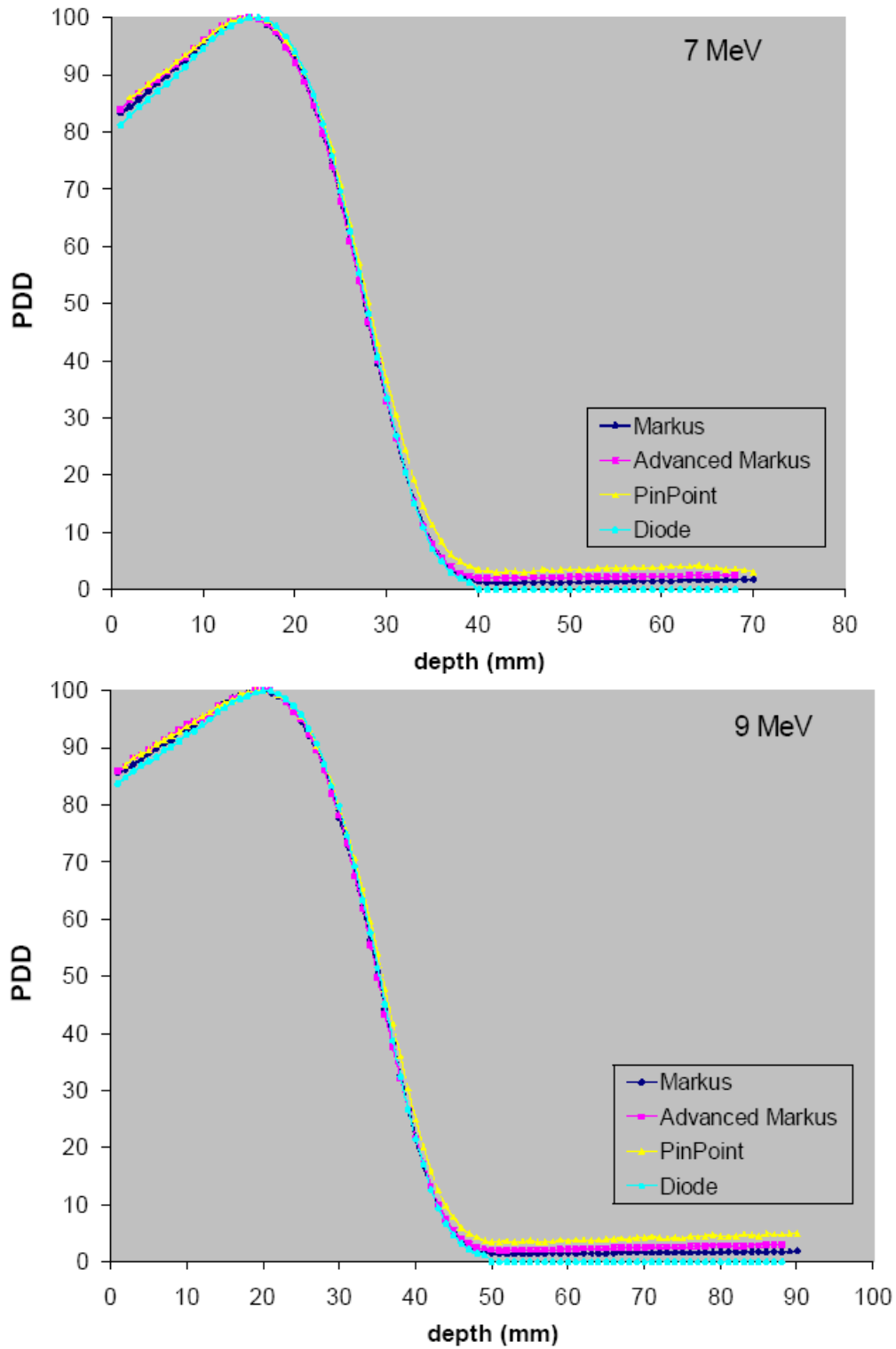


**Figure 3-6:** Comparison of the PDD as measured with the Markus, Advanced Markus, PinPoint chambers and diode detector for 10 cm x 10 cm reference field for energies 7 and 9 MeV

Figures 3-5, 3-6, 3-7 and 3-8 show the normalised PDD curves for the small-field cone system and the Periscopic electron cone system respectively for the different cones in each system. These figures show the field size and energy dependence of the PDD for the flat-end cones and the bevel-end cones. The following characteristics were observed for the bevelled cones:

1. decrease in depth dose with decrease in field diameter and increase in energy (the depth-dose measured along the clinical central-axis is less for bevelled cones than for straight cones of the same size)
2.  $d_{\max}$ , shifts closer to the surface
3. there is an increase in surface dose with decrease in field diameter
4. the descending part of the PDD becomes steeper with increase in energy

These characteristics are observed for both the small-field cone system and the periscopic electron cone system. The decrease in depth dose was more significant for the 2 cm cone than for the other straight end cones of different diameters (3 to 8 cm) of the small-field cone system. The 10 cm x 10 cm PDD was added to figures 3-5 to 3-8 to show the decrease in depth dose, for the cone system in comparison to the reference field. For the small field applicator system the decrease in depth dose and shift in  $d_{\max}$  was observed for all PDD curves when compared to the reference applicator PDD. The decrease in depth dose and shift in  $d_{\max}$  was more significant for the 2 and 3 cm applicators (straight and bevelled). No significant decrease in depth dose between the reference field and the straight end cones of the periscopic system was observed

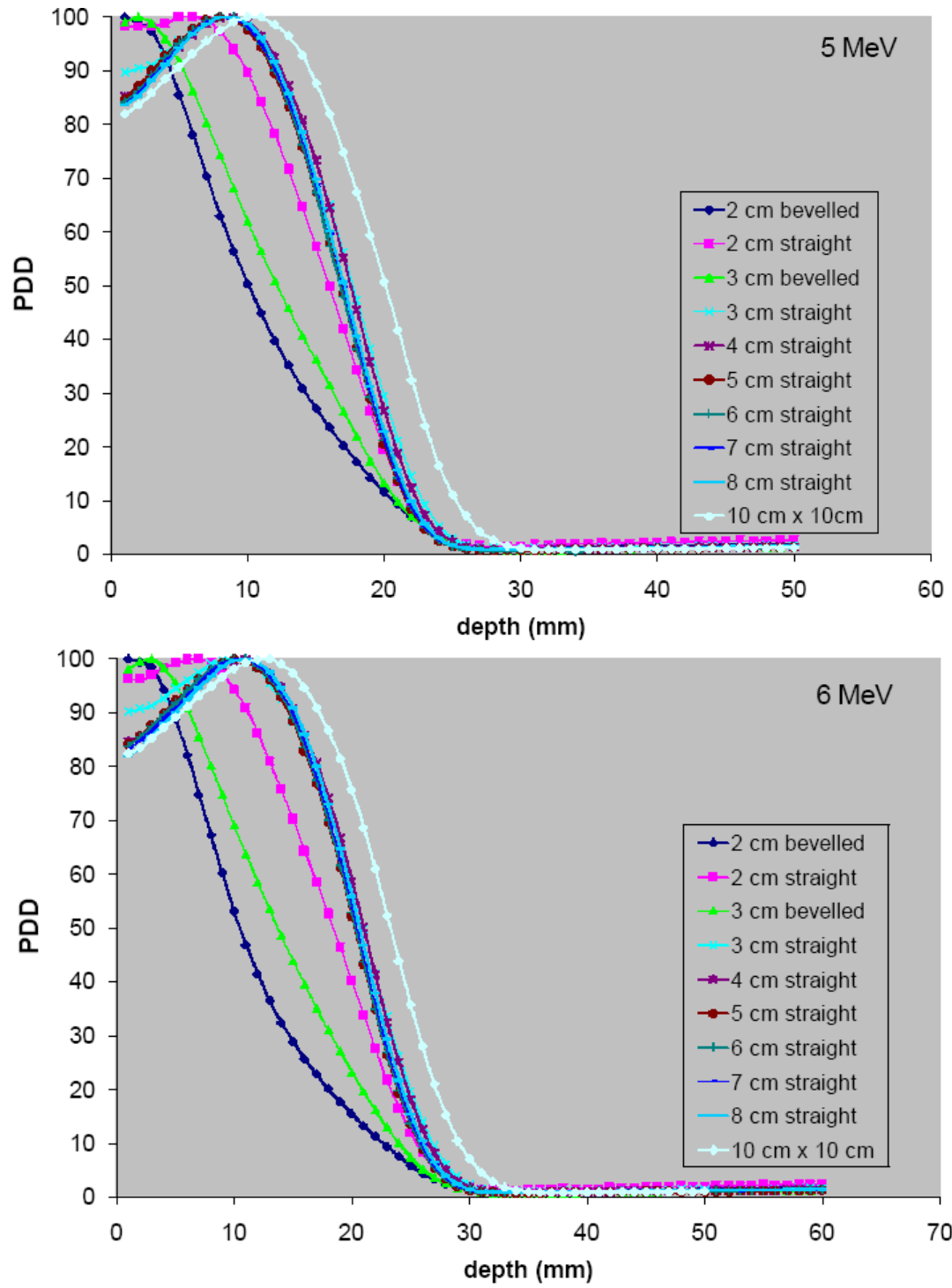


Figure 3-7: PDD measured along the clinical central-axis for different cones for the small field applicator system cones for energies 5 and 6 MeV (bevel angle 45°)

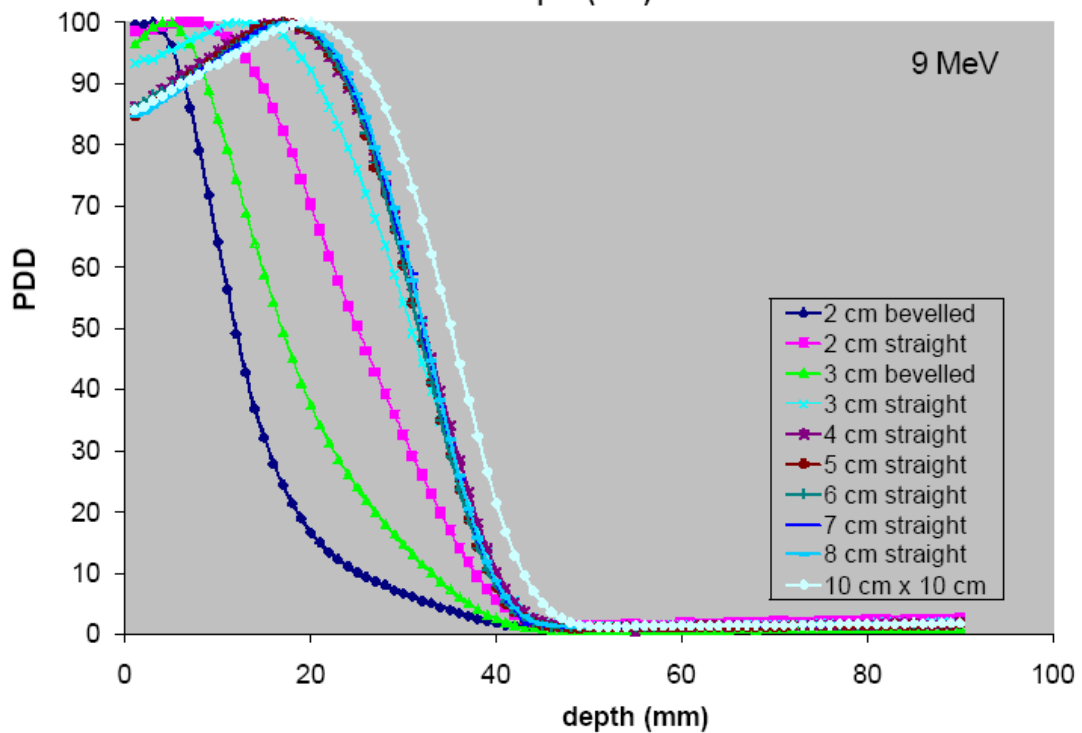
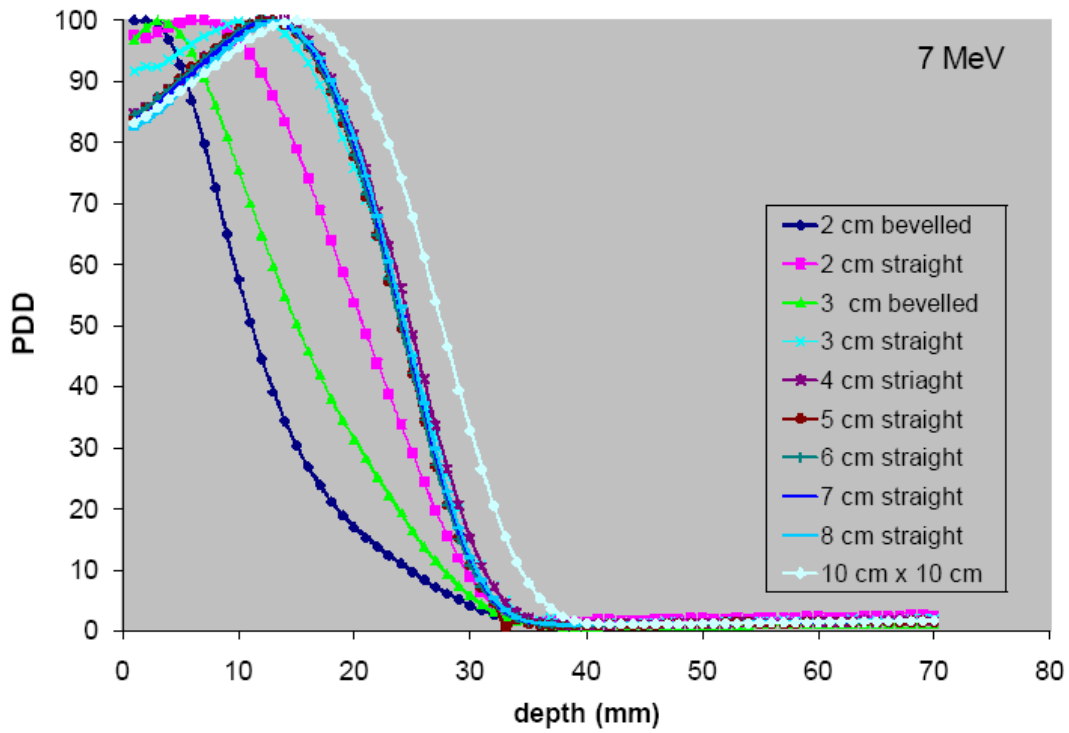
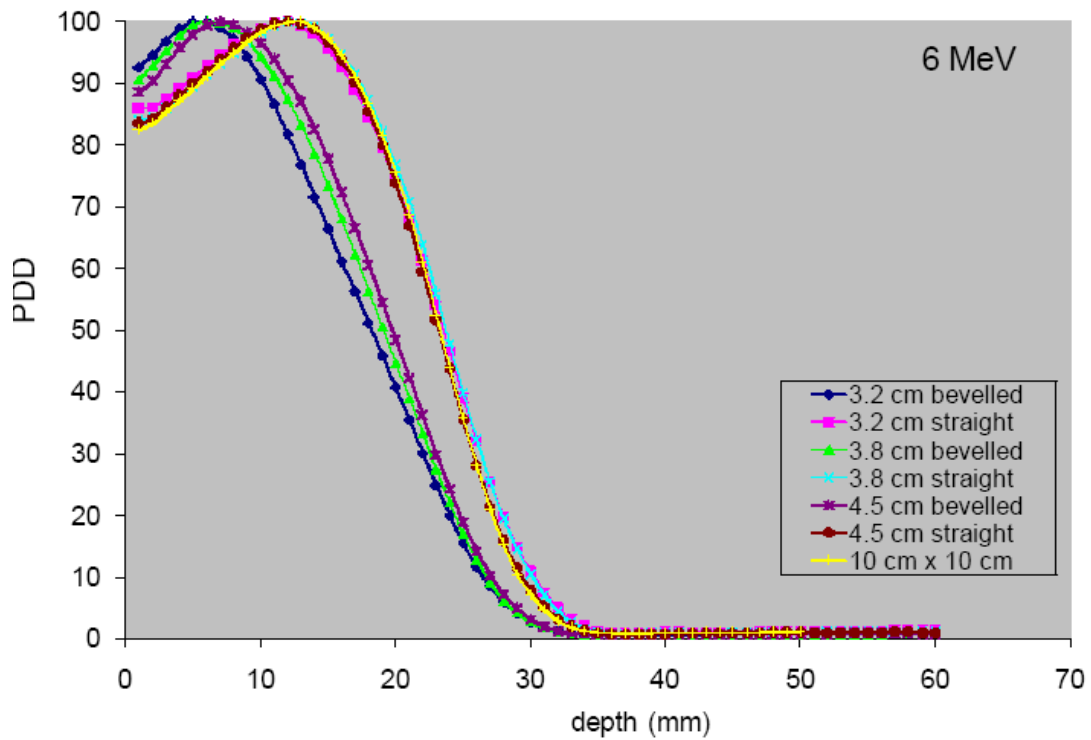
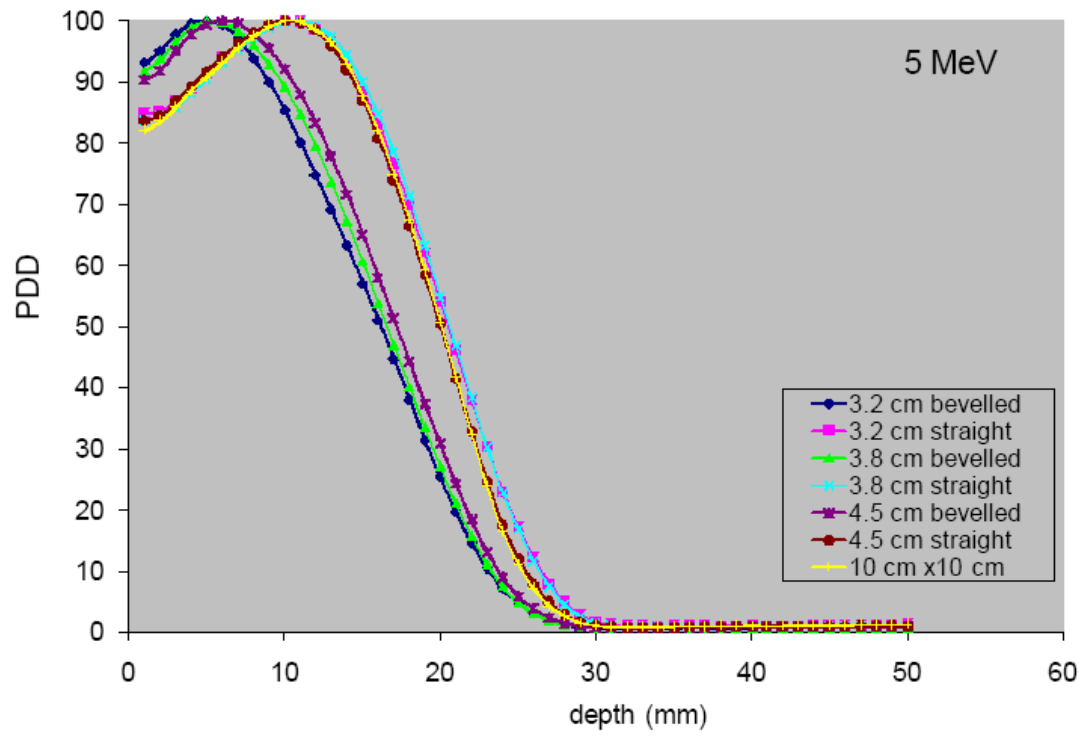
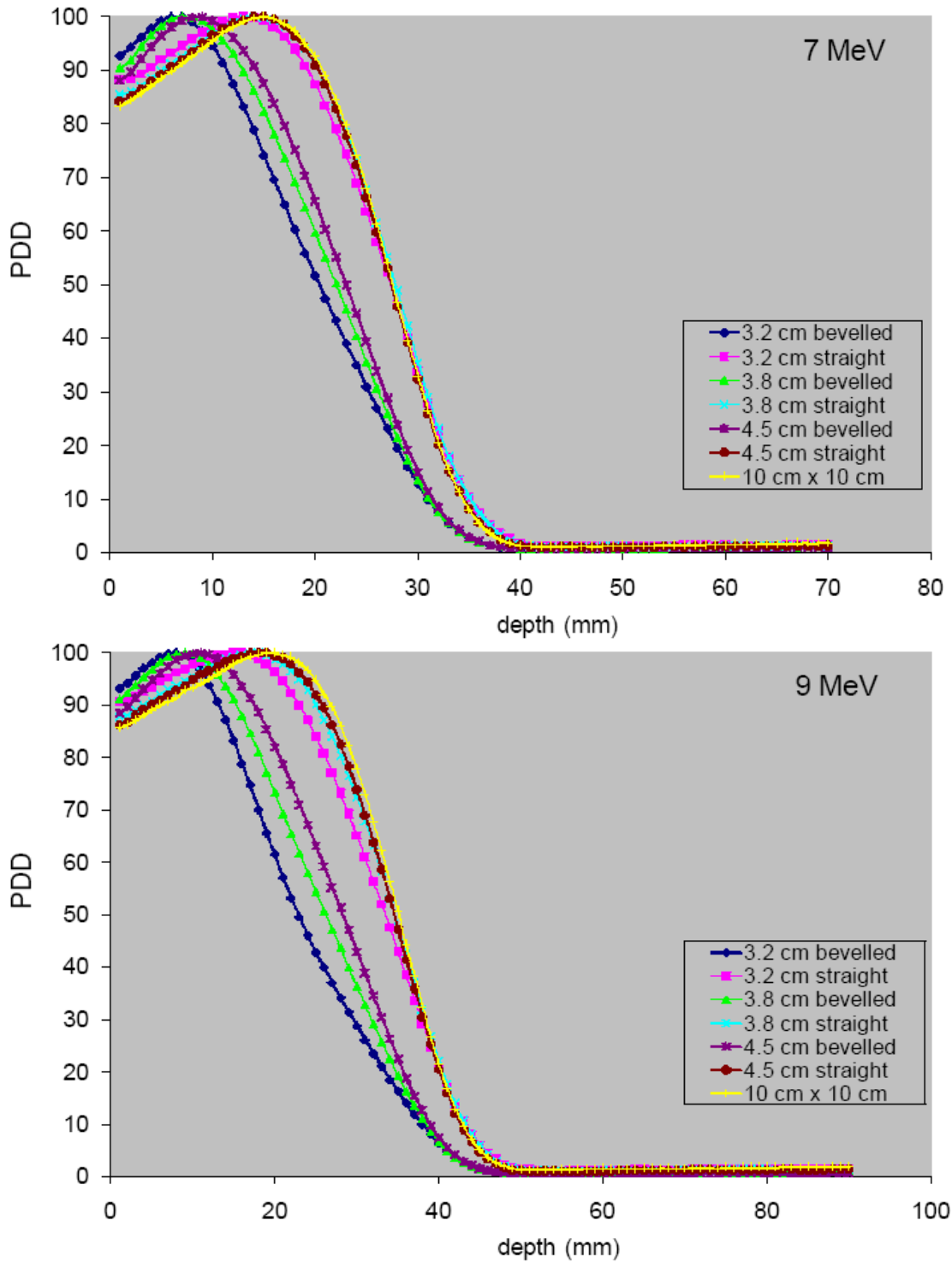


Figure 3-8: PDD measured along the clinical central-axis for different cones for the small field applicator system cones for energies 7 and 9 MeV (bevel angle 45°) (Markus chamber)



**Figure 3-9: PDD measured along the clinical central-axis for the different cones for the Periscopic electron cone system cones for energies 5 and 6 MeV (bevel angle 30°)**



**Figure 3-10: PDD measured along the clinical central-axis for the different cones for the Periscopic electron cone system cones for energies 7 and 9 MeV (bevel angle 30°) (7 MeV and 9 MeV) (Markus chamber)**

Figures 3-9 to 3-14 show the selected PDD curves as measured with all detectors, for the small-field cone system. Figures 3-15 and 3-18 show PDD curves as measured with the all detectors, for the Periscopic electron cone system, for cones with inner diameters 4.5 cm straight and bevel end cones.

Tables 3-4 to 3-7 are a summary of the electron depth dose characteristics for the small-field cone system. For the smaller cones (2 and 3 cm) with straight ends, a 2-13% increase in surface dose is observed. The  $d_{\max}$  for the 8-4 cm cones are within  $\pm 2$  mm, however for the 2 and 3 cm cones the  $d_{\max}$  shifts towards the surface. The therapeutic depth is between 80% and 90% isodose levels thus the depth of the 80% and 90% are indicated on the table.

Tables 3-8 to 3-11 are a summary of the electron depth dose characteristics for the Periscopic electron cone system. The surface dose for the straight end cone was found to be fairly constant. There was an increase in surface dose for the bevelled cones in comparison to the straight ended cones.

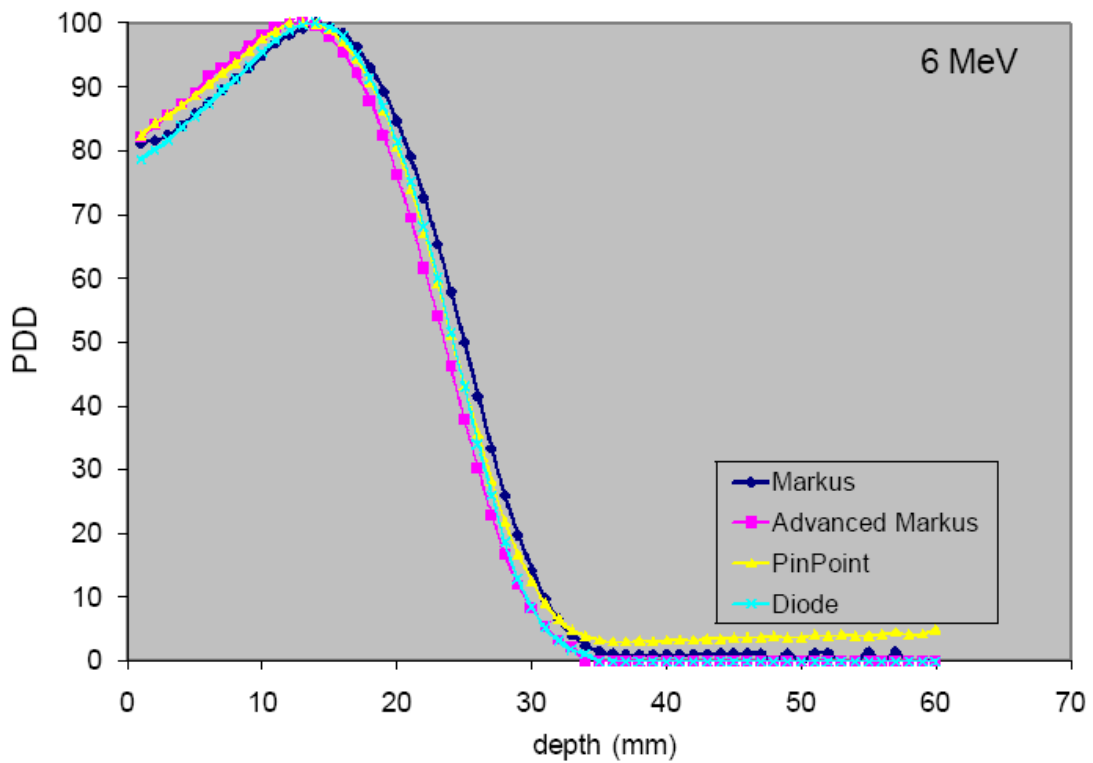
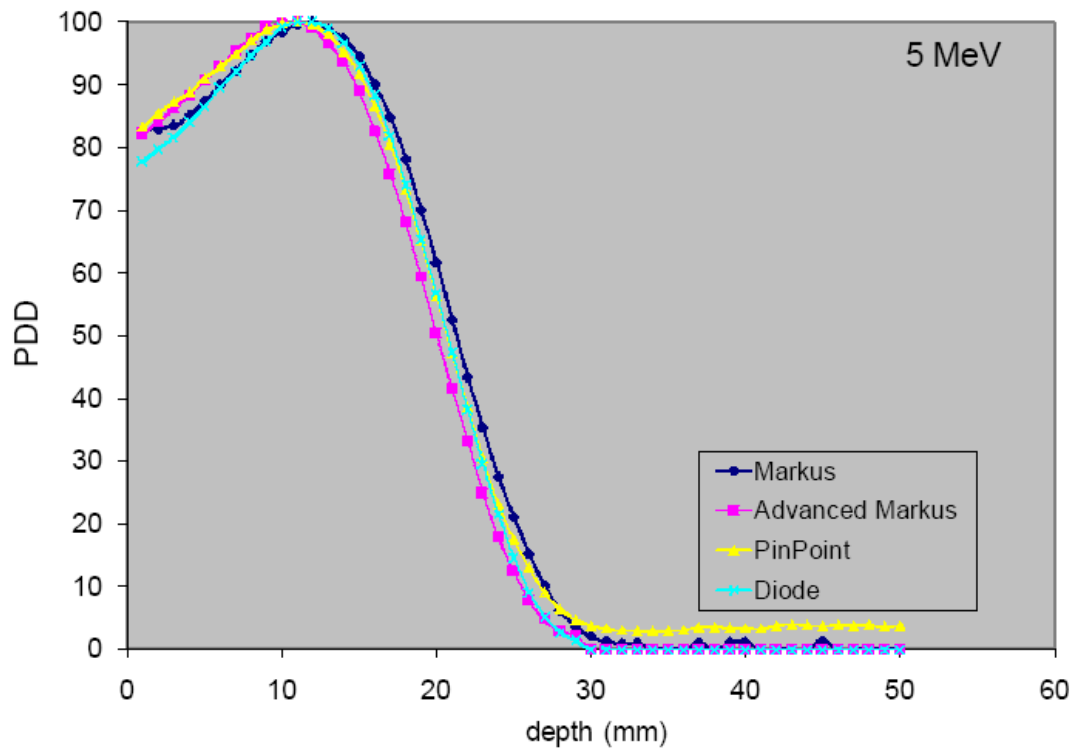


**Figure 3-11: Comparison of the PDD as measured with the Markus, Advanced Markus, PinPoint and the diode detector for the 8 cm cone for energies 5 and 6 MeV (small field cone system)**

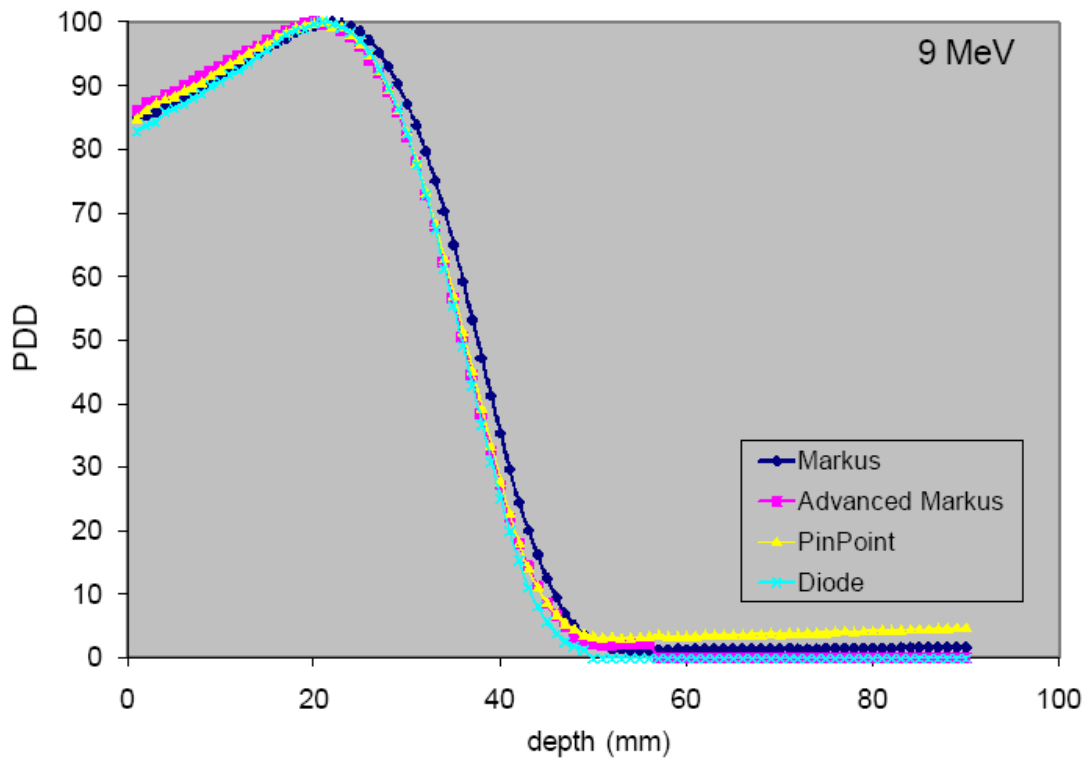
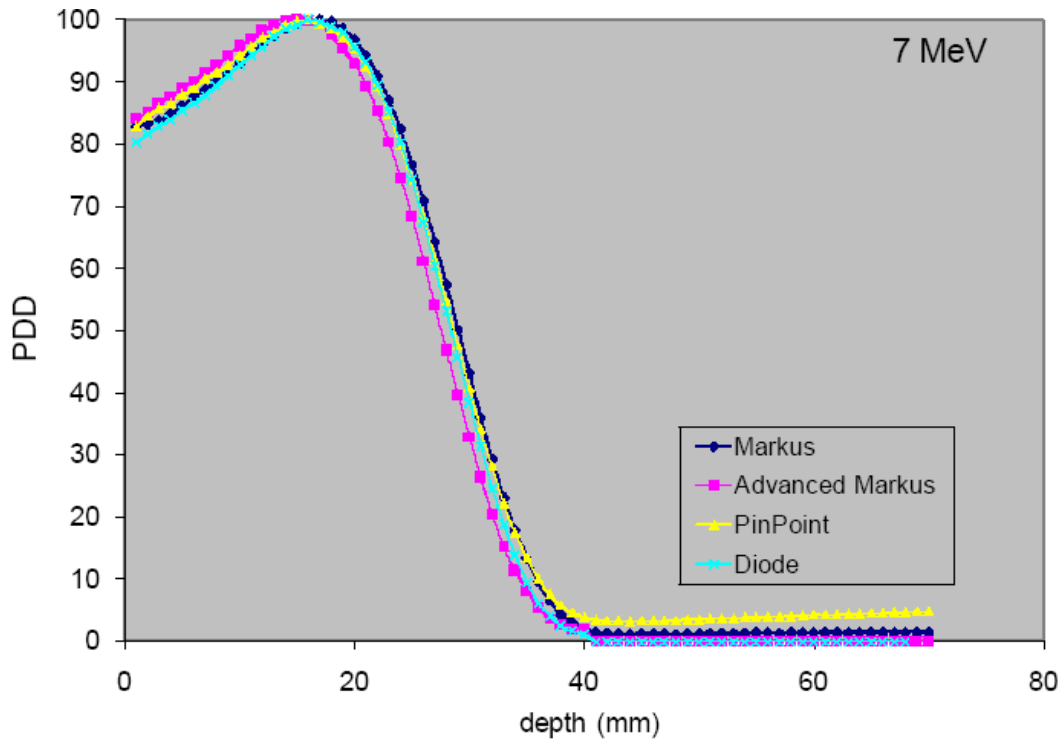
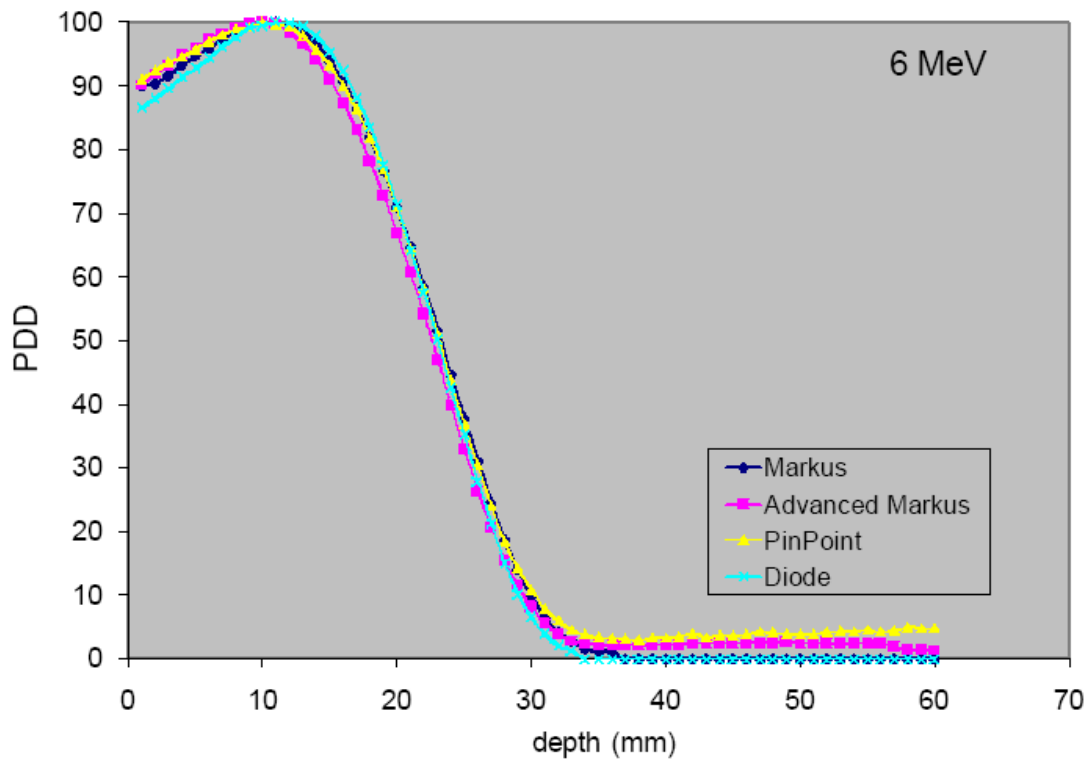
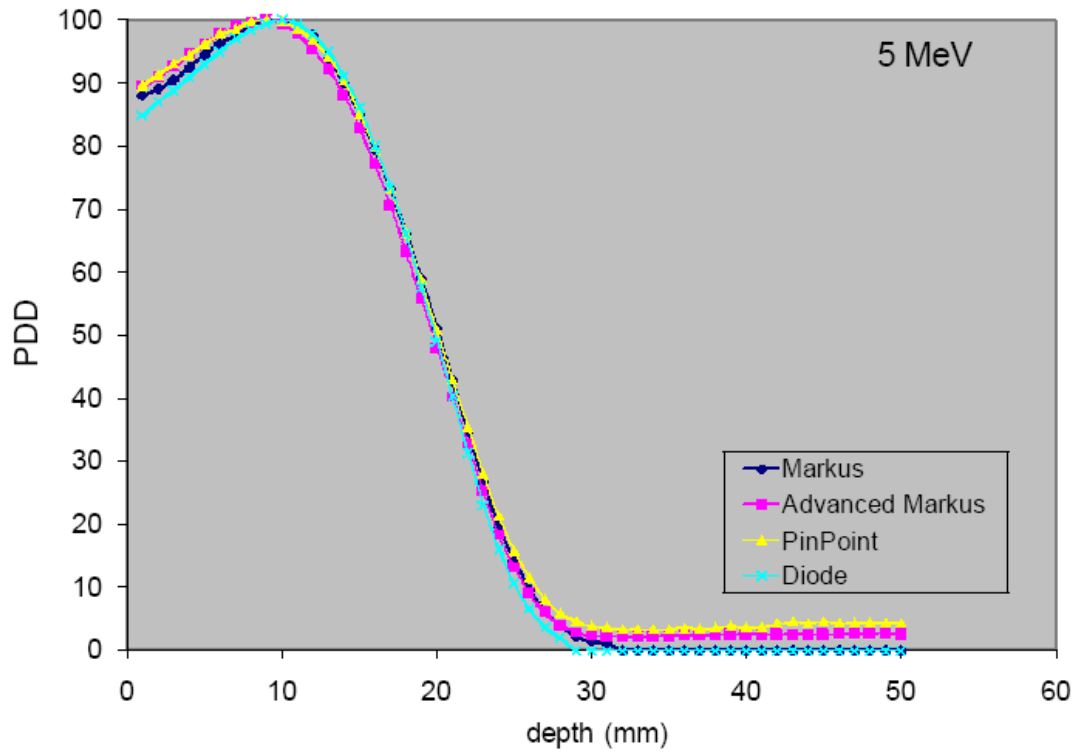
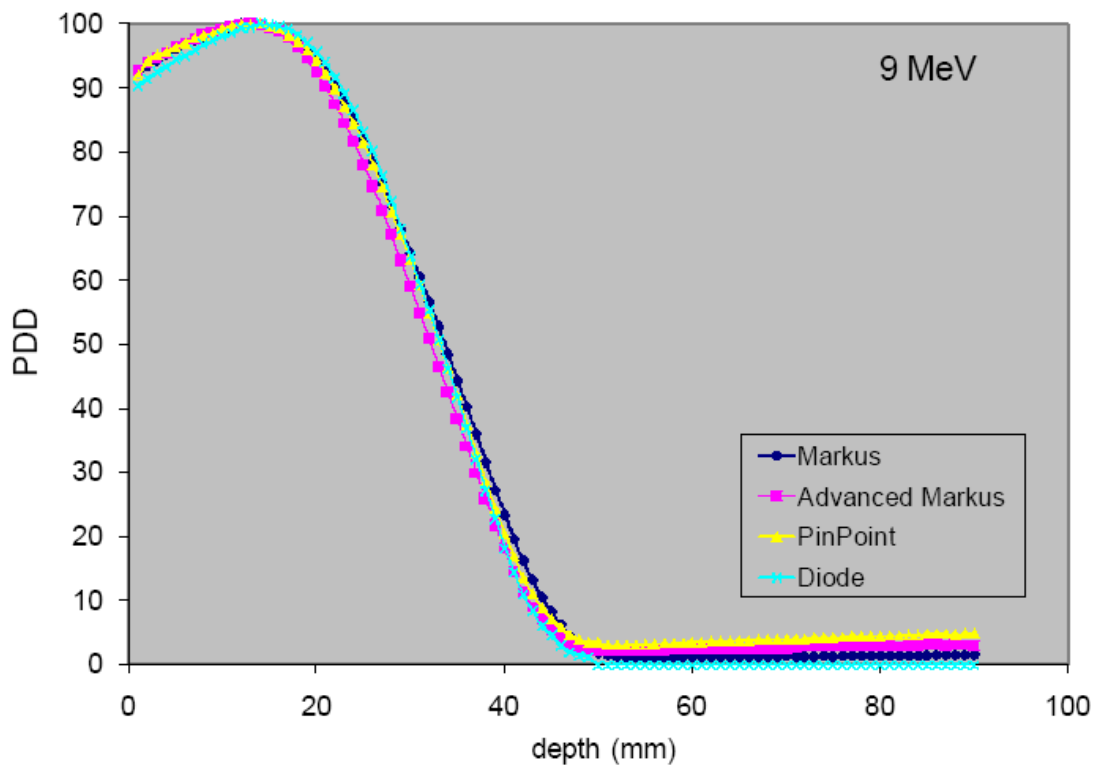
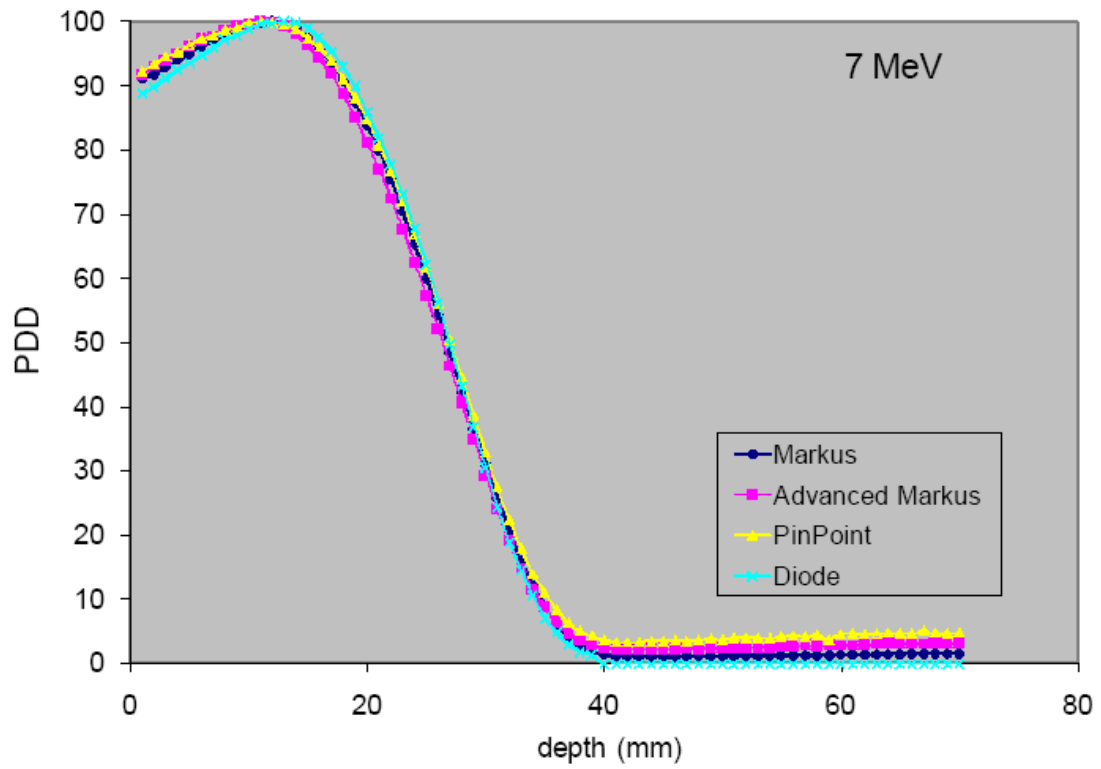


Figure 3-12: Comparison of the PDD as measured with the Markus, Advanced Markus, PinPoint and the diode detector for the 8 cm cone for energies 7 and 9 MeV (small field cone system)



**Figure 3-13: Comparison of the PDD as measured with the Markus, Advanced Markus, PinPoint and the diode detector for the 3 cm straight cone for energies 5 and 6 MeV (small field cone system)**



**Figure 3-14: Comparison of the PDD as measured with the Markus, Advanced Markus, PinPoint and the diode detector for the 3 cm straight cone for energies 7 and 9 MeV (small field cone system)**

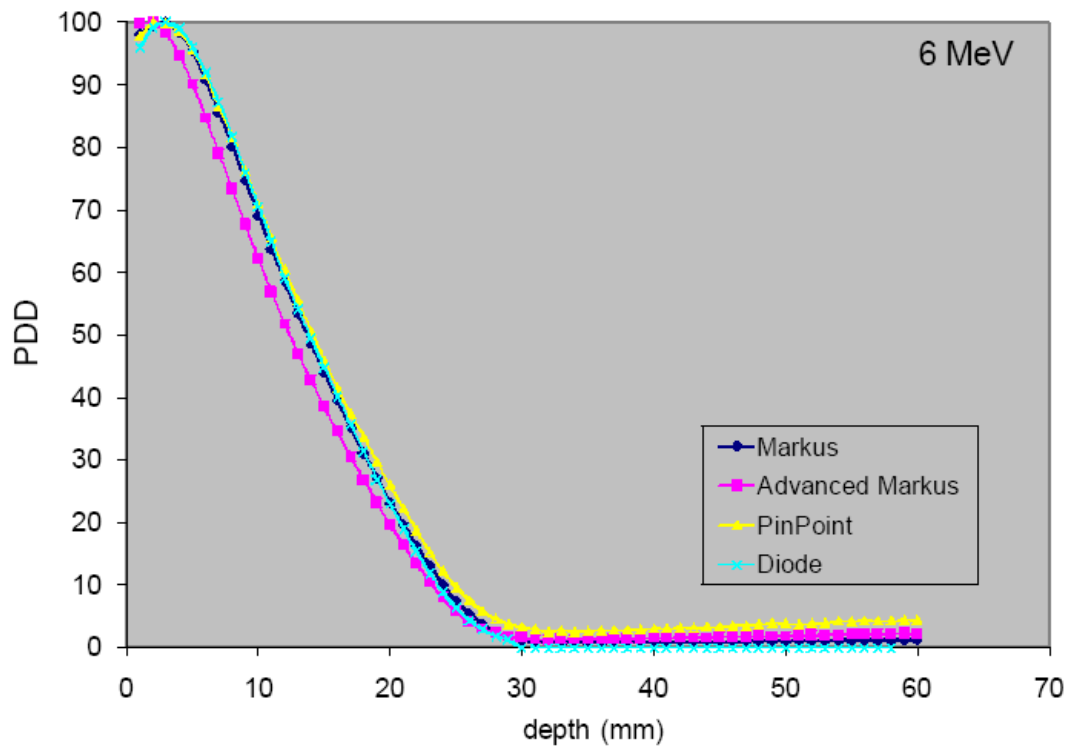
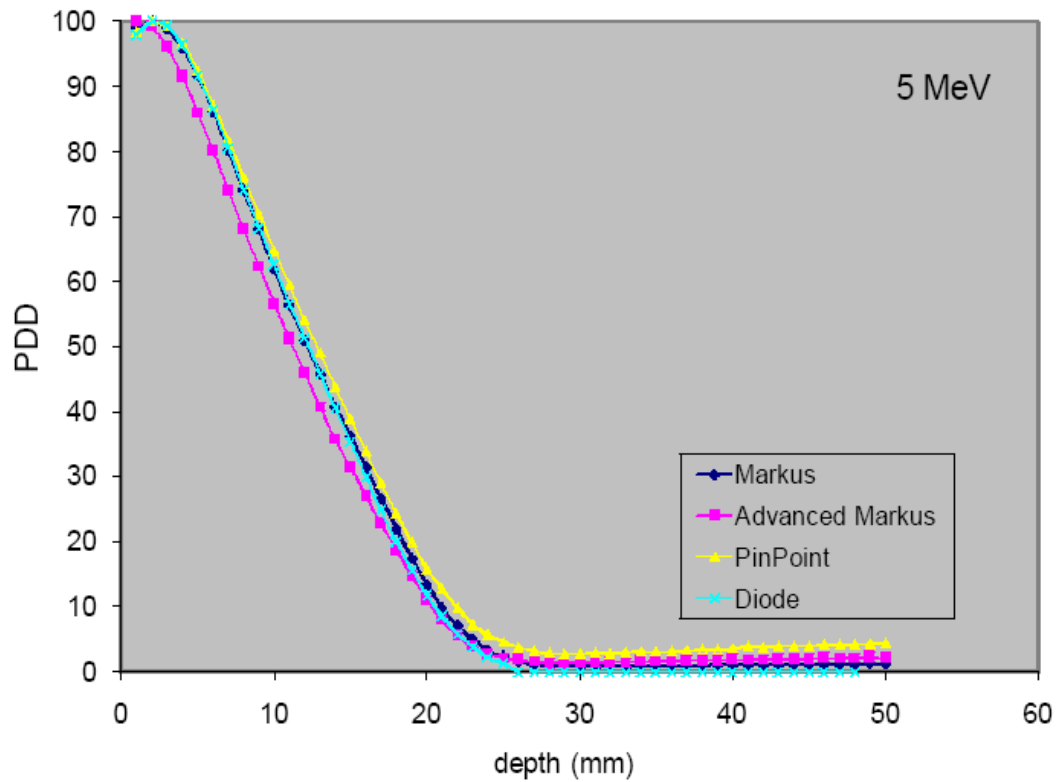


Figure 3-15: Comparison of the PDD as measured with the Markus, Advanced Markus, PinPoint and the diode detector for the 3 cm bevelled cone for energies 5 and 6 MeV (small field cone system) (bevel angle 45°)

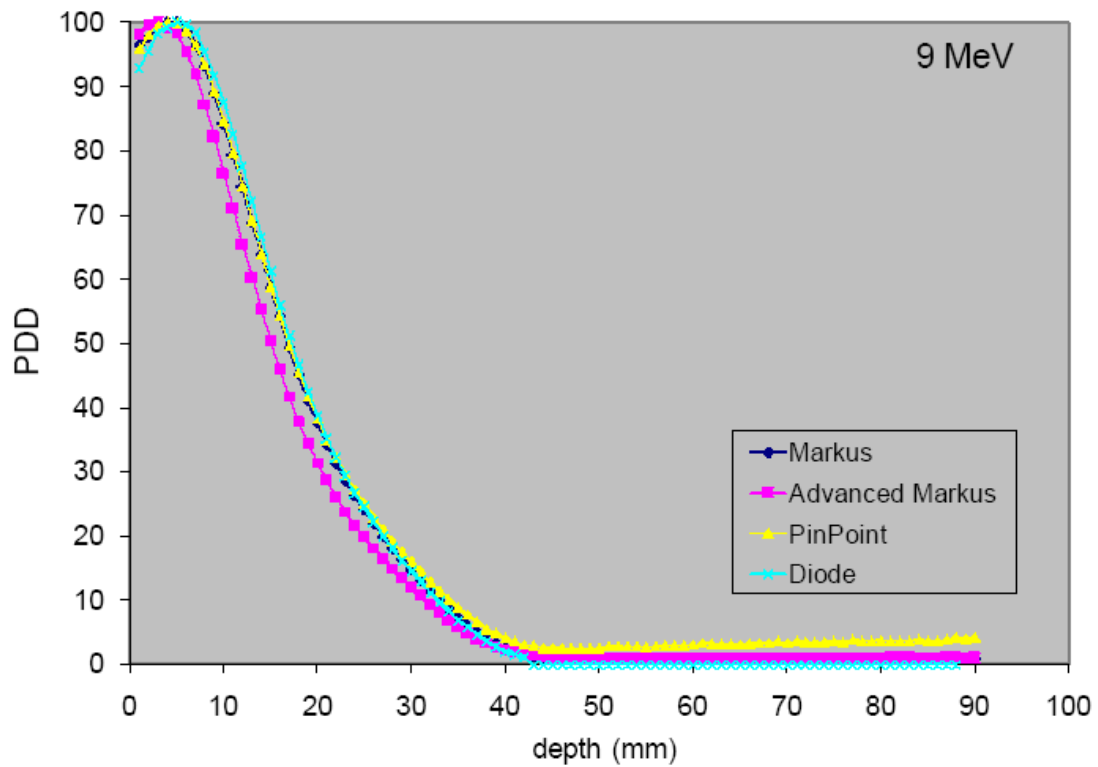
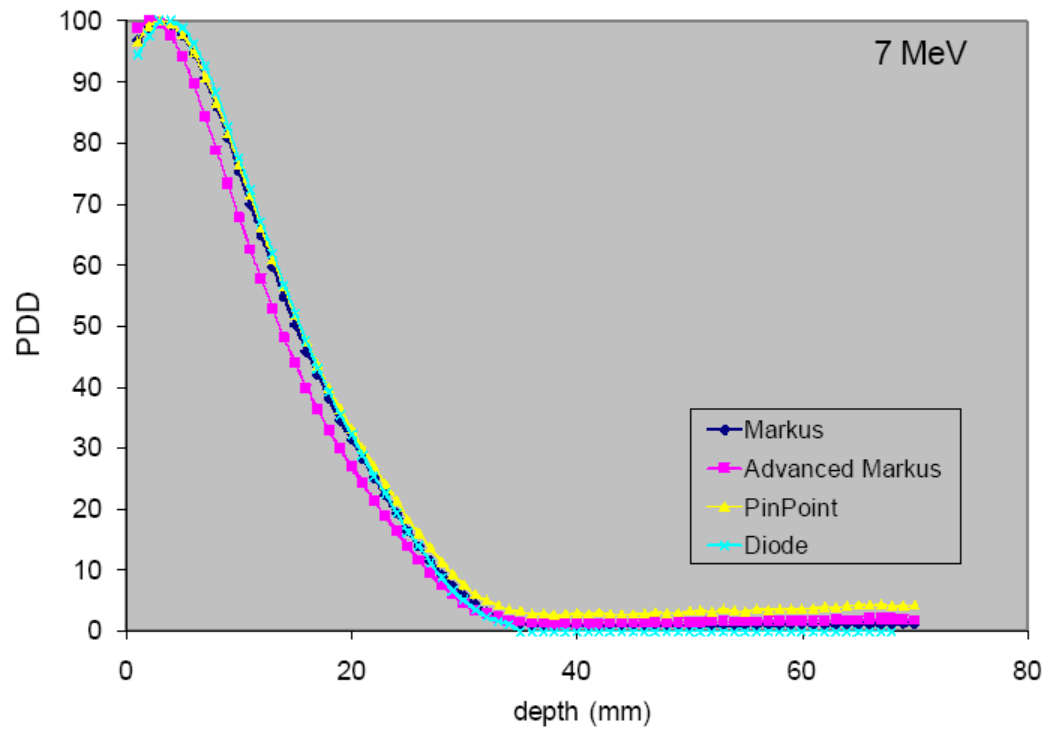
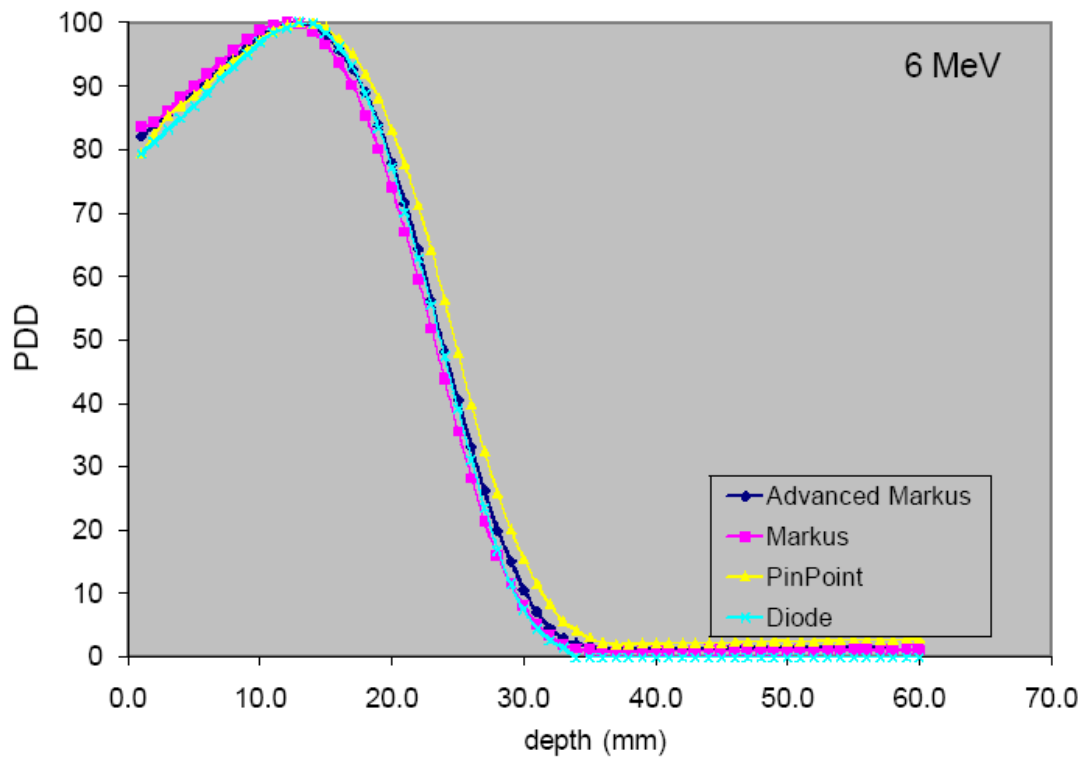
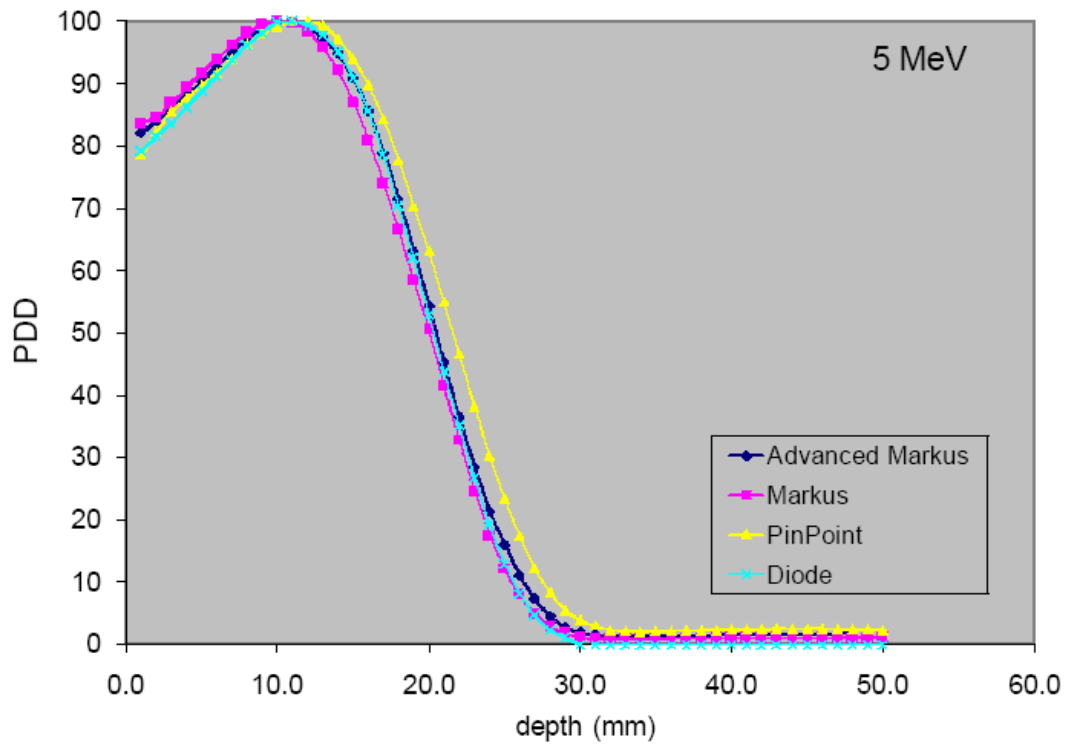


Figure 3-16: Comparison of the PDD as measured with the Markus, Advanced Markus, PinPoint and the diode detector for the 3 cm bevelled cone for energies 7 and 9 MeV (small field cone system) (bevel angle 45°)



**Figure 3-17: Comparison of the PDD as measured with the Markus, Advanced Markus, PinPoint and the diode detector for the 4.5 cm straight cone for energies 5 and 6 MeV (periscopic electron cone system)**

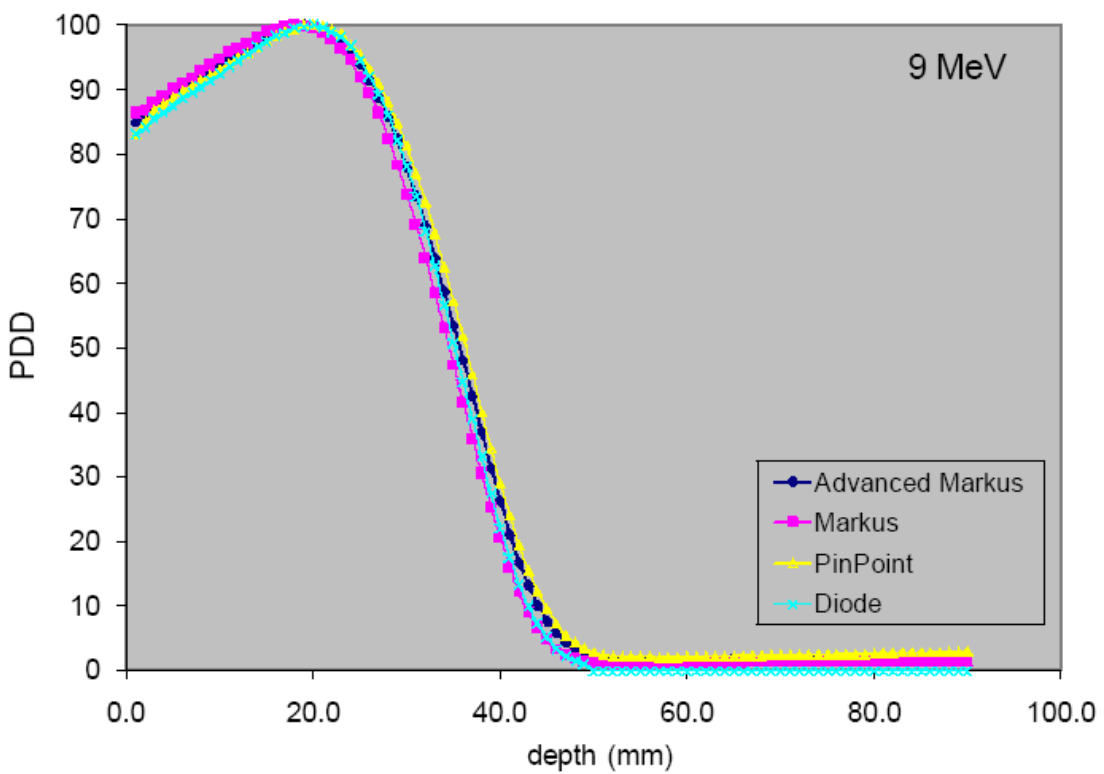
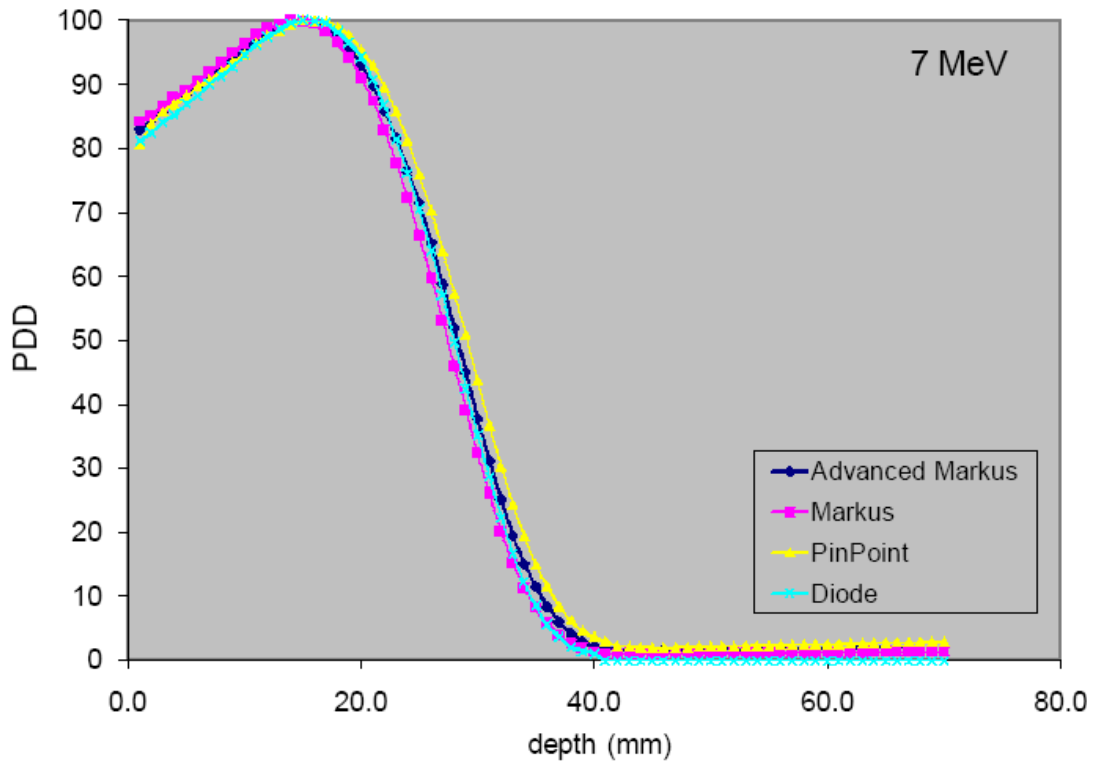
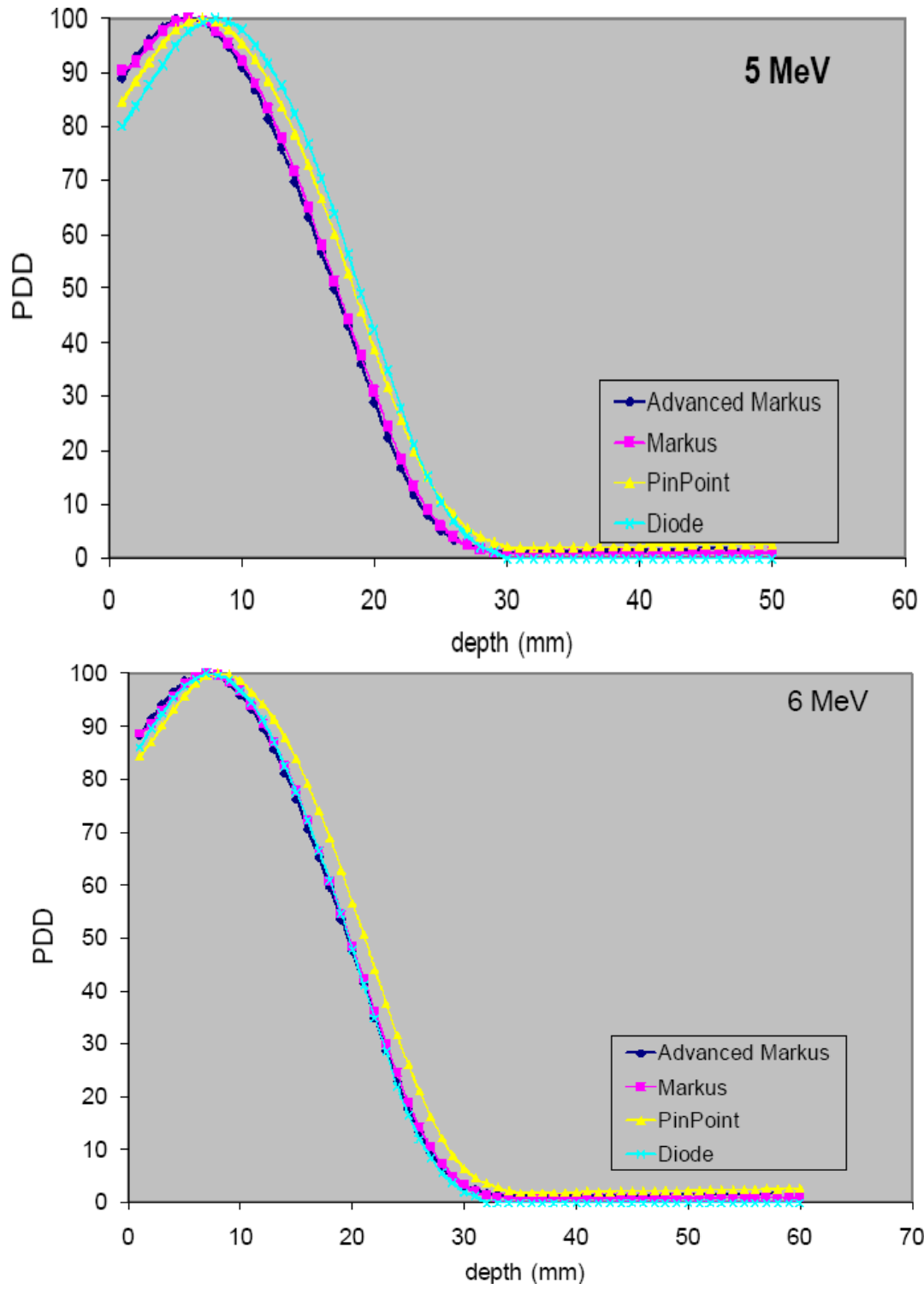
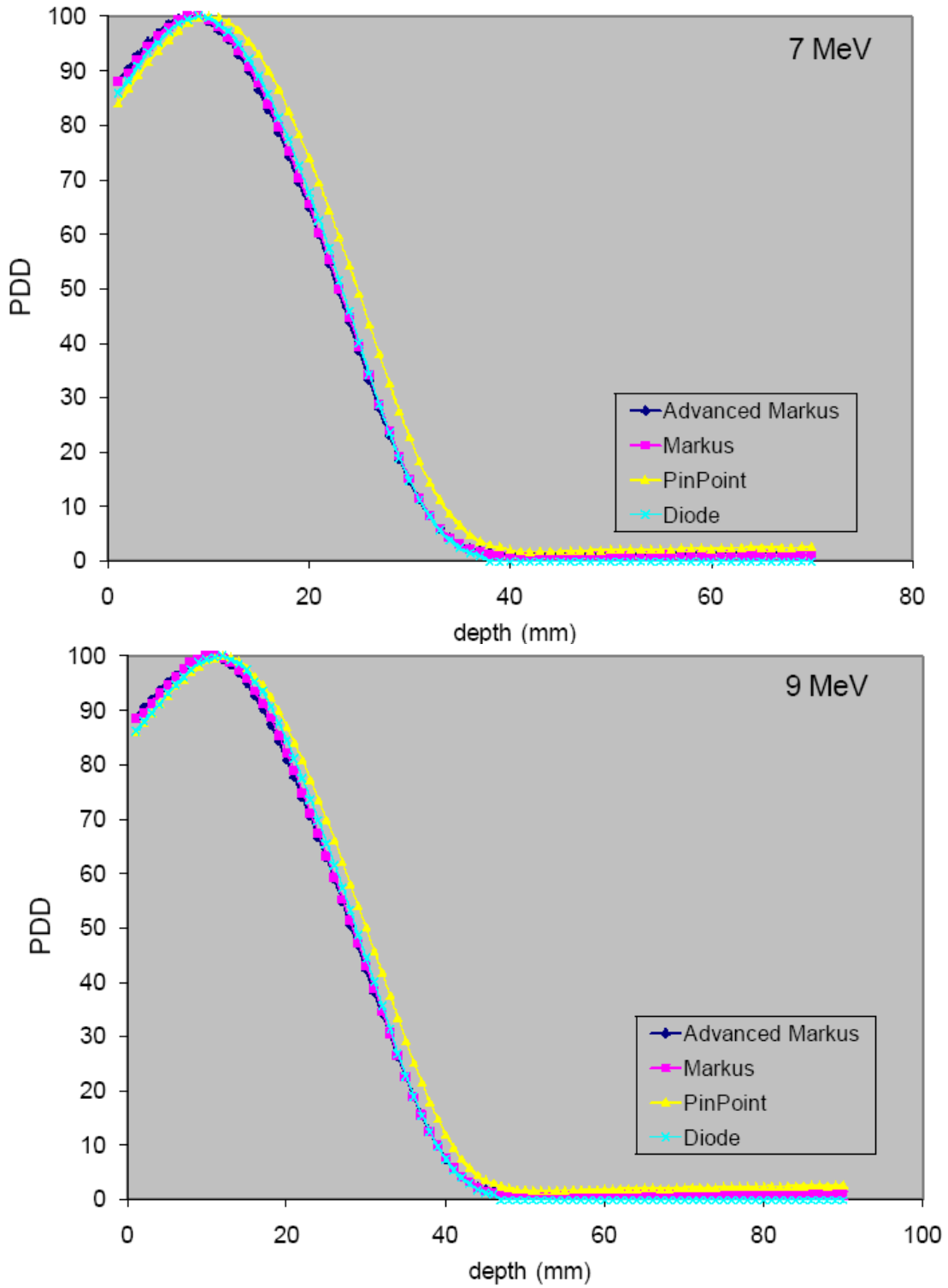


Figure 3-18: Comparison of the PDD as measured with the Markus, Advanced Markus, PinPoint and the diode detector for the 4.5 cm straight cone for energies 7 and 9 MeV (periscopic electron cone system)



**Figure 3-19: Comparison of the PDD as measured with the Markus, Advanced Markus, PinPoint and the diode detector for the 4.5 cm bevelled cone for energies 5 and 6 MeV (periscopic electron cone system)**



**Figure 3-20: Comparison of the PDD as measured with the Markus, Advanced Markus, PinPoint and the diode detector for the 4.5 cm bevelled cone for energies 7 and 9 MeV (periscopic electron cone system) (bevel angle 30°)**

**Table 3-6: Summary of the electron depth dose characteristics as measured with the Markus chamber (small-field cone system)**

		Markus				
		Depth (mm)				
	approximate surface dose (%)	d <sub>max</sub>	90%	80%	50%	30%
<b>5 MeV</b>						
Applicator						
2 cm circle	96	7	11	13	18	21
3 cm circle	87	9	14	16	20	23
4 cm circle	85	11	16	17	21	23
5 cm circle	83	11	15	17	21	23
6 cm circle	82	11	15	17	21	23
7 cm circle	82	12	16	18	21	23
8 cm circle	83	12	16	18	21	24
2 cm circle <sup>a</sup>	101	1	4	6	10	14
3 cm circle <sup>a</sup>	98	2	5	7	12	16
<b>6 MeV</b>						
Applicator						
2 cm circle	96	7	12	15	21	24
3 cm circle	90	11	16	18	23	26
4 cm circle	84	12	18	20	24	27
5 cm circle	83	13	18	20	24	27
6 cm circle	82	13	18	20	24	27
7 cm circle	82	14	19	20	25	27
8 cm circle	81	14	19	21	25	27
2 cm circle <sup>a</sup>	101	1	5	6	11	15
3 cm circle <sup>a</sup>	97	3	6	8	14	18

<sup>a</sup> bevel angle 45°

		Markus				
		Depth (mm)				
	approximate surface dose (%)	d <sub>max</sub>	90%	80%	50%	30%
<b>7 MeV</b>						
Applicator						
2 cm circle	99	5	14	16	23	28
3 cm circle	90	12	18	21	27	30
4 cm circle	85	14	21	23	28	31
5 cm circle	83	15	21	24	28	31
6 cm circle	84	16	22	24	28	31
7 cm circle	83	16	22	24	29	32
8 cm circle	83	17	22	24	29	32
2 cm circle <sup>a</sup>	100	1	5	7	11	15
3 cm circle <sup>a</sup>	95	3	7	9	15	20
<b>9 MeV</b>						
Applicator						
2 cm circle	97	9	17	20	28	35
3 cm circle	92	12	22	26	34	38
4 cm circle	88	18	26	30	36	40
5 cm circle	84	21	28	31	37	40
6 cm circle	86	21	30	31	37	40
7 cm circle	85	21	29	31	37	41
8 cm circle	85	22	29	32	38	41
2 cm circle <sup>a</sup>	100	3	6	8	12	16
3 cm circle <sup>a</sup>	95	4	9	11	17	23

**Table 3-7: Summary of the electron depth dose characteristics as measured with the Advanced Markus chamber (small-field cone system)**

		Advanced Markus				
		Depth (mm)				
	approximate surface dose (%)	d <sub>max</sub>	90%	80%	50%	30%
<b>5 MeV</b>						
Applicator						
2 cm circle	93	6	11	13	18	21
3 cm circle	88	9	14	16	20	22
4 cm circle	83	10	14	16	20	23
5 cm circle	82	10	15	16	20	22
6 cm circle	82	10	14	16	20	22
7 cm circle	82	10	15	16	20	22
8 cm circle	80	11	15	16	20	22
2 cm circle <sup>a</sup>	101	1	3	5	9	13
3 cm circle <sup>a</sup>	101	1	4	6	11	15
<b>6 MeV</b>						
Applicator						
2 cm circle	94	6	12	14	20	24
3 cm circle	88	10	15	18	23	25
4 cm circle	84	11	17	19	23	26
5 cm circle	82	12	17	19	23	26
6 cm circle	83	12	17	19	23	26
7 cm circle	82	13	18	19	24	26
8 cm circle	80	13	17	19	24	26
2 cm circle <sup>a</sup>	102	1	4	5	9	14
3 cm circle <sup>a</sup>	99	2	5	7	12	17
<sup>a</sup> bevel angle 45°						

		Advanced Markus				
		Depth (mm)				
	approximate surface dose (%)	d <sub>max</sub>	90%	80%	50%	30%
<b>7 MeV</b>						
Applicator						
2 cm circle	95	7	13	16	23	28
3 cm circle	90	11	18	20	26	30
4 cm circle	85	14	20	22	28	31
5 cm circle	83	14	20	23	27	30
6 cm circle	85	15	21	23	28	30
7 cm circle	83	15	21	23	28	30
8 cm circle	83	15	21	23	28	30
2 cm circle <sup>a</sup>	101	1	4	6	10	14
3 cm circle <sup>a</sup>	98	2	6	8	14	19
<b>9 MeV</b>						
Applicator						
2 cm circle	96	7	15	18	26	33
3 cm circle	92	13	21	24	32	37
4 cm circle	87	17	25	28	34	38
5 cm circle	84	19	26	29	35	38
6 cm circle	87	19	26	29	35	38
7 cm circle	86	20	28	30	36	40
8 cm circle	85	20	28	30	36	39
2 cm circle <sup>a</sup>	100	1	5	7	10	14
3 cm circle <sup>a</sup>	97	3	7	9	15	21

Table 3-8: Summary of the electron depth dose characteristics as measured with the PinPoint chamber (small-field cone system)

	PinPoint					
	approximate surface dose (%)	Depth (mm)				
		d <sub>max</sub>	90%	80%	50%	30%
<b>5 MeV</b>						
Applicator						
2 cm circle	92	7	12	14	19	23
3 cm circle	88	9	14	16	20	23
4 cm circle	84	10	15	16	20	23
5 cm circle	82	11	15	17	21	23
6 cm circle	82	10	15	17	21	23
7 cm circle	80	11	15	17	21	23
8 cm circle	81	11	15	17	21	23
2 cm circle <sup>a</sup>	100	2	5	6	11	15
3 cm circle <sup>a</sup>	97	2	5	7	13	17
<b>6 MeV</b>						
Applicator						
2 cm circle	93	7	13	16	22	25
3 cm circle	90	10	16	18	23	26
4 cm circle	85	11	17	19	23	26
5 cm circle	84	12	17	19	23	26
6 cm circle	82	13	18	20	24	26
7 cm circle	80	13	18	20	24	27
8 cm circle	80	13	18	20	24	27
2 cm circle <sup>a</sup>	99	2	5	7	11	16
3 cm circle <sup>a</sup>	96	2	6	8	14	19

<sup>a</sup> bevel angle 45°

	PinPoint					
	approximate surface dose (%)	Depth (mm)				
		d <sub>max</sub>	90%	80%	50%	30%
<b>7 MeV</b>						
Applicator						
2 cm circle	95	6	15	17	24	29
3 cm circle	91	11	18	21	28	31
4 cm circle	86	14	21	23	28	31
5 cm circle	84	15	21	23	28	31
6 cm circle	84	15	21	24	28	31
7 cm circle	82	15	21	24	29	31
8 cm circle	81	16	22	24	29	32
2 cm circle <sup>a</sup>	98	2	6	7	12	16
3 cm circle <sup>a</sup>	94	3	7	9	15	21
<b>9 MeV</b>						
Applicator						
2 cm circle	96	8	17	20	28	35
3 cm circle	90	14	22	25	33	38
4 cm circle	86	17	26	29	35	39
5 cm circle	85	19	27	30	35	39
6 cm circle	86	19	27	30	36	39
7 cm circle	84	20	28	30	36	39
8 cm circle	84	21	28	31	36	40
2 cm circle <sup>a</sup>	98	2	6	8	12	16
3 cm circle <sup>a</sup>	94	4	9	11	17	23

**Table 3-9: Summary of the electron depth dose characteristics as measured with the Diode detector (small-field cone system)**

	Diode detector					
	approximate surface dose (%)	Depth (mm)				
		d <sub>max</sub>	90%	80%	50%	30%
<b>5 MeV</b>						
Applicator						
2 cm circle	88	8	13	15	19	22
3 cm circle	83	10	14	16	20	22
4 cm circle	79	11	15	17	20	23
5 cm circle	79	11	15	17	20	22
6 cm circle	78	11	15	17	20	23
7 cm circle	76	12	15	17	21	23
8 cm circle	78	11	16	17	21	23
2 cm circle <sup>a</sup>	97	2	4	6	10	14
3 cm circle <sup>a</sup>	96	2	5	7	12	16
<b>6 MeV</b>						
Applicator						
2 cm circle	90	9	14	16	22	25
3 cm circle	85	11	17	19	23	26
4 cm circle	80	13	18	20	24	26
5 cm circle	80	13	18	20	23	26
6 cm circle	80	13	18	20	24	26
7 cm circle	78	14	18	20	24	27
8 cm circle	77	14	18	20	24	27
2 cm circle <sup>a</sup>	97	2	5	6	10	14
3 cm circle <sup>a</sup>	93	3	6	8	14	18

<sup>a</sup> bevel angle 45°

	Diode detector					
	approximate surface dose (%)	Depth (mm)				
		d <sub>max</sub>	90%	80%	50%	30%
<b>7 MeV</b>						
Applicator						
2 cm circle	93	9	15	18	24	29
3 cm circle	88	13	19	21	27	30
4 cm circle	81	16	21	23	28	31
5 cm circle	80	16	21	23	28	31
6 cm circle	82	16	22	24	28	31
7 cm circle	82	17	22	24	29	31
8 cm circle	79	16	22	24	28	31
2 cm circle <sup>a</sup>	99	2	5	7	11	14
3 cm circle <sup>a</sup>	91	4	8	10	15	21
<b>9 MeV</b>						
Applicator						
2 cm circle	95	9	17	20	28	34
3 cm circle	89	14	23	26	33	37
4 cm circle	82	20	27	29	35	39
5 cm circle	82	20	27	30	35	39
6 cm circle	84	20	28	30	36	39
7 cm circle	82	21	28	31	36	40
8 cm circle	82	21	29	32	37	40
2 cm circle <sup>a</sup>	96	3	6	8	11	15
3 cm circle <sup>a</sup>	90	5	9	12	17	23

**Table 3-10: Summary of the electron depth dose characteristics as measured with the Markus chamber (periscopic electron cone system)**

	Markus					
	approximate surface dose (%)	Depth (mm)				
		d <sub>max</sub>	90%	80%	50%	30%
<b>5 MeV</b>						
Applicator						
3.2 cm circle	84	10	15	16	21	23
3.8 cm circle	83	11	15	17	21	23
4.5 cm circle	83	10	14	16	20	22
3.2 cm circle <sup>b</sup>	91	5	9	11	16	19
3.8 cm circle <sup>b</sup>	90	5	10	12	17	20
4.5 cm circle <sup>b</sup>	89	6	11	13	17	20
<b>6 MeV</b>						
Applicator						
3.2 cm circle	86	12	17	19	24	26
3.8 cm circle	84	12	17	19	24	26
4.5 cm circle	83	12	17	19	23	26
3.2 cm circle <sup>b</sup>	90	5	10	12	18	22
3.8 cm circle <sup>b</sup>	88	6	11	14	19	23
4.5 cm circle <sup>b</sup>	87	7	12	15	20	23
<sup>b</sup> bevel angle 30°						

	Markus					
	approximate surface dose (%)	Depth (mm)				
		d <sub>max</sub>	90%	80%	50%	30%
<b>7 MeV</b>						
Applicator						
3.2 cm circle	88	13	19	22	27	31
3.8 cm circle	85	14	20	23	28	31
4.5 cm circle	83	14	20	23	27	30
3.2 cm circle <sup>b</sup>	91	6	11	14	20	25
3.8 cm circle <sup>b</sup>	89	7	13	16	22	26
4.5 cm circle <sup>b</sup>	87	9	14	17	23	27
<b>9 MeV</b>						
Applicator						
3.2 cm circle	91	16	23	26	33	38
3.8 cm circle	88	17	25	28	35	38
4.5 cm circle	86	18	26	29	35	38
3.2 cm circle <sup>b</sup>	92	8	13	16	23	30
3.8 cm circle <sup>b</sup>	90	9	15	18	26	32
4.5 cm circle <sup>b</sup>	87	11	18	21	28	33

**Table 3-11: Summary of the electron depth dose characteristics as measured with the Advanced Markus chamber (periscopic electron cone system)**

		Advanced Markus				
		Depth (mm)				
	approximate surface dose (%)	d <sub>max</sub>	90%	80%	50%	30%
<b>5 MeV</b>						
Applicator						
3.2 cm circle	85	9	14	16	20	22
3.8 cm circle	83	10	14	16	20	22
4.5 cm circle	80	10	15	17	20	23
3.2 cm circle <sup>b</sup>	90	5	9	11	16	19
3.8 cm circle <sup>b</sup>	85	6	10	12	17	20
4.5 cm circle <sup>b</sup>	85	6	10	12	17	20
<b>6 MeV</b>						
Applicator						
3.2 cm circle	86	10	16	18	23	26
3.8 cm circle	83	11	17	19	23	26
4.5 cm circle	80	12	18	20	24	26
3.2 cm circle <sup>b</sup>	90	6	10	12	18	22
3.8 cm circle <sup>b</sup>	86	7	12	15	20	23
4.5 cm circle <sup>b</sup>	85	7	12	14	20	23
<sup>b</sup> bevel angle 30°						

		Advanced Markus				
		Depth (mm)				
	approximate surface dose (%)	d <sub>max</sub>	90%	80%	50%	30%
<b>7 MeV</b>						
Applicator						
3.2 cm circle	89	12	18	21	27	30
3.8 cm circle	86	13	19	22	27	30
4.5 cm circle	82	15	21	23	28	31
3.2 cm circle <sup>b</sup>	91	6	11	14	21	25
3.8 cm circle <sup>b</sup>	88	8	14	16	23	27
4.5 cm circle <sup>b</sup>	86	8	14	17	23	27
<b>9 MeV</b>						
Applicator						
3.2 cm circle	90	14	22	25	23	37
3.8 cm circle	88	16	24	27	33	38
4.5 cm circle	84	19	27	30	36	39
3.2 cm circle <sup>b</sup>	93	7	13	16	23	30
3.8 cm circle <sup>b</sup>	89	10	16	19	27	30
4.5 cm circle <sup>b</sup>	87	10	17	20	28	33

**Table 3-12: Summary of the electron depth dose characteristics as measured with the PinPoint chamber (periscopic electron cone system)**

	PinPoint					
	approximate surface dose (%)	Depth (mm)				
		d <sub>max</sub>	90%	80%	50%	30%
<b>5 MeV</b>						
Applicator						
3.2 cm circle	83	9	14	17	20	23
3.8 cm circle	77	10	15	17	21	23
4.5 cm circle	75	12	16	18	22	24
3.2 cm circle <sup>b</sup>	88	5	10	12	17	20
3.8 cm circle <sup>b</sup>	83	6	11	13	18	21
4.5 cm circle <sup>b</sup>	81	7	12	14	18	21
<b>6 MeV</b>						
Applicator						
3.2 cm circle	83	11	16	19	23	26
3.8 cm circle	79	12	17	19	24	27
4.5 cm circle	76	13	19	21	25	27
3.2 cm circle <sup>b</sup>	89	6	11	13	19	23
3.8 cm circle <sup>b</sup>	84	7	13	15	20	24
4.5 cm circle <sup>b</sup>	82	8	13	16	21	24
<sup>b</sup> bevel angle 30°						

	PinPoint					
	approximate surface dose (%)	Depth (mm)				
		d <sub>max</sub>	90%	80%	50%	30%
<b>7 MeV</b>						
Applicator						
3.2 cm circle	86	13	19	22	27	31
3.8 cm circle	82	14	21	23	28	31
4.5 cm circle	78	15	22	24	29	32
3.2 cm circle <sup>b</sup>	90	7	12	15	21	26
3.8 cm circle <sup>b</sup>	85	9	14	17	23	26
4.5 cm circle <sup>b</sup>	81	10	16	19	25	29
<b>9 MeV</b>						
Applicator						
3.2 cm circle	88	15	23	26	34	38
3.8 cm circle	84	17	26	29	35	39
4.5 cm circle	81	20	27	30	37	40
3.2 cm circle <sup>b</sup>	91	8	14	16	24	30
3.8 cm circle <sup>b</sup>	87	10	17	20	28	33
4.5 cm circle <sup>b</sup>	84	12	19	22	30	35

**Table 3-13: Summary of the electron depth dose characteristics as measured with the Diode detector (periscopic electron cone system)**

	Diode detector					
	approximate surface dose (%)	Depth (mm)				
		d <sub>max</sub>	90%	80%	50%	30%
<b>5 MeV</b>						
Applicator						
3.2 cm circle	79	11	15	16	20	22
3.8 cm circle	77	11	15	17	21	23
4.5 cm circle	77	11	15	17	20	23
3.2 cm circle <sup>b</sup>	85	6	10	12	17	20
3.8 cm circle <sup>b</sup>	84	6	10	12	17	20
4.5 cm circle <sup>b</sup>	84	6	10	12	17	20
<b>6 MeV</b>						
Applicator						
3.2 cm circle	80	12	17	19	23	26
3.8 cm circle	79	13	18	20	24	26
4.5 cm circle	77	13	18	20	24	26
3.2 cm circle <sup>b</sup>	85	7	11	14	19	23
3.8 cm circle <sup>b</sup>	84	7	12	14	20	23
4.5 cm circle <sup>b</sup>	83	7	12	14	20	23
<sup>b</sup> bevel angle 30°						

	Diode detector					
	approximate surface dose (%)	Depth (mm)				
		d <sub>max</sub>	90%	80%	50%	30%
<b>7 MeV</b>						
Applicator						
3.2 cm circle	84	14	20	22	27	30
3.8 cm circle	80	15	21	23	28	31
4.5 cm circle	80	15	21	23	28	31
3.2 cm circle <sup>b</sup>	87	8	13	15	22	26
3.8 cm circle <sup>b</sup>	85	8	14	17	23	26
4.5 cm circle <sup>b</sup>	84	9	15	17	23	27
<b>9 MeV</b>						
Applicator						
3.2 cm circle	85	16	23	26	33	37
3.8 cm circle	83	19	26	29	35	38
4.5 cm circle	82	20	27	30	35	39
3.2 cm circle <sup>b</sup>	89	9	14	17	24	31
3.8 cm circle <sup>b</sup>	87	10	17	20	28	33
4.5 cm circle <sup>b</sup>	84	12	18	21	29	33

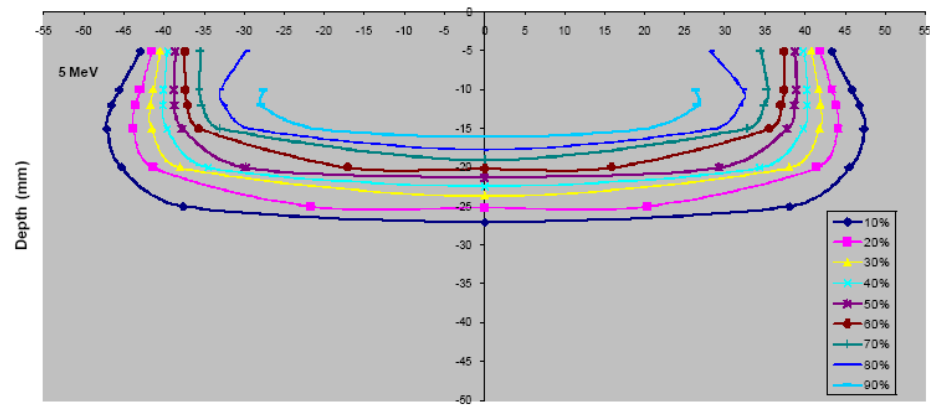
### 3.3.2 Two dimensional relative beam data (isodose curves)

104 isodose charts were generated from interpolation of PDD curves and the off-axis profile data for all cone-energy combinations and for each detector used. The PDD and the off-axis profiles were measured along the clinical central-axis (equal to the geometric central axis for straight cones figure 2-1) at SSD 100 cm. Off-axis profiles were measured from depths 45, 35, 30 and 25 mm to 5 mm for electron energies 9, 7, 6 and 5 MeV respectively, in steps of 5 mm. Measurements points on the off-axis profiles were taken in steps of 1 mm. The off-axis profiles were normalised to the central-axis value, which corresponded to the PDD at the depth of the off-axis measurement.

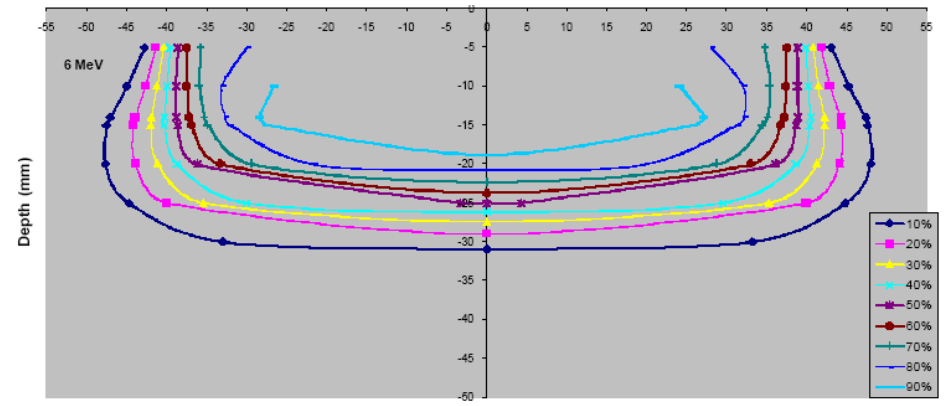
Figures 3-19, 3-20 3-21, 3-22 and 3-23 show the isodose charts for the small-field cone system as generated from the data obtained with measurements using the Markus chamber for straight end cones of inner diameter 8, 5 and 3 cm and the 3 cm bevel end cone. Figures 3-24, 3-25 and 3-26 likewise show the isodose charts for the Periscopic electron cone system, generated from the data obtained with measurements using the Markus chamber for the 4.5 cm (straight and bevel end) cone. According to McCullough and Anderson (1982), it is important to note that a bevelled cone provides an elliptical treatment field, the minor axis of the cone is equal to the inner diameter and the major axis increases by  $(\cos\theta)^{-1}$ , where  $\theta$  is the bevel angle.

The isodose charts in figures 3-19, 3-20, 3-21 and 3-24 are typical of isodose charts generated for cylindrical cones with straight ends. While figures 3-22 and 3-25 are typical of isodose charts for cylindrical cones with bevel ends generated from data along the major axis of the cone. For bevel cones isodose curves were also generated from data measured along the minor axis of the cone. These isodose curves are similar to those of the straight end cones. Figures 3-23 and 3-26 show isodose charts for bevel end cones, generated from data on the minor axis of the cone.

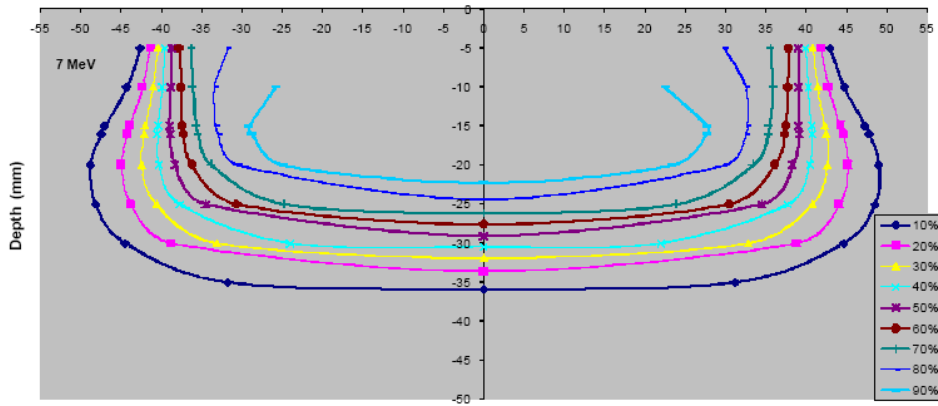
The isodose charts are at a scale of 1:1 and are typical of isodoses generated by the other detectors.



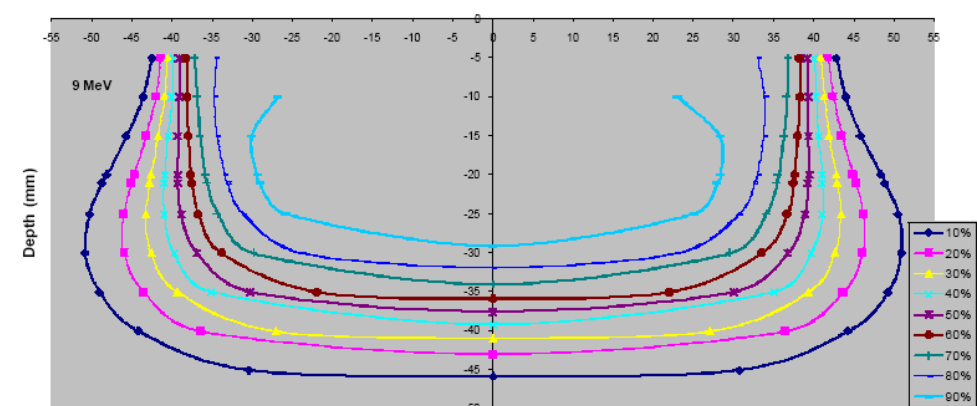
(a)



(b)



(c)



(d)

**Figure 3-21: Isodose charts for the 8 cm straight cone (small cone system) for electron energies (a) 5, (b) 6, (c) 7, and (d) 9 MeV measured with the Markus chamber**

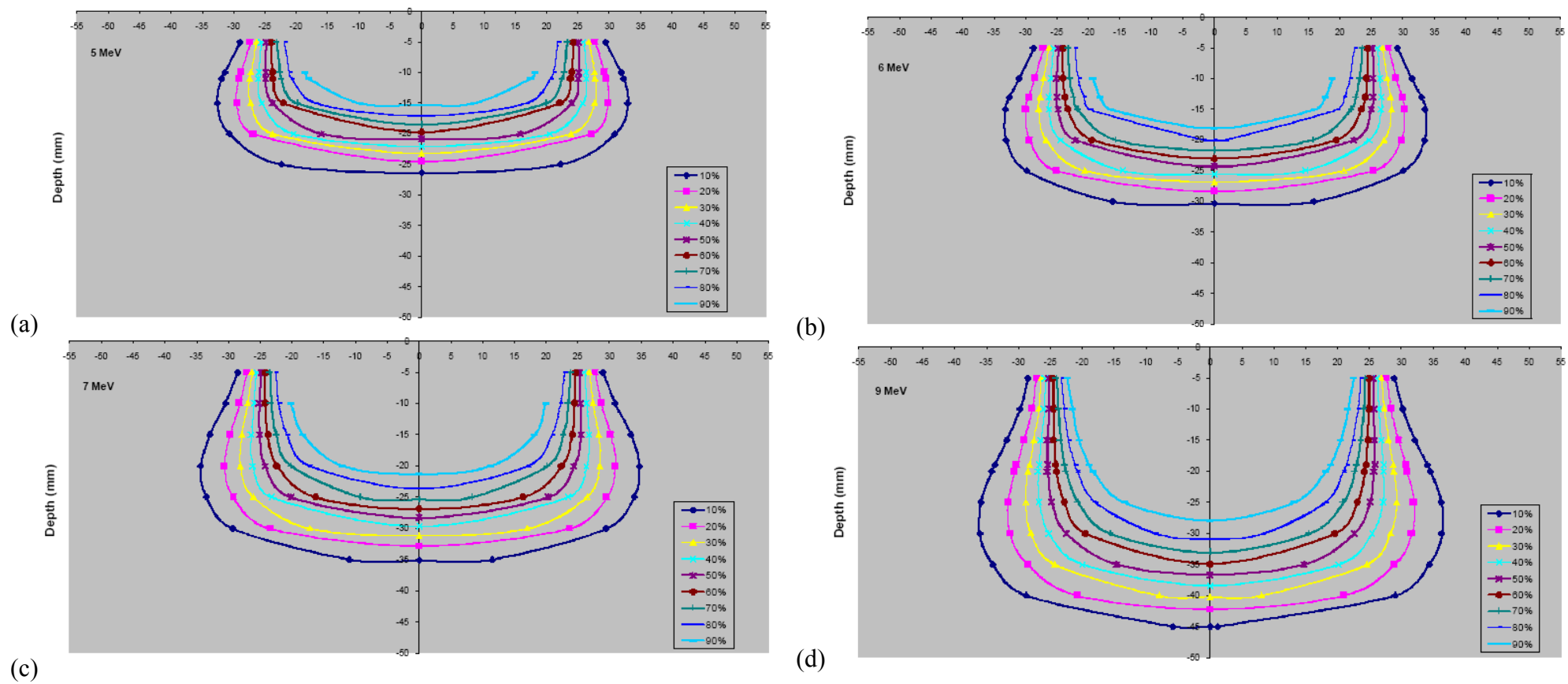
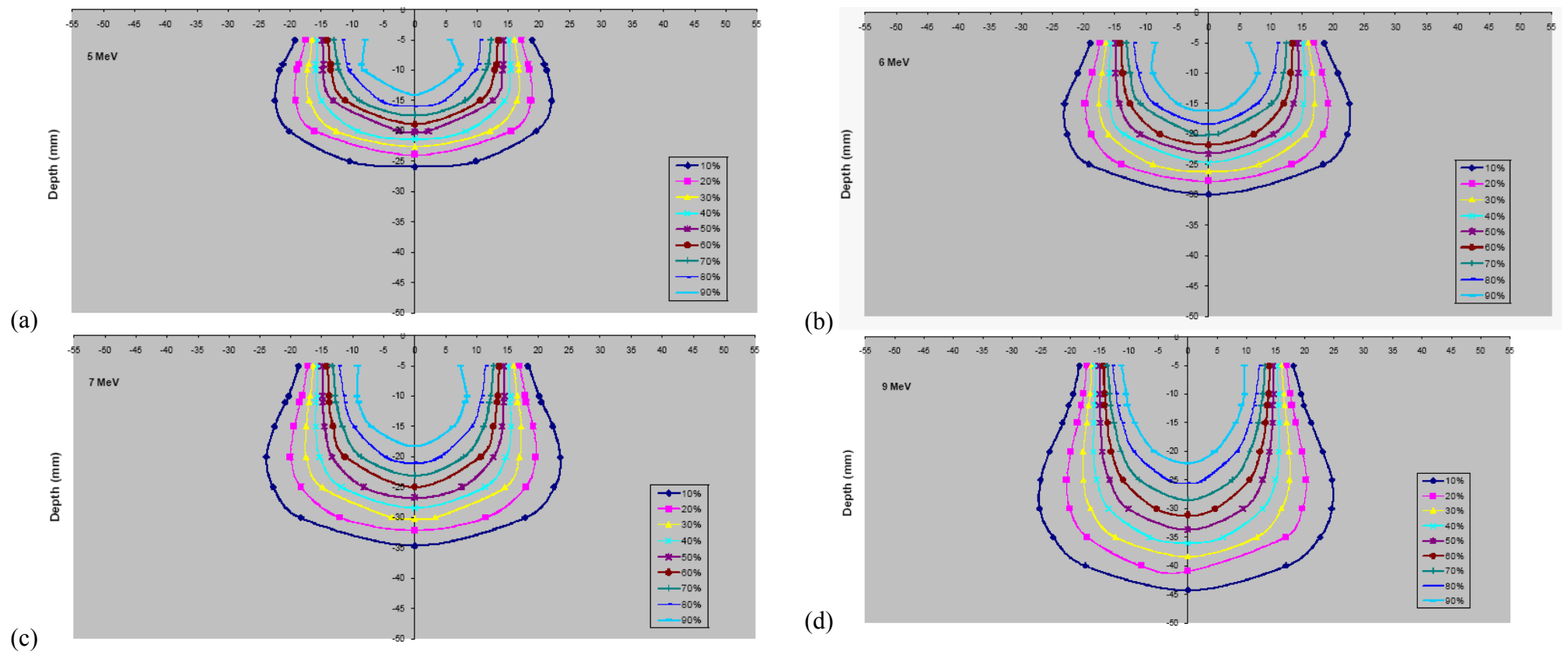
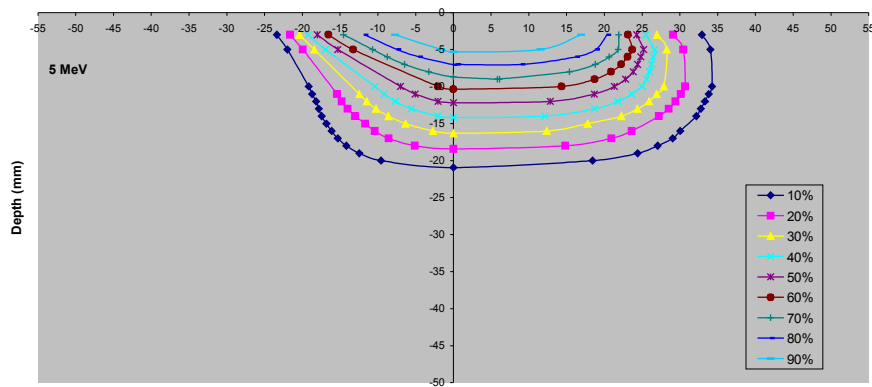


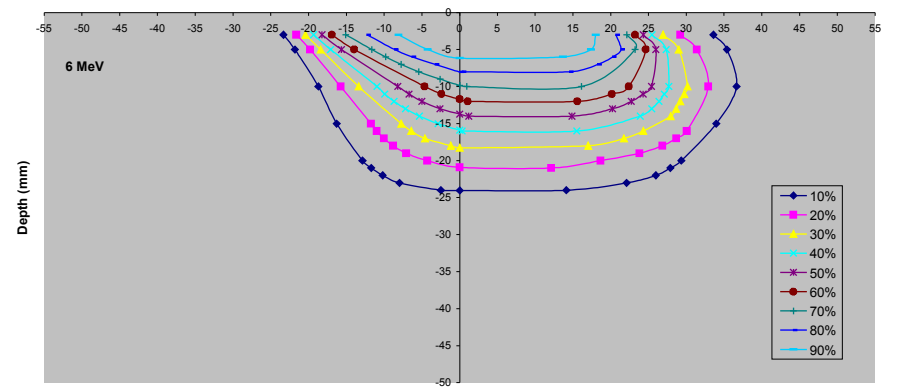
Figure 3-22: Isodose charts for the 5 cm straight cone (small cone system) for electron energies (a) 5, (b) 6, (c) 7, and (d) 9 MeV measured with the Markus chamber



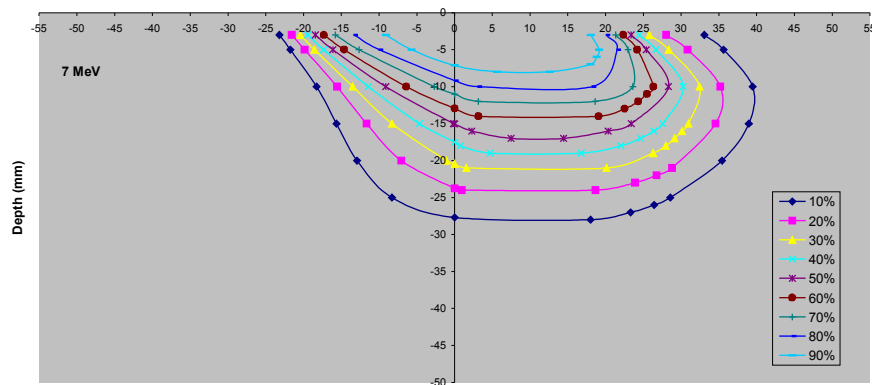
**Figure 3-23: Isodose charts for the 3 cm straight cone (small cone system) for electron energies (a) 5, (b) 6, (c) 7, and (d) 9 MeV measured with the Markus chamber**



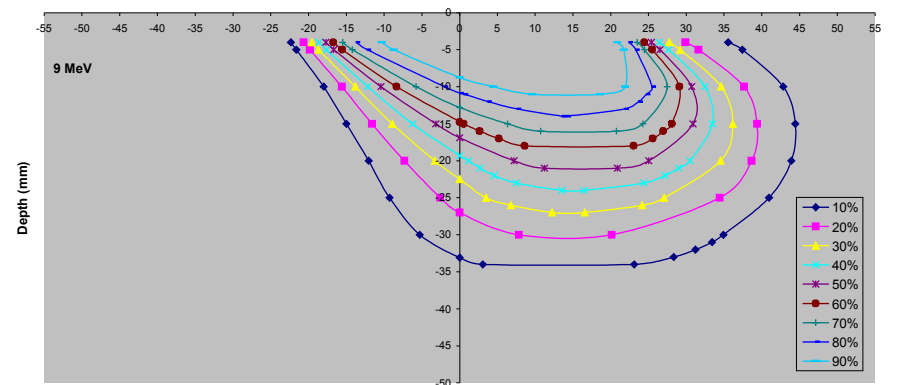
(a)



(b)

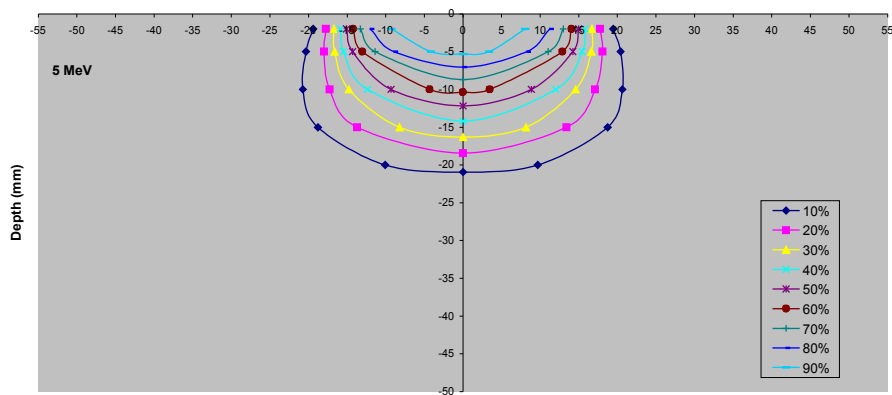


(c)

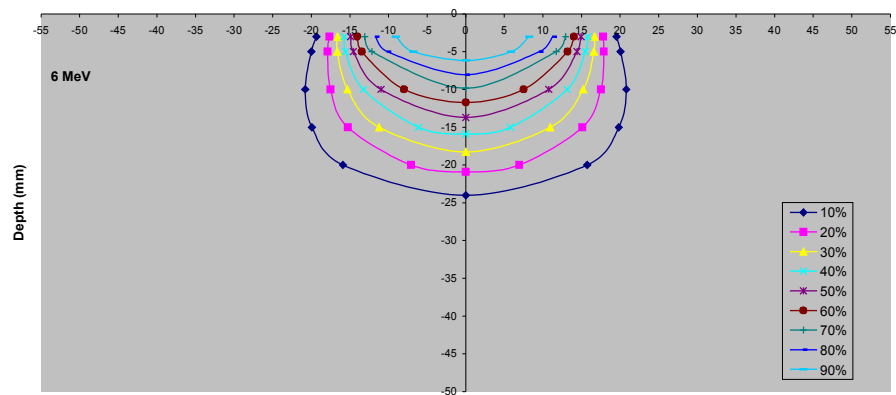


(d)

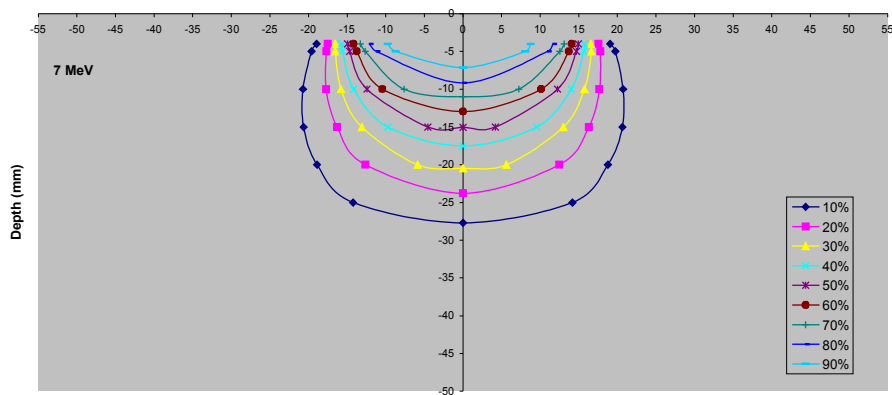
Figure 3-24: Isodose charts for the 3 cm bevelled cone (bevel angle 45°) (small cone system) for electron energies (a) 5, (b) 6, (c) 7, and (d) 9 MeV measured with the Markus chamber, measured along the major elliptical axis of the cone)



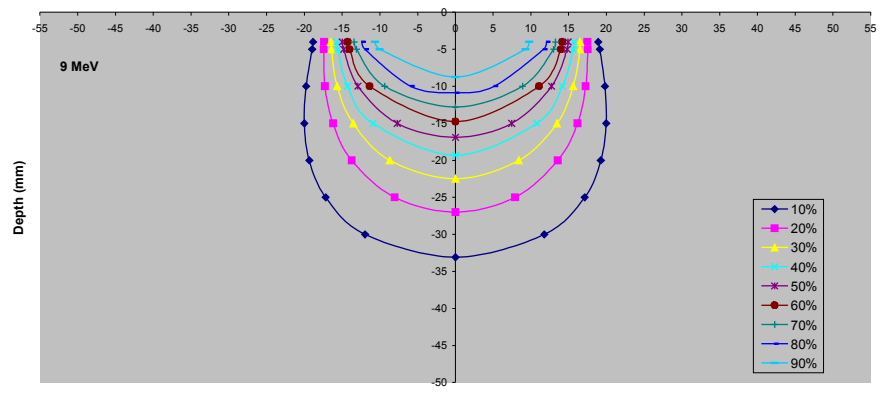
(a)



(b)

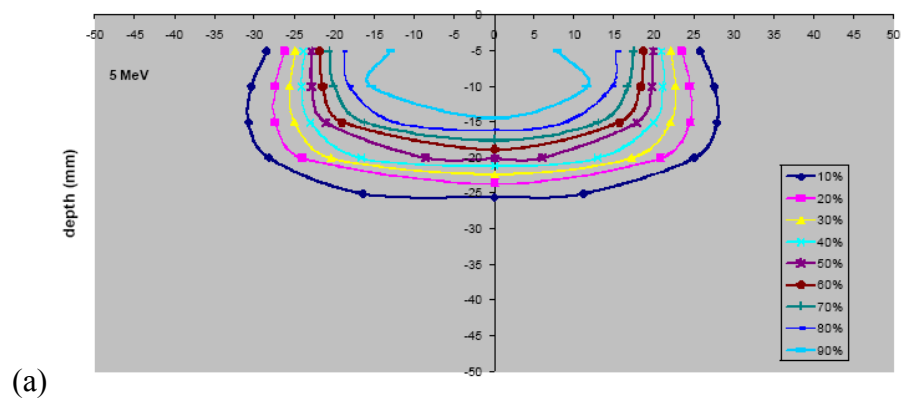


(c)

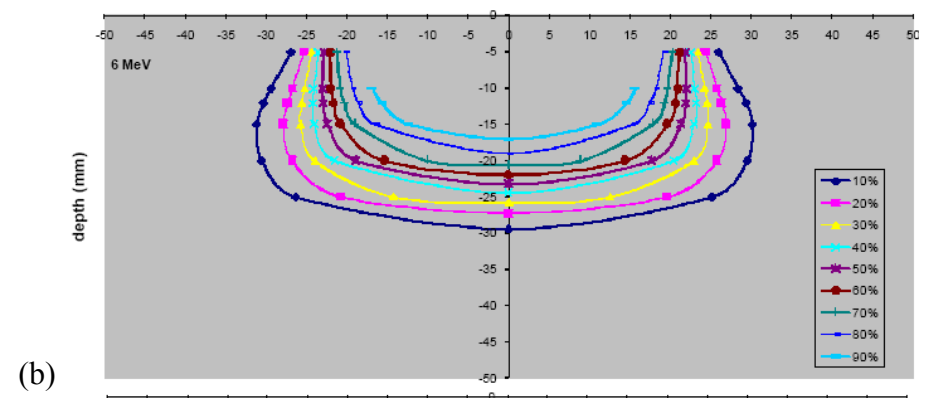


(d)

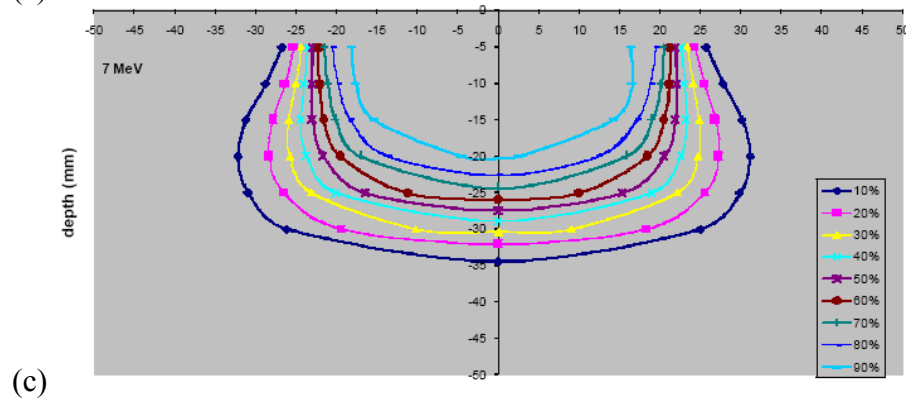
**Figure 3-25: Isodose charts for the 3 cm bevelled applicator (bevel angle 45°) (small applicator system) for electron energies (a) 5, (b) 6, (c) 7, and (d) 9 MeV measured with the Markus chamber, measured along the minor elliptical axis of the applicator**



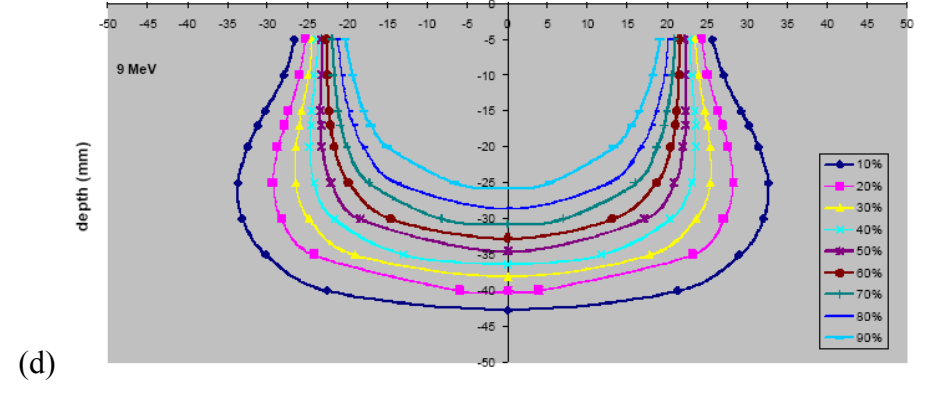
(a)



(b)



(c)



(d)

**Figure 3-26: Isodose charts for the 4.5 cm straight cone (periscopic electron system) for electron energies (a) 5, (b) 6, (c) 7, and (d) 9 MeV measured with the Markus chamber**

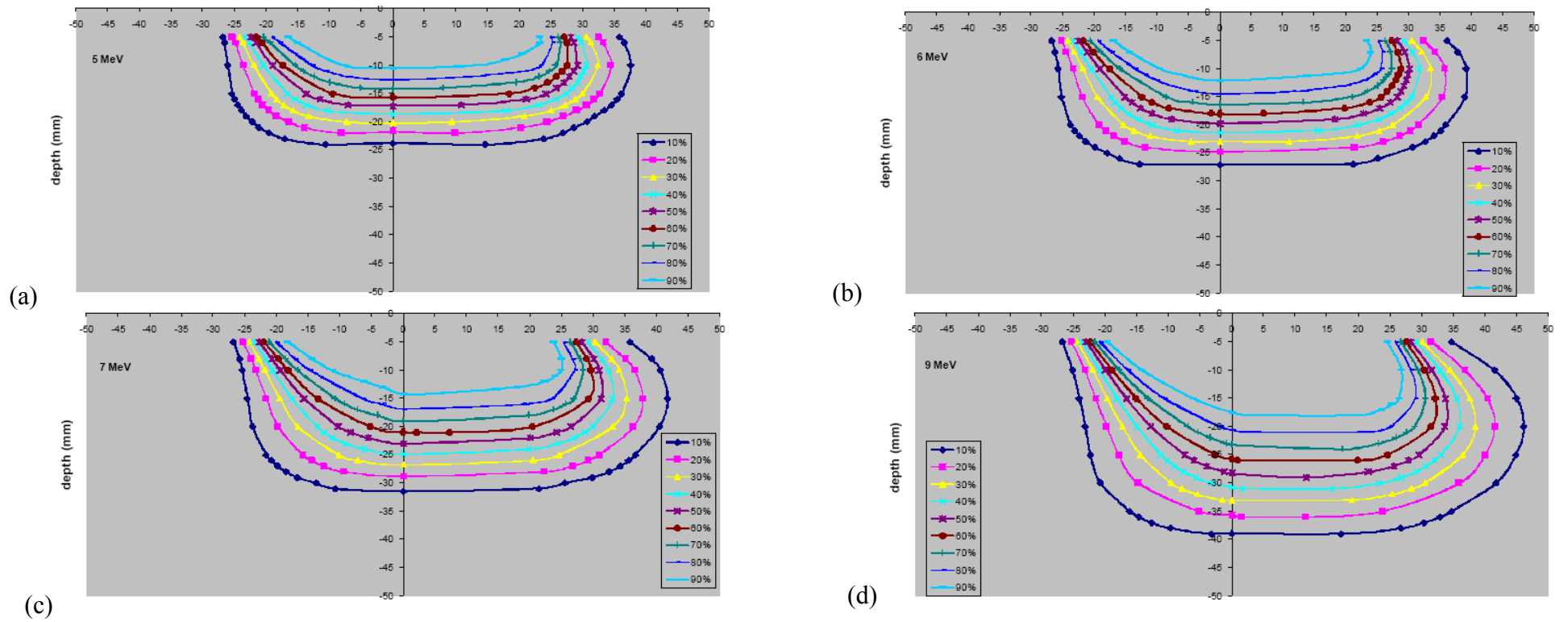
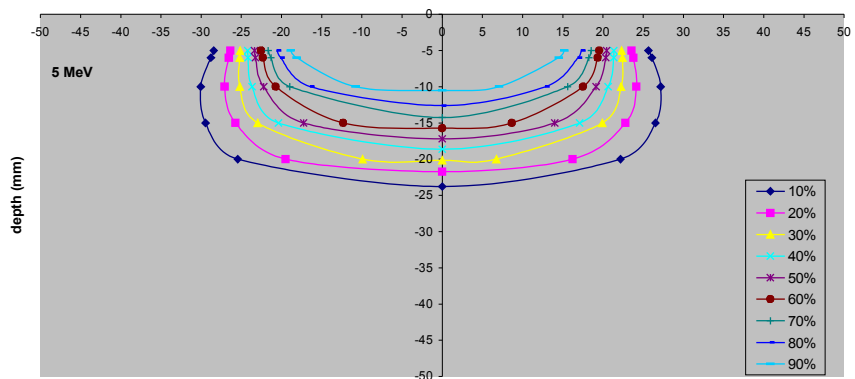
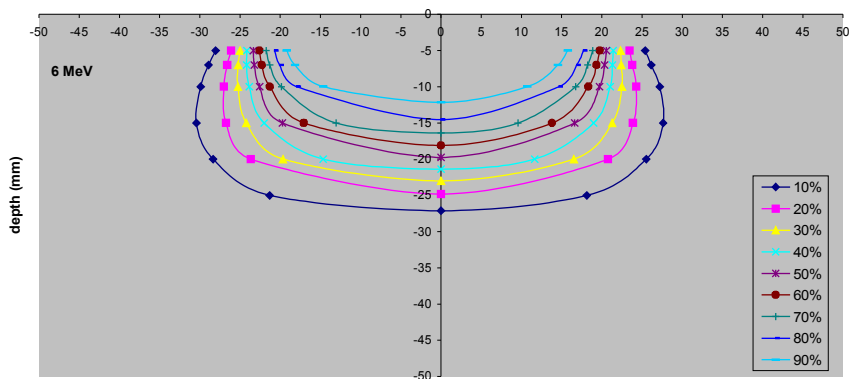


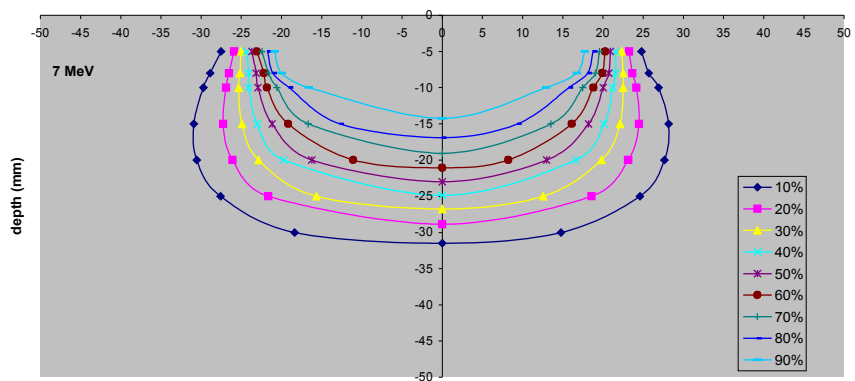
**Figure 3-27: Isodose charts for the 4.5 cm bevelled cone (bevel angle 45°) (periscopic electron system) for electron energies (a) 5, (b) 6, (c) 7, and (d) 9 MeV measured with the Markus chamber, measured along the major elliptical axis of the cone**



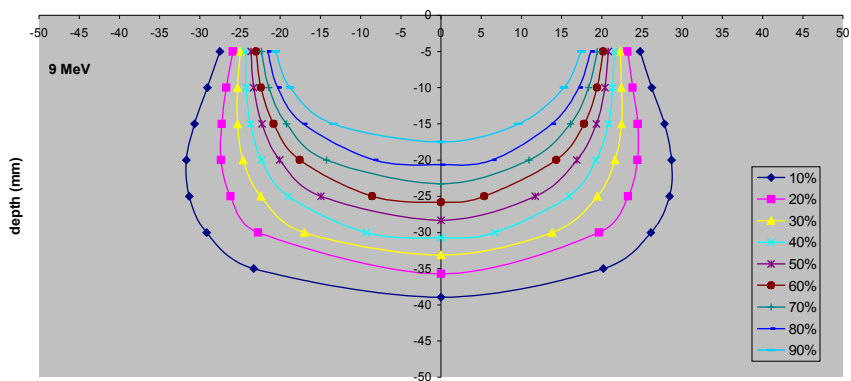
(a)



(b)



(c)



(d)

Figure 3-28: Isodose charts for the 4.5 cm bevelled applicator (bevel angle  $45^\circ$ ) (periscopic electron cone system) for electron energies (a) 5, (b) 6, (c) 7, and (d) 9 MeV measured with the Markus chamber, measured along the minor elliptical axis of the applicator

Figures 3-27, 3-28 and 3-29 show a comparison of isodose curves for cones of inner diameter 8 cm, 3 cm straight and 3 cm bevelled cones for small-field cone system. The isodose curves as generated from data captured with the Markus, Advanced Markus and PinPoint chambers and diode detector are seen to differ especially in the penumbra region. Figures 3-30 and 3-31 show a comparison of isodose curves for the Periscopic electron cone system for cones with inner diameter 4.5 cm straight and bevel end generated from data of measurements using of all the detectors.

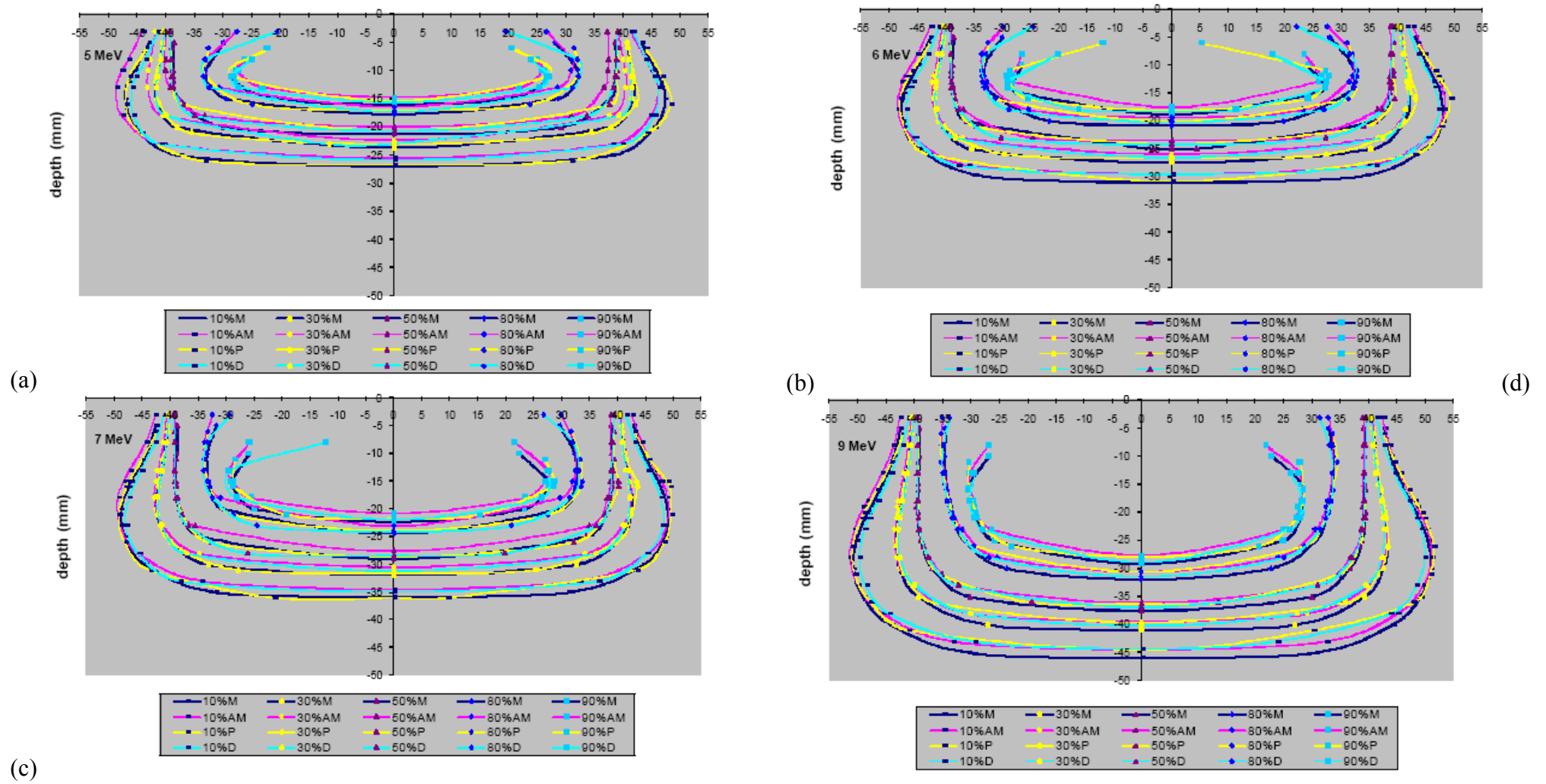


Figure 3-29: Comparison of isodose curves as measured with the Markus (M), Advanced Markus (AM), PinPoint (P) and Diode (D) detector for energies for the 8 cm straight cone (small cone system) (a) 5 MeV (b) 6 MeV (c) 7 MeV and (d) 9 MeV

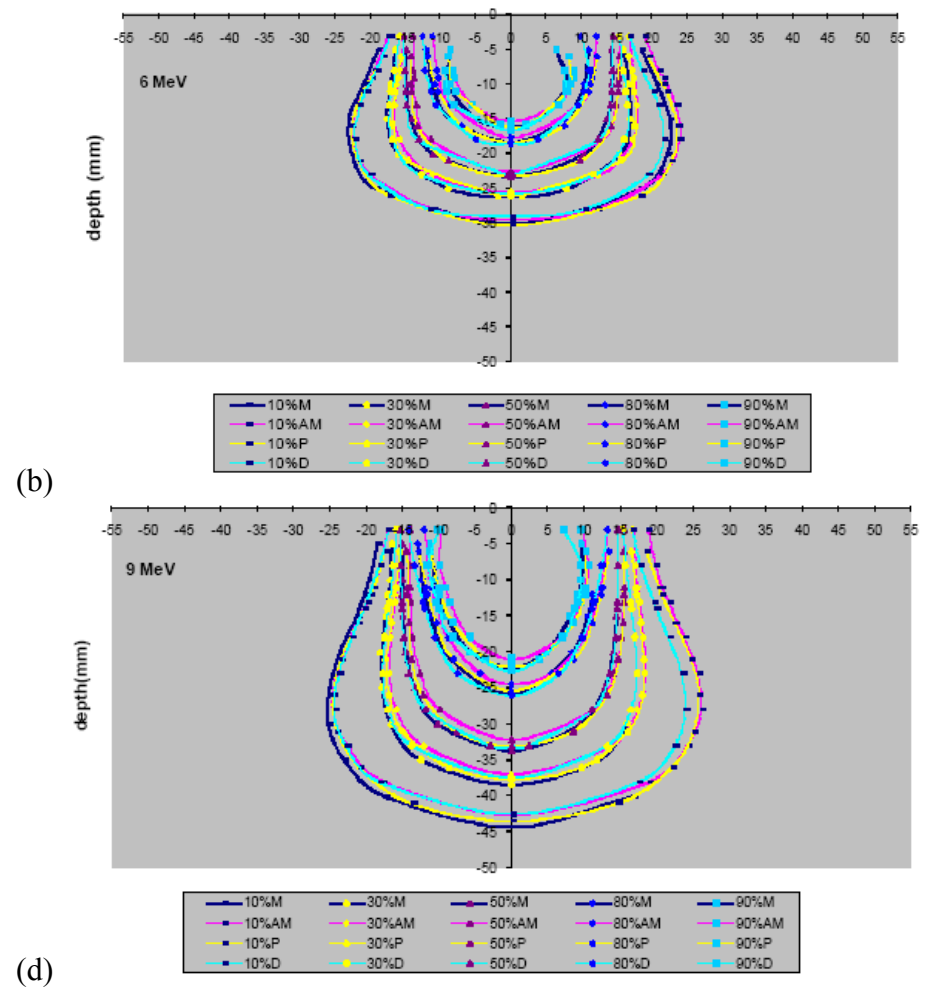
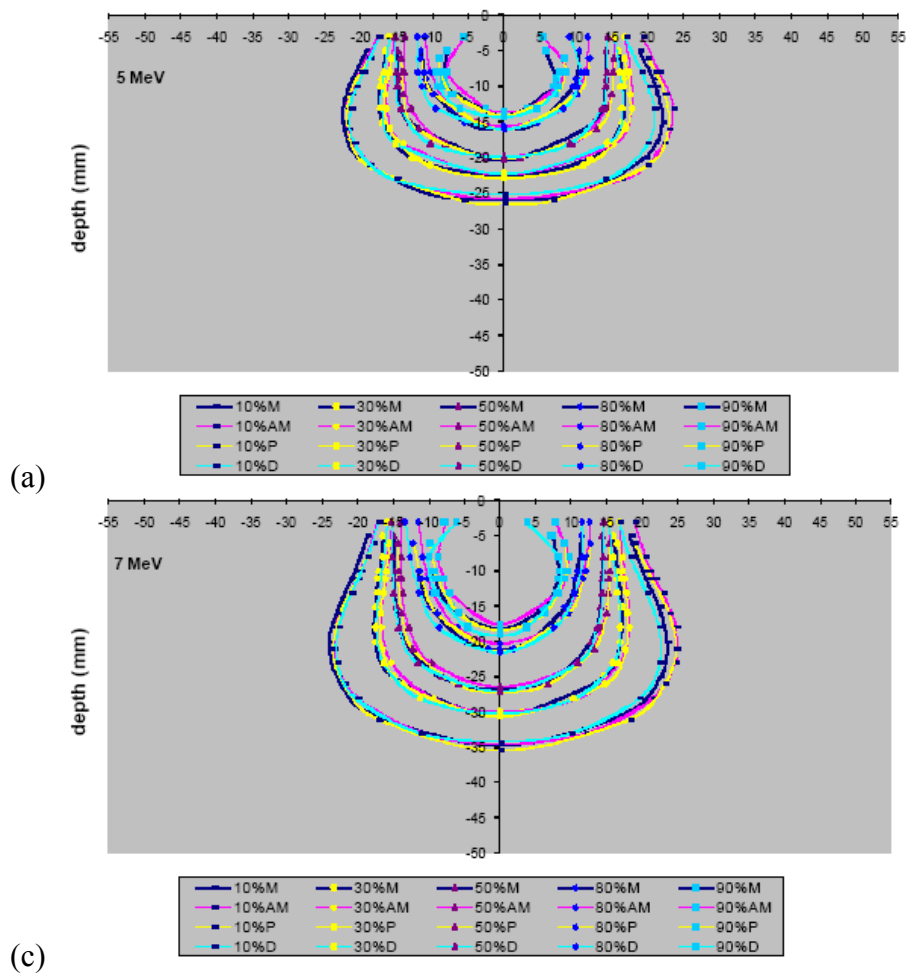


Figure 3-30: Comparison of isodose curves as measured with the Markus (M), Advanced Markus (AM), PinPoint (P) and Diode (D) detector for energies for the 3 cm straight cone (small cone system) (a) 5 MeV (b) 6 MeV (c) 7 MeV and (d) 9 MeV

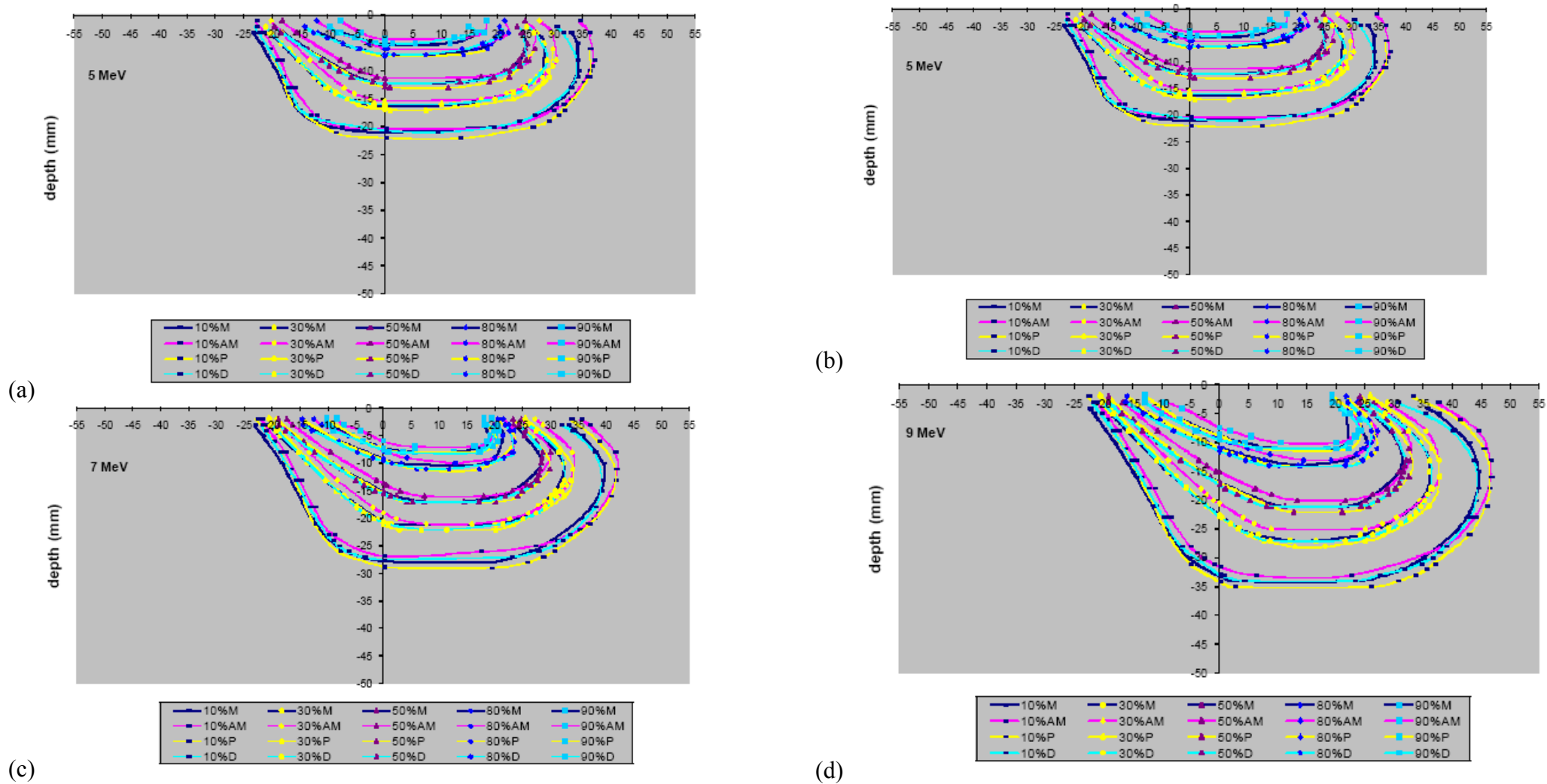


Figure 3-31: Comparison of isodose curves as measured with the Markus (M), Advanced Markus (AM), PinPoint (P) and Diode (D) detector for energies for the 3 cm bevelled cone (bevel angle 45°) (small cone system) (a) 5 MeV (b) 6 MeV (c) 7 MeV and (d) 9 MeV

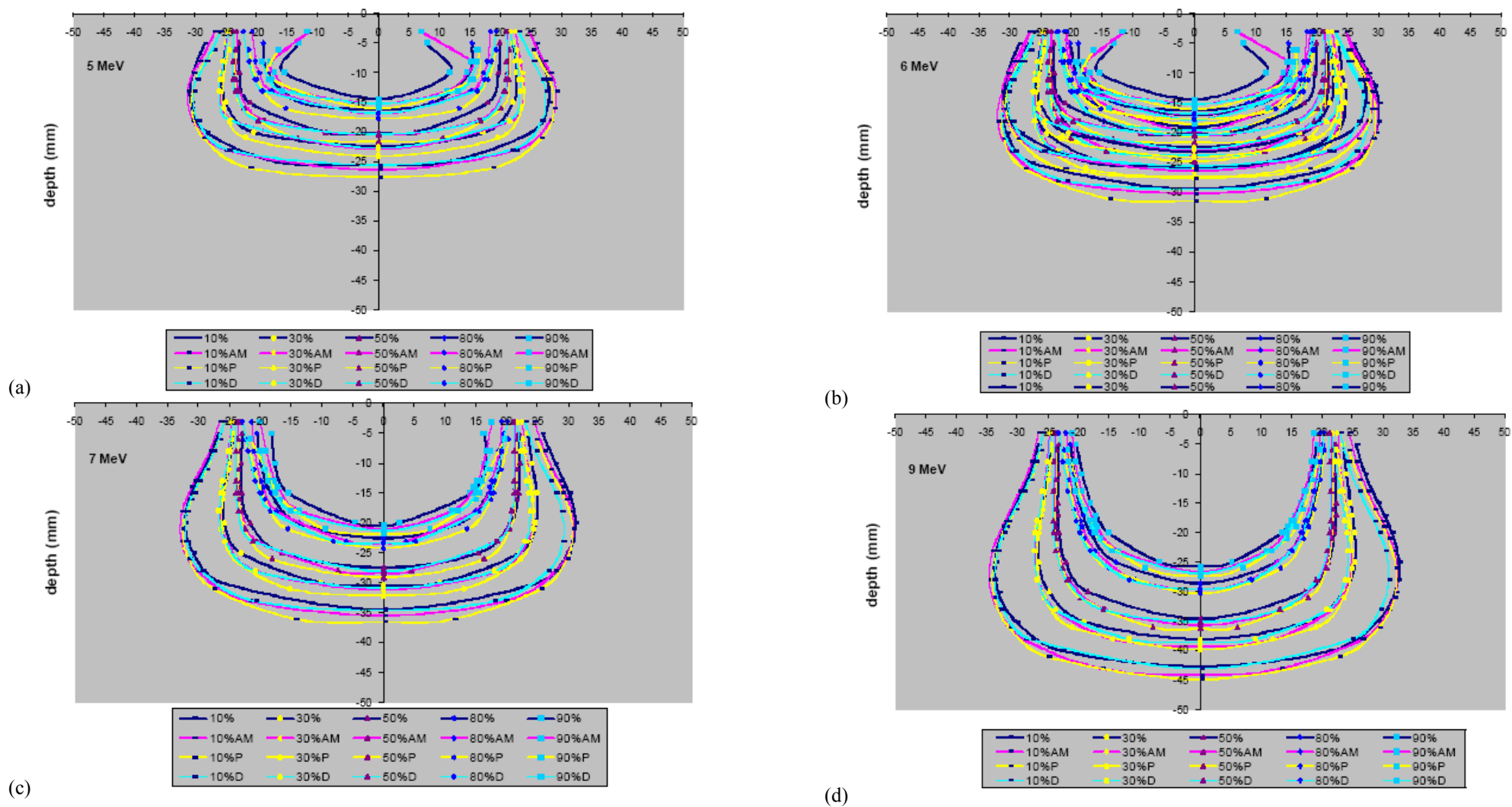


Figure 3-32: Comparison of isodose curves as measured with the Markus (M), Advanced Markus (AM), PinPoint (P) and Diode (D) detector for energies for the 4.5 cm straight cone (periscopic electron cone system) (a) 5 MeV (b) 6 MeV (c) 7 MeV and ( d) 9 MeV

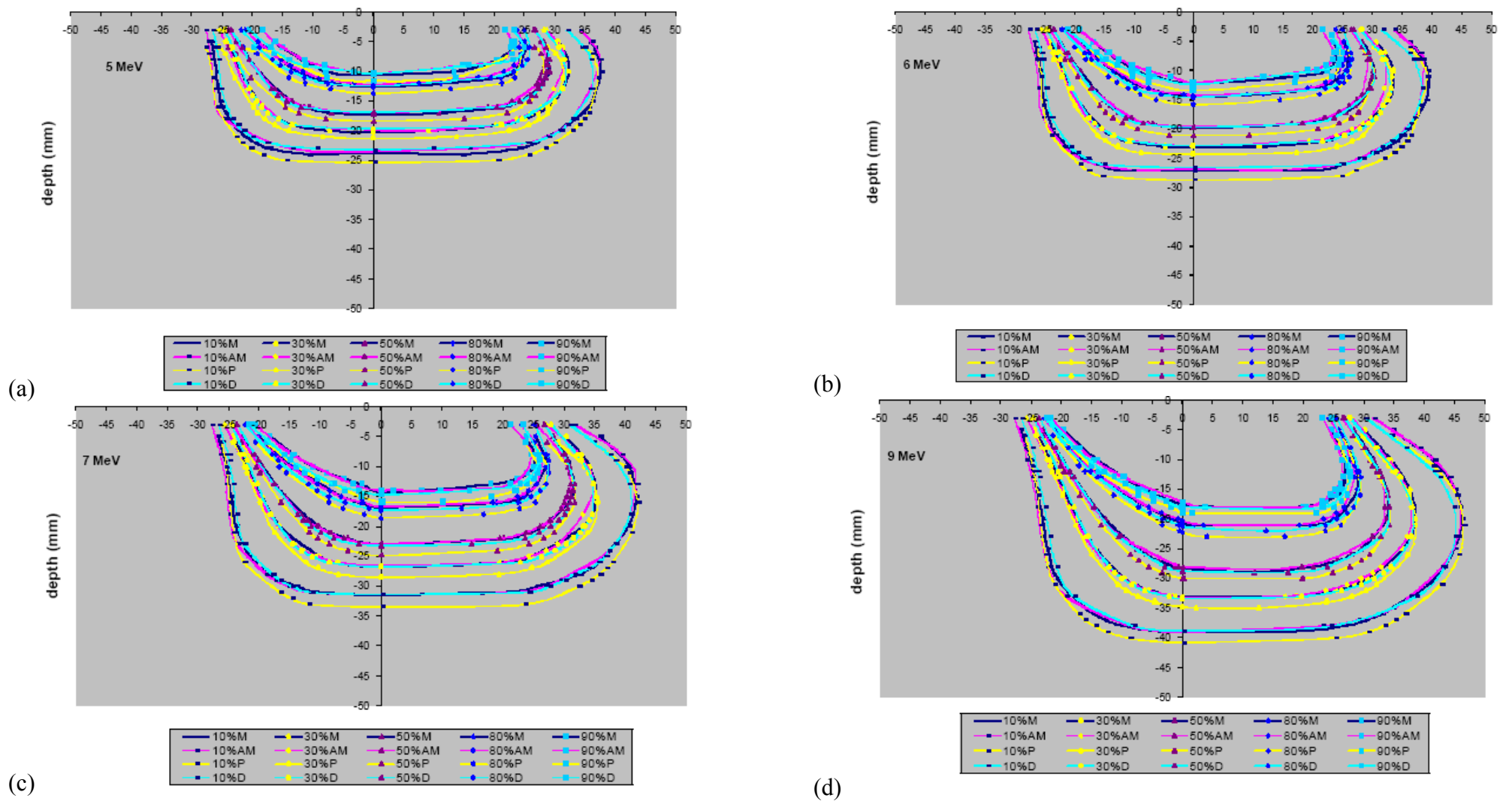


Figure 3-33: Comparison of isodose curves as measured with the Markus (M), Advanced Markus (AM), PinPoint (P) and Diode (D) detector for energies for the 4.5 cm bevelled cone (bevel angle 30°) (periscopic electron cone system) (a) 5 MeV (b) 6 MeV (c) 7 MeV and (d) 9 MeV

### 3.3.3 SSD corrections on air gap

For all the small-field and the periscopic cones, the SSD and the source-cone-end-distance (SCED) are equal (i.e. there is flush contact with the water surface) thus the air gap ( $g$ ) is zero (figure 2-1). However for the bevelled cones of inner diameter 2 and 3 cm (small-field cone system), the SSD and SCED are not equal, that is  $g$  is not zero. Thus a GF correction must be made for the 2 and 3 cm bevelled cones

Table 3-14 below show the ISF for the two bevelled cone (2 and 3 cm). The ISF was calculated at individual  $d_{\max}$  for each energy-cone combination, using all the detectors. The values obtained for the ISF for the different detectors are the same and thus are shown only in one table. ISF is used to correct for the  $g$ .

**Table 3-14: Inverse square factors for the 2 and 3 cm bevelled cones for the small field cone system**

Energy	5	6	7	9
Applicator				
2 cm <sup>a</sup> (SCED=99.4 cm)	0.988	0.988	0.988	0.988
3 cm <sup>a</sup> (SCED=99.2 cm)	0.988	0.988	0.988	0.988

<sup>a</sup>bevel angle 45°

The GF was calculated from measurements with the air gap ( $g \neq 0$ ) and measurements taken when the cone made flush contact with the water surface ( $g = 0$ ). The GF for the 2 and 3 cm bevel ended cones was measured with  $g$  of 6 and 8 mm respectively was for the ionisation chamber measurements as follows:

$$GF = \frac{\left[ \frac{(M_{IORT}(s_w, air)_{IORT})_g}{(M_{IORT}(s_w, air)_{IORT})_{g=0}} \right]}{ISF} \quad 3-11$$

and for diode detector:

$$GF = \frac{[(M_{IORT})_g / (M_{IORT})_{g=0}]}{ISF}$$

3-12

Table 3-14 shows the air gap corrections as calculated from measurements using the Markus, Advanced Markus, PinPoint chambers and diode detector. GF values were less than 1 which means that the output for these cones is overestimated if this correction is not applied because there are fewer electrons scattered to  $d_{max}$ .

**Table 3-15: Gap factors for the 2 and 3 bevelled cones (bevel angle 45°) for the small field cone system**

		Markus		Advanced Markus	
		2 cm circle <sup>a</sup>	3 cm circle <sup>a</sup>	2 cm circle <sup>a</sup>	3 cm circle <sup>a</sup>
Measured gap (g) [mm]		6	8	6	8
Energy [MeV]	5	0.861 ± 0.002	0.943 ± 0.001	0.862 ± 0.001	0.902 ± 0.004
	6	0.914 ± 0.001	0.930 ± 0.004	0.874 ± 0.001	0.902 ± 0.000
	7	0.914 ± 0.001	0.924 ± 0.000	0.874 ± 0.001	0.874 ± 0.001
	9	0.918 ± 0.003	0.913 ± 0.001	0.902 ± 0.000	0.902 ± 0.000

		PinPoint		Diode Detector	
		2 cm circle <sup>a</sup>	3 cm circle <sup>a</sup>	2 cm circle <sup>a</sup>	3 cm circle <sup>a</sup>
Measured gap (g) [mm]		6	8	6	8
Energy [MeV]	5	0.904 ± 0.003	0.934 ± 0.002	0.961 ± 0.001	1.008 ± 0.001
	6	0.915 ± 0.002	0.929 ± 0.000	0.733 ± 0.001	0.984 ± 0.001
	7	0.925 ± 0.002	0.920 ± 0.002	1.006 ± 0.002	0.967 ± 0.001
	9	0.933 ± 0.002	0.929 ± 0.001	0.998 ± 0.002	0.974 ± 0.002

<sup>a</sup> bevel angle 45°

## CHAPTER 4      DISCUSSION

Electron beams are widely used as a modality for IORT and this is due to the unique characteristics that make them ideal for IORT. Because of the added collimation of the IORT system there is an increase in low-energy scattered electrons at the edges of the field, this gives rise to a lack of charged particle equilibrium. The lack of charged particle equilibrium for IORT results in a decrease in mean energy at a given depth, this has an effect on the stopping-power ratios between water and the detector material and this in turn has an effect on the dosimetry of IORT beams. Two collimator systems were studied the small-field cone system and the periscopic system. The periscopic system is designated for IORT and intracavitary use. However the small-field cone system is not for IORT use. The two systems are similar in the way the electron beams are collimated, and the dosimetry has similar challenges. According to Björk *et al* (2004) there are extensive measurement techniques in small-field beams, however comparisons with different detectors in the same irradiation geometry have not been thoroughly studied. Thus no reference data exists to which the data obtained in this study can be compared to for the different detectors used.

### 4.1    Absolute dosimetry

#### 4.1.1    Output measurements

The linac being commissioned for IORT studies is not a dedicated machine for IORT use but is already in use for conventional treatment. The linac was commissioned to deliver 1 cGy/MU at  $d_{\max}$  for the reference electron applicator 10 cm x 10 cm at SSD 100 cm for all electron energies. The Advanced Markus and PinPoint chambers were used for the output measurements as they had calibration factors traceable to international laboratories. For the Advanced Markus chamber the percent error from the expected value of 1 cGy/MU was between 0.1% and 3.2%, while for the PinPoint the percent error was between 0.9% and 5.1%. The IAEA protocol TRS-398 (IAEA 2000) was used for the calculation of the output and determining  $k_{QE}$  which corrects for the difference in irradiation beam between the reference beam and the user beam.

$k_{Q_E}$  values quoted for the PinPoint (type-31006) in table 7.III of the IAEA TRS-398 (IAEA 2000) are not available for beam qualities ( $R_{50}$ ) less than 4.00 g.cm<sup>-2</sup>. Thus the values of  $k_{Q_E}$  used were extrapolated from the available data and this introduced errors in the output calculations. Table 7.III of the IAEA TRS-398 (IAEA 2000) does not provide  $k_{Q_E}$  values for the Advanced Markus chamber, however  $k_{Q_E}$  values are quoted for the Markus chamber. Because some dimensions of the Advanced Markus chamber and the Markus chamber are the same, these values were used, and errors could have been introduced in the output should the  $k_{Q_E}$  values be different for the Advanced Markus.

#### 4.1.2 Output factor measurements

The peak in OF (table 3-12) for the 6 cm cone may be explained by the number of scattered electrons from the inner walls of the cone that reach the central-axis at  $d_{\max}$ . The contribution to the fluence at  $d_{\max}$  for consists of primary electrons (no initial scatter) and secondary electrons scattered from the inner walls of the cone. According to Nyerick *et al* (1991), for lower energies, it is more likely that the scattered electrons from the upper portion of the cone will re-scatter at lower portions and will be absorbed, thus initial rise in OF is energy dependent. However the number of scattered electrons increases with cone diameter due to an increase in solid angle relative to the source subtended by the cone (Nyerick *et al* 1991) but for the larger cones (7 and 8 cm), the effect is countered by the fact that the some of the scattered electrons do not reach the central-axis and this is more significant for higher energies where the electrons are scattered in a more forward direction and hence the decrease in OF for the 7 and 8 cm.

OF were determined according to the IAEA TRS-398 protocol (IAEA 2000) for the non-reference fields. The uncertainty in output factor measurements was estimated to be  $\pm 0.2\%$  (1 SD) for the Markus and Advanced Markus chambers and diode detectors and  $\pm 0.4\%$  (1 SD) for the PinPoint measurement for the PinPoint chamber for the Small field cone system. For the Periscopic system the uncertainty was found to be  $\pm 0.4\%$  for the Markus, Advanced Markus and Diode detector and  $\pm 0.9\%$  for the

PinPoint chamber. The uncertainty in OF is based on the uncertainty in the dosimeter reading for the IORT field and the reference field.

The aim of the study was to provide a comparison of data obtained by the different detectors used. Because the Markus chamber is widely used in electron dosimetry and has a relatively small volume, the position of the proximal electrode is well known and, the measuring point is thus also well known. Therefore all measurements with the other detectors (Advanced Markus chamber, PinPoint chamber and diode detector) were referenced to the Markus chamber.

For the small-field cone system the percent difference in OF between the Markus and the Advanced Markus was less than 2.6%, with the PinPoint chamber it was less than 2.5%, and for the Diode detector it was less than 2.6%, for the straight ended cones. For the bevelled cones the percent difference in OF between the Markus and the Advanced Markus chamber was less than 3.9%, and the PinPoint chamber less than 4.8%, and for the diode detector it was less than 2.5%.

For the Periscopic electron cone system the percent difference in OF between the Markus and the Advanced Markus was less than 1.2%, with the PinPoint chamber it was less than 1.9%, and for the diode detector less than 1.2% for the straight cones. For the bevelled cones the percent difference in OF between the Markus and the Advanced Markus chamber was less than 1.9%, and the PinPoint chamber less than 2.8%, and for the diode detector it was less than 4.2%.

The  $s_{w,air}$  for electron beams used from table 7.V of the IAEA TRS-398 protocol (IAEA 2000) are a function of beam quality and relative depth ( $d/R_{50}$ ). The IAEA protocol TRS-398 (IAEA 2000) was used to calculate the OF. The  $s_{w,air}$  factors used were taken from table 7.V (IAEA 2000), for both the reference field and IORT field. However IORT fields do not meet the criteria for broad beam geometry and thus, using  $s_{w,air}$  for broad beams for IORT fields may introduce the error as determined in the OF.

## 4.2 Relative dosimetry

In the study a comparison was made of PDD measured with different detectors. The accuracy of the diode detector was verified by comparing the PDD curves obtained with the diode for the reference field with the PDD obtained with the Markus chamber. Measurements obtained with the diode were offset by 2 mm. Measurements from the Advanced Markus chamber and the PinPoint chamber were also offset by 2 mm and - 1 mm respectively. It therefore appears as though the nature of the detector system is not as precise.

The relative ionisations were converted to depth dose curves using the  $S_{w,air}$ . Fluence Corrections for the Parallel-Plate chambers (Markus and Advanced Markus) and the diode detector were assumed to be unity however fluence correction factors must be applied for cylindrical chambers (PinPoint). The fluence correction for the PinPoint chamber for the beams qualities used is not known and thus was not applied to the depth dose curves. The percent difference in the surface dose between the Markus chamber and the Advanced Markus chamber was between 0.1% and 3.7%, the PinPoint chamber between 1.5% and 7.9, and the diode detector between 0.1 % and 3.5%.

Björk *et al* (2004) found the  $S_{w,air}$  changed between different irradiation conditions – reference beam and IORT beams. The  $S_{w,air}$  used corresponds to the broad beam geometry and  $R_{50}$  used to interpolate  $S_{w,air}$  was for the reference beams. Using  $R_{50}$  from the IORT beams introduces errors in the  $S_{w,air}$  especially for smaller fields (2 cm and 3 cm).

The PDD is affected by variation in secondary jaw setting (x-ray jaws). The x-ray jaw setting for the small-field cone system is fixed at 17 cm x 17 cm and the beam is then further collimated by the collimator system. Thus for the small-field electron cone system the PDD is independent of the x-ray jaw setting. However for the Periscopic electron cone system, the x-ray jaw setting is not fixed. The x-ray jaw setting used in this study was 19 cm x 19 cm (secondary jaw setting for standard electron applicators). Wilenzick *et al* (unpublished work) used the periscopic electron cone

system and studied the effects of variation of the collimator setting on OF, beam profiles and concluded that the 10 cm x 10 cm x-ray jaw setting was optimal. Their study was however conducted for higher energy electrons (12, 15 and 18 MeV).

A comparison of the isodose curves for the different detectors showed that there was disagreement between curves especially in the penumbra region. This can be attributed to the spatial resolution of the detectors. The PinPoint chamber over responded in the penumbra regions when compared to the Markus chamber especially for the smaller fields.

The ISF corrects for the air gap only. On the other hand the GF corrects for the inaccuracy of the ISF due to the change in scatter. ISF may be applied to a geometrical situation where the treatment surface is at an SSD of 100 cm. However if the 2 and 3 cm bevel applicators are in flush contact then, the GF must be applied to take into consideration the difference in scatter when  $g \neq 0$  and  $g = 0$ .

## CHAPTER 5      CONCLUSIONS AND RECOMMENDATIONS

1. The Markus chamber, Advanced Markus chamber and the Diode maybe used for the relative dosimetry of small electron fields such as have been studied.
2. The Markus chamber should be cross-calibrated such that the absorbed dose calibration factor is obtained and a comparative study of output measurements made.
3. The diode detector should be cross-calibrated such that an absorbed dose calibration factor is obtained, and comparative studies could be conducted for output measurements using the diode detector.
4. It is recommended that the PinPoint not be used for absolute dosimetry, unless  $k_{QE}$  values can be determined for the beam qualities being used.
5.  $k_{QE}$  values should also be determined for the Advanced Markus such that the error introduced by using  $k_{QE}$  values for the Markus chamber is quantified.
6. It is possible to orientate the PinPoint chamber in two directions, with the stem of the chamber parallel to the beam and secondly with the stem of the chamber perpendicular to the beam. Further studies should be conducted with the PinPoint oriented in both positions to determine which orientation is more suitable for small-field electron dosimetry measurements.
7. Monte Carlo simulations should be used to generate  $S_{w,air}$  for the small electron fields.
8. A comparison of  $S_{w,air}$  obtained by Monte Carlo simulation for such collimator systems, would allow for the determination of the error introduced in using  $S_{w,air}$  for broad beam geometry situations.

9. A comparative dosimetric study should also be conducted for higher energy electrons.

## REFERENCES

- AAPM 1983 A Protocol for the Determination of Absorbed Dose from High Energy Photon and Electron Beams *Med. Phys.* **10** 741-771
- AAPM 1991 Clinical electron-beam dosimetry: Report of the AAPM Radiation Therapy Committee Task Group 25 *Med. Phys.* **18** 73-109
- AAPM 1999 Protocol for Clinical Reference Dosimetry of High-Energy Photons and Electrons Task Group 51 *Med. Phys.* **26** 1847-1870
- Abe M 1984 Intraoperative Radiotherapy – Past Present and Future *Int. J. Radiat. Oncol. Biol. Phys.* **10** 1987-1990.
- Beddar A S, Kubu M L, Domanovic M A, Ellis R J, Kinsella T I and Sibata C H 2001 A New Approach to Intraoperative Radiation Therapy *AORN J.* **74** 500-505
- Biggs P J, Epp E R, Ling C C, Novack D H and Micheals H B 1981 Dosimetry, Field Shaping and Other Considerations for Intraoperative Electron Therapy, *Int. J. Radiat. Oncol. Biol. Phys.* **7** 875-884.
- Biggs P J 1985 The Physics of Intraoperative radiotherapy using high energy electron beams, *Nuclear Instruments and Methods in Physics Research* **B10/11** 1102-1106
- Björk P, Knöös T and Nilsson P 2000a Comparative Dosimetry of Diode and Diamond Detectors in Electron Beams for Intraoperative Radiation Therapy *Med. Phys.* **27** 2580-2588.
- Björk P, Knöös T, Nilsson P and Larsson K 2000b Design and Dosimetry Characteristics of a Soft-Docking System for Intraoperative Radiation Therapy *Int. J. Radiat. Oncol. Biol. Phys.* **47** 527-533.
- Björk P, Knöös T and Nilsson P 2002 Dosimetry Characteristics of Degraded Electron Beams Investigated by Monte Carlo calculations in a Setup for Intraoperative Radiation Therapy *Phys. Med. Biol.* **47** 239-256.
- Björk P, Knöös T and Nilsson P 2004 Measurements of Output Factors with Different Detector Types and Monte Carlo calculations of Stopping-Power Ratios for Degraded Electron beams *Phys. Med. Biol.* **49** 4493-4506.
- Bova F J 1995 Clinical Electron Beam Physics *Radiation Therapy Physics* ed. Smith A R (New York: Springer-Verlag)
- Conkey C, Stern E D, Thomas P A, Morrale B and Roseman D L 1987 Intraoperative Radiation Therapy: Procedures and Protocols *AORN Journal* **46** 226-236
- Dahl R A, and McCullough E C 1989 Determination of Accurate Dosimetric Parameters

for Bevelled Intraoperative Electron Beam Applicators *Med. Phys.* **16** 130-131

Ellis R J, Nag S and Kinsella T J 2000 Alternative Technique of Intraoperative Radiotherapy *Eur. J. Surg. Oncol.* **26** S25-S27

Fraass BA, Miller, R W, Kinsella T J, Sindelar W F, Harrington F S, Yeakel, K, Van de Geijn J and Glatstein E, 1985 Intraoperative Radiation Therapy at the National Cancer Institute: Technical Innovations and Dosimetry *Int. J. Radiat. Oncol. Biol. Phys.* **11** 1299-1311.

Hogstrom K R, Boyer A L, Shill A S, Ochransky T G, Kirsner S M, Krissel F and Rich T 1990 Design of Metallic Electron Beam Cones for an Intraoperative Therapy Linear Accelerator *Int. J. Radiat. Oncol. Biol. Phys.* **18** 1223-1232

IAEA 1987 Absorbed dose Determination in Photon and Electron Beams: An International Code of Practice Technical Report Series no. 277 (International Atomic Energy Agency: Vienna)

IAEA 1997 The Use of Plane-Parallel Ionisation Chambers in High-Energy Electron and Photon Beams: An International Code of Practice for Dosimetry Technical Report Series no. 381 (International Atomic Energy Agency: Vienna)

IAEA 2000 Absorbed Dose Determination in External Beam Radiotherapy: An International Code of Practice for Dosimetry based on Standards of Absorbed Dose to Water Technical Report series no. 398 (International Atomic Energy Agency: Vienna)

ICRU 2004 Prescribing, Recording, and Reporting Electron Beam Therapy ICRU report 71 International Commission of Radiation Units and Measurements (ICRU) (Britain: Oxford University Press)

Khan F M 2003 The Physics of Radiation Therapy 3<sup>rd</sup> ed. (Philadelphia USA: Lippincott Williams and Wilkins)

Klevenhagen S C 1985 Physics of Electron beam therapy: Medical Physics Handbook (Adam Hilger Ltd: Boston USA)

McCullough E C and Anderson J A 1982 The Dosimetric Properties of an Applicator System for Intraoperative Electron Beam Therapy Utilising a Clinac-18 Accelerator *Med. Phys.* **9** 261-268

Nyerick C E 1991 Dosimetry Characteristics of Metallic Cones for Intraoperative Radiotherapy *Int. J. Radiat. Oncol. Biol. Phys.* **21** 501-510

Olsen D R, Paulsen T H, Heyerdal H, Tveit K M, Wiig J N, Gierscksy K E and Storaas A 1995 Field Homogeneity of Bevelled Intraoperative Electron Beams - The Influence Of Virtual Focus Distance *Medical Dosimetry* **20** 105-109

Palta J R and Suntharalingam N 1989 A Non-Docking Intraoperative Electron Beam Applicator System *Int. J. Radiat. Oncol. Biol. Phys.* **17** 411-417

Palta J R, Biggs P J, Hazle J D, Huq S M, Dahl R A, Ochransky T G, Soen J, Dobelbower R R and McCullough E C 1995 Intraoperative Electron Beam Radiation Therapy: Technique, Dosimetry, and Dose Specification: A report of Task Group 48 of the Radiation Therapy Committee, American Association of Physicist in Medicine *Int. J. Radiat. Oncol. Biol. Phys.* **33** 725-746.

Podgorsak E B and Podgorsak M B 1999 Special Techniques in Radiotherapy In Van Dyk J, 1999 *The Modern Technology of Radiation Oncology: A compendium for Medical Physicists and Radiation Oncologist* (Madison: Medical Physics Publishing)

Sharma S C, Wilson D L and Jose B, 1984 Dosimetry of Small Field for Therac 20 Electron Beams *Med. Phys.* **11** 697-702.

Sharma S C, Johnson M W and Gossman M S, 2005 Practical Consideration for Electron Beam Small Field Size Dosimetry *Medical Dosimetry.* **30** 104-106.

Strydom W, Parker W and Olivares M 2005 Electron Beam: Physical and Clinical Aspects. In Podgorsak, E. B. (ed.) 2005 *Radiation Oncology Physics: A Handbook for Teachers and Students.* (Vienna: IAEA.)

van der Merwe D G 1994 The Effects of Tissue Inhomogeneities on The Energy Spectrum and Dosimetry in Electron Radiation Therapy PhD Thesis University of the Witwatersrand, Johannesburg

Venselaar J L M and Bierhuizen H W J, 1998 A Solution for the treatment of small lesions using electron beams from a Saturne, linear accelerator with continuous variable trimmers; Dosimetric aspects *Medical Dosimetry* **23** 99-103

Verellen D 2006 Physics of Stereotactic Radiosurgery and Stereotactic Body Radiation Therapy: Proceeding of the SAAPMB Congress March 2006 Cape Town South Africa

Willet C G, Czito B G and Tyler D S 2007 Intraoperative Radiation Therapy *J. Clin. Oncol.* **8** 971-977

Wilenzick R M, Kubrich W S, Douglas G A and White C A (unpublished work) Evaluation of a Commercial Applicator System for Intraoperative Radiotherapy

[www.elimpex.com/products/radiation-therapy/chambers/30331.pdf](http://www.elimpex.com/products/radiation-therapy/chambers/30331.pdf)